Charge air configurations for propulsion diesel engines aboard fast naval combatants

a simulation study on efficiency and performance

SDPO.18.005.m.
Delft University of Technology

Joris Quirinus Rusman

TU Delft
Ministerie van Defensie

Charge air configurations for propulsion diesel engines aboard fast naval combatants

a simulation study on efficiency and performance

by

Joris Quirinus Rusman

to obtain the degree of Master of Science
at the Delft University of Technology,
to be defended publicly on Wednesday February 7, 2018 at 14:00.

Report number:	SDPO.18.005.m	
Student number:	4019253	
Project duration:	January 1, 2017 – February 7, 2018	
Thesis committee:	ir. K. Visser, Rear-Admiral (ME) ret.,	TU Delft
	LTZ1 (TD) MSc. R.D. Geertsma,	TU Delft, supervisor
	Dr. ir. R. Pecnik,	TU Delft
	LTZ1 (TD) ir. F.J. Driegen,	DMO, supervisor

An electronic version of this thesis is available at `http://repository.tudelft.nl/`.

TU Delft

Abstract

The time a naval combatant can be deployed for a mission is limited by its dependency on supplies. At a certain point the ship needs to leave the area of operations to be replenished in a harbour or by a support ship. Moreover, the Royal Netherlands Navy has a societal obligation to reduce its environmental impact, in particular on global warming. Therefore, the Royal Netherlands Navy (RNLN) wants to reduce the fossil fuel dependency of its fleet significantly [50]. One of the methods to reduce fossil fuel dependency of ships is to reduce their energy requirement.

The operational profile of fast naval combatants for the RNLN requires that the ships operate on the diesel engines for 90 percent of the time, often in part load. In part load, the turbocharger cannot supply the engine with the right amount of charge air. This results in a limited operating envelope for the diesel engine, and a decreased efficiency in part load. This is caused by the matching of a turbocharger, which is a compromise between high efficiency in the design point, and off design performance. However, in part load, advanced charge air configurations can potentially resolve this and improve the results as shown by Grimmelius et al.[15] and Zhang et al [56].

This study investigates the effect of advanced charge air configurations on the efficiency and acceleration performance of diesel engines in hybrid configurations aboard fast naval combatants. First, two mean value first principle diesel engine models based on the work of Geertsma et al. [12] were used to model the diesel engine. Next, the models were partly validated with ship data. We found that an approach using compressor maps and a motion based turbocharger model was most accurate. Then, a parallel-sequential turbocharger and a hybrid electric turbocharger were incorporated into the model. A hybrid turbocharger is a turbocharger with an electric machine coupled to the turbocharger shaft. The electric machine can increase the turbocharger speed to boost the charge air pressure in motor mode. Also, in generator mode excessive power from the turbocharger shaft can be taken out and utilized elsewhere. It was concluded that the application of advanced charge air configurations can significantly improve the engine efficiency in part load. For example, in a diesel hybrid propulsion configuration with power take-off this can lead to an efficiency increase of almost 10% at 20% load in comparison with a single charged engine. Furthermore, hybrid turbocharging enables extending the operating envelope of a parallel-sequential turbocharged engine with up to 25% at 60% engine speed. This enables the engine to deliver constant torque from 600 to 1000 rpm. With these concepts therefore, both improved efficiency and improved acceleration performance can be achieved.

Contents

List of Figures

List of Tables

Nomenclature

Acronyms

bsfc	brake specific fuel consumption [g/kWh]
FAT	factory acceptance test
MOE	measures of effectiveness
MOP	measures of performance
MVFP	mean value first principle
OES	Operationele energie strategie [50]
PTI	power take in
PTO	power take off
RTBO	reduced time before overhaul
VTG	variable turbine geometry

Greek Symbols

α_{TC}	radial acceleration of the TC $[rad/s^2]$
β	Zinner pulse correction factor
β	power correction factor
χ	ratio of specific heats of air and exhaust gas
δ	fuel addition factor
ϵ_{INL}	heat exchange effectiveness
η_{pu}	ratio of combustion air to trapped mass [-]
η_{scav}	scavenge efficiency
η_{sc}	scavenge efficiency
γ	specific heat ratio
λ	air excess ratio [-]
λ^*	pseudo air excess ratio [-]
ω_{TC}	radial speed of the TC $[rad/s]$
ϕ_{com}	dimension less flow rate
π	pressure ratio
π_{sc}	Pressure difference between inlet and outlet of the cylinder [Pa]
Ψ	non dimensional flow coefficient
ψ	dimension head parameter
ψ_0	enthalpy coefficient
σ_f	stoichiometric air to fuel ratio [-]
σ_f	stoiciometric air to fuel ratio
τ	temperature ratio
$\tau_{TC-mech}$	mechanical time constant

Roman Symbols

$\dot{m}_{in}$	mass flow entering [kg/s]
$\dot{m}_{out}$	mass flow leaving [kg/s]
$\dot{Q}$	heat flow [kJ/s]
$\dot{W}$	work [kJ/s]
η_{comb}	combustion efficiency
η_q	heat release efficiency
$A_{sc,eff}$	effective scavenge area of the cylinder $[m^2]$
h	enthalpy [kJ]
h	enthalpy per unit mass [kJ/kg]
h^L	Lower heating value [kJ/kg]
I_{TC}	Moment of inertia $[kgm^2]$
m_1	trapped mass [kg]
m_f	fuel mass [kg]
n_{bld}	polytropic expansion coefficient
n_e	engine speed [Hz]
$p_{c,buchi}$	Büchi pressure [Pa]
p_c	inlet receiver pressure [Pa]
q_{hl}	specific heat loss in kJ/kg
q_{ii}	heat release [kJ/kg]
R_{air}	universal gas constant $= 8,31446 JK^{-1}mol^{-1}$
s_{sl}	slip ratio
T	Temperature [K]
T_{bld}	blowdown temperature [K]
$T_{ev,est}$	exhaust valve temperature estimate [K]
X_{ii}	heat ratio
i	number of cylinders
k	number of revolutions per cycle
n	engine speed [Hz]

Subscripts

cyl_out	flow out of the cylinder
id	assuming no heat loss
is	assuming isentropic conditions
BPV	bypass valve
com	compressor
cv	control volume
EC	exhaust closure
eng	engine
IC	inlet closure
ind	induction
ind	induction
INL	inlet
IR	inlet receiver
OR	outlet receiver
sc	scavange
sc	scavenge
sc-tr	trapped
TC	turbocharger
tur	turbine

1

Introduction

The time a naval combatant can be deployed for a mission is limited by its dependency on supplies. At a certain point, the ship needs to leave the area of operations to be replenished at a harbour or by a support ship. Increasing energy requirements during operation have a big impact on the effectiveness and deployment of the Royal Netherlands Navy. In the future, the Royal Netherlands Navy wants to reduce the energy requirements of their fleet significantly, as seen in Figure 1. The aim is to improve the logistic dependency of the ships, but also for environmental and economic reasons. The motivation is further elaborated in the Operationele Energie Strategie (OES) [50].

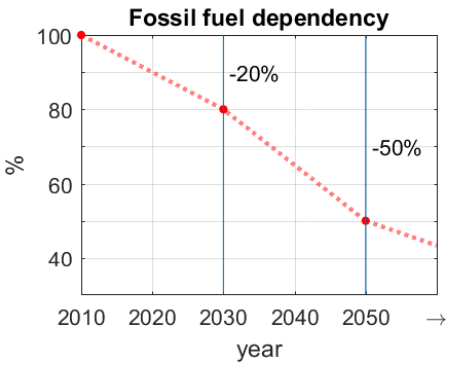

Figure 1: OES Targets [50]

The objective of decreasing the energy requirements can be addressed in three ways. First, one could not use the ship that often or sail at a lower speed to reduce fuel consumption. However, reducing the ships speed is not always possible without impacting the mission of the ship. Also, the effectiveness of the ship would be reduced considerably by the longer transit time. Second, one could sail on alternative fuels such as hydrogen or bio diesel, reducing the dependency on fossil energy sources. However, none of the alternative fuels is commonly used or available nowadays, so this will increase the logistic dependency in the field. For example, if hydrogen is not available in harbour one has to travel further to the next harbour. Third, one could improve the design of the ship so it uses less fuel and produces less emissions. For example, if the ship is fitted with very efficient engines the logistic dependency on fuel reduces, as do the emissions. Another option would be to design a more slender ship, which uses less energy to reach a certain speed. The advantage of increasing the efficiency is that this approach is complementary to the other approaches.

Currently, the Royal Netherlands Navy is working on the replacement of the Karel Doorman class frigates. The main task of this ship is anti submarine warfare. The envisioned propulsion plant consists of a hybrid diesel configuration, which enables the ship to use a silent propulsion mode for submarine hunting. A problem frequently encountered on diesel driven naval combatants is overloading of the diesel engines. In the past the Karel Doorman class frigates have experienced problems with their diesel engines . This resulted in poor acceleration performance as the control strategy was designed very conservatively to protect the engine from overloading [51].

Vollbrandt [52] studied the acceleration performance of a diesel hybrid configuration aboard a fast naval combatant and compared it to a combined diesel or gas turbine configuration. It was concluded that the acceleration performance of diesel hybrid configurations can be comparable and in specific cases even better than combined diesel or gas turbine configurations. This is important, since generally diesel engines are more efficient than gas turbines. Therefore, the choice for diesel engines instead of gas turbines would directly contribute to the goal of improving the efficiency of the ship. Geertsma et al. [13] quantitatively compared hybrid diesel-electric

and gas-turbine-electric propulsion. They showed that fuel consumption and emission can be reduced with respect to the gas- turbine-electric configuration, while maintaining an acceleration performance close to that of gas-turbine-electric propulsion.

The operational profile of a fast naval combatant is depicted in Figure 2. It can be seen that more than 90% of the operation time the ship sails at speeds lower than 21 knots, and operates on the diesel engines. Also, during a substantial part of this 90% the diesel engines are used in part load. Especially in part load, diesel engines are prone to thermal overloading. Thermal overloading of the diesel engine limits the acceleration performance of diesel driven naval combatants as shown by Vollbrandt and Geertsma et al. In both studies the air excess ratio (3.26) was used as an indicator for the thermal loading of the diesel engine. The air excess ratio depends on the charge air pressure, provided by the turbocharger. Therefore, the turbocharger has a significant influence on the efficiency, operating envelope and acceleration performance of the ship. The turbocharger configuration and matching is an integral part of the engine design. The matching of a turbocharger is a compromise between high efficiency in the design point, and off design performance. Away from the design point, the turbocharger cannot supply the engine with the right amount of charge air. This results in a limited operating envelope for the diesel engine and a decreased efficiency in part load. Advanced charge air configurations can potentially resolve this and improve the results of Vollbrandt and Geertsma et al. even further, which raises the question:

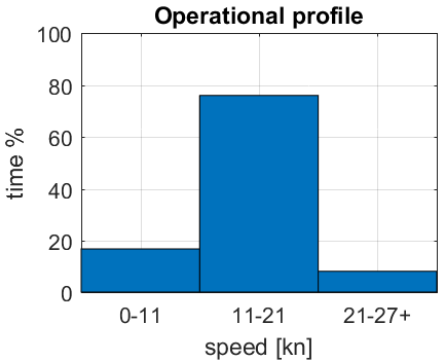

Figure 2: Operational profile [52]

Can the efficiency and performance of diesel hybrid configurations aboard fast naval combatants be improved by applying advanced charge air configurations?

This main question can be subdivided into the three following sub-questions:

- What is the effect of advanced charge air configurations on the efficiency of the diesel engine?
- What is the effect of advanced charge air configurations on the operating envelope of the diesel engine?
- What is the effect of advanced charge air configurations on the acceleration performance of the diesel engine?

Many studies into turbochargers, fuel efficiency and performance of ships of ships have been performed at the TU Delft, for which several diesel engine models have been developed. Examples are the work of Vrijdag et al.[55], Schulten et al. [40] and Grimmelius et al. [15]. Often, complex models are used, which rely on compressor and turbine maps belonging to the specific engines. Examples can be found in the work of Schulten et al. [40] and Sapra et al.[38]. These maps are not included in FAT and project guide data, and therefore they are hard to acquire. For comparative studies like this, the overall system performance is of interest. Simpler models can save a lot time and effort, with accurate enough results for the overall system performance. Recently Geertsma et al. [12] and Loonstijn [34] proposed improvements to a Mean Value First Principle (MVFP) diesel engine model proposed by [35] et al., to create a more realistic model of the turbocharged diesel engine aboard a ship. However, an extensive validation with regards to the accuracy of these models to predict performance of diesel engines with advanced charge air concepts still remains open for investigation. Therefore, we want to answer the following question:

Is it possible to model advanced charge air configurations by means of a simple mean value first principle diesel engine model and validate this model by measurements

in operational conditions?

The aim of this study is to investigate the effect of advanced charge air configurations on the efficiency and acceleration performance of diesel hybrid configurations aboard fast naval combatants. This research will contribute in four parts to this goal. First, a general summary and classification of charge air systems will be presented. Second, a MVFP model with a power balance based turbocharger and a MVFP model with a motion based turbochager are investigated to determine whether it is feasible to use a MVFP engine model for comparative studies into advanced turbocharging. Next, a MVFP model will be validated with data acquired at a measuring campaign aboard a fast naval combatant. Finally, the validated model will be used to investigate the application of advanced charge air configurations to show the effect on the energy efficiency, acceleration performance, design, and emissions of fast naval combatants.

2

Charge air systems

The aim of charge air systems is to increase the amount of air trapped in the cylinder. Due to the larger amount of air, more fuel can be injected in a cycle. This will result in a higher specific power of the engine. Further, the efficiency of the engine tends to improve because mechanical an heat losses increase at a lower rate then the specific power.

If the energy to compress the charge air is obtained from the hot exhaust gasses by means of a turbine, the process is called turbocharging. In search of an ever increasing efficiency and performance, different charge air systems have been developed which are nowadays becoming more and more important. Figure 4 shows several different charge air systems and their influence on the torque characteristic of the diesel engine.

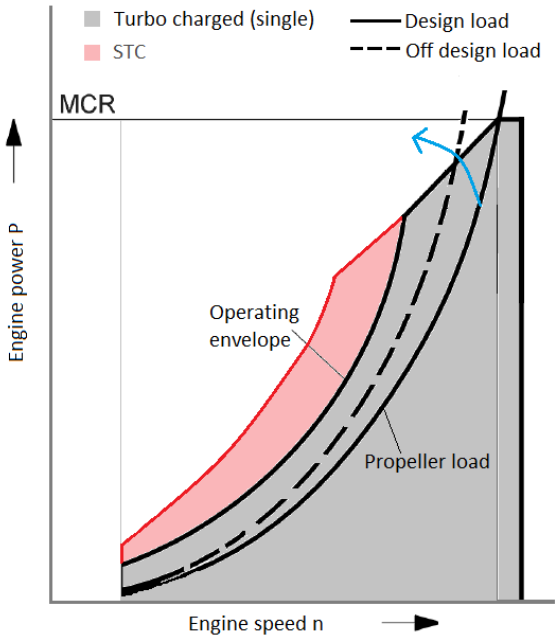

Figure 3: Extended operating envelope [26]

The benefit of improving the torque characteristic is illustrated in Figure 3. By increasing the operating envelope of the diesel engine, a bigger power margin with respect to the propeller load is achieved. The power margin can be utilized to apply a power take-off or could be used as 'reserve' to ensure performance in off design loads, for example high sea states.

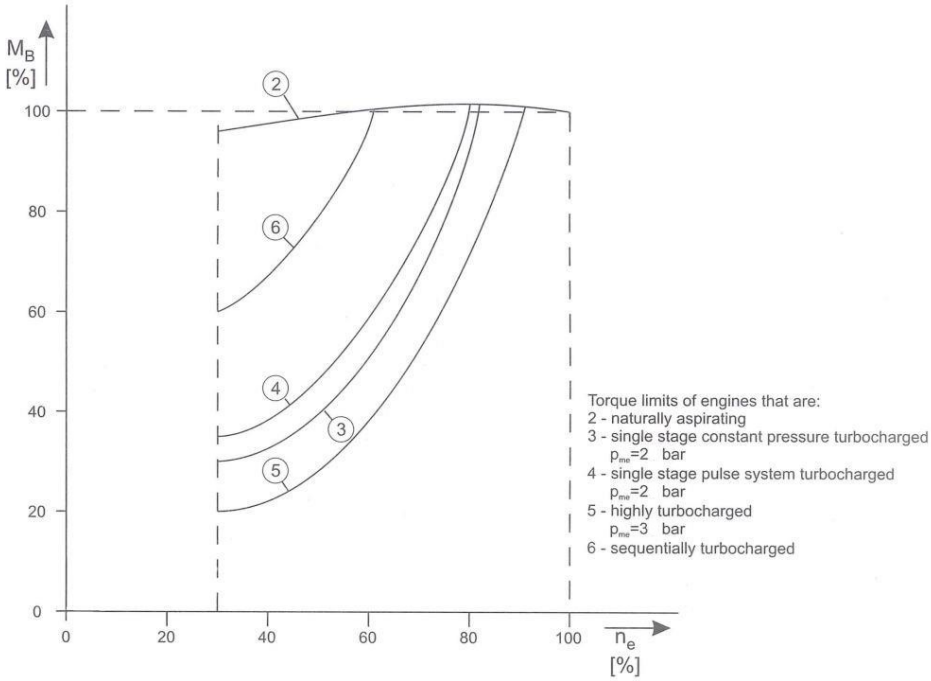

Figure 4: Torque characteristics of diesel engines of equal nominal rated power, with various types of charge air systems [26]

2.1. Principles

A turbocharger consists of a compressor and a turbine connected via a shaft as seen in Figure 5. The turbine is driven by hot exhaust gases and drives the compressor. The compressor will compresses ambient air to a certain pressure, and can then be cooled in an intercooler to increase the density further.

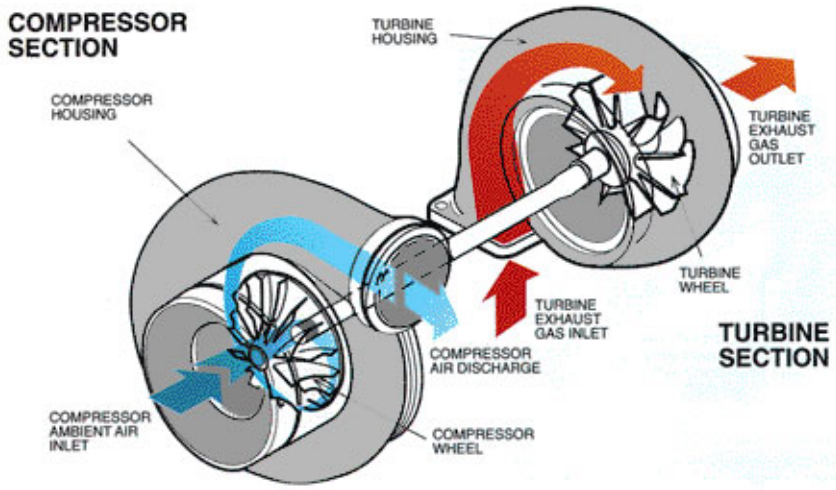

Figure 5: Basic components of a turbocharger system [2]

2.1.1. Supercharging

In case of engines equipped with a supercharger, the amount of charge air pressure is increased by means of a mechanically driven compressor. This means more air is available for the combustion process, therefore the amount of fuel injected per cycle can be increased. The power to drive the mechanical compressor is provided by the engine itself, as can be seen in Figure 6. Although less common, the mechanical compressor can sometimes be driven by an electric machine. Su-

perchargers are applied to widen the operating envelope and increase the specific power of the diesel engine. The increase in efficiency of the engine is minor in comparison with turbocharged engines because the supercharger is not driven by a waste stream, but by the crankshaft, subtracting power from the engine. An advantage of the supercharger is that it does not increase the back pressure after the diesel engine. Therefore, a supercharger can be successfully applied in configurations where the pressure in the exhaust is an important design criteria. For example, submarine diesel engines have to cope with varying back pressure in the exhaust system due to waves blocking the exhaust pipe.

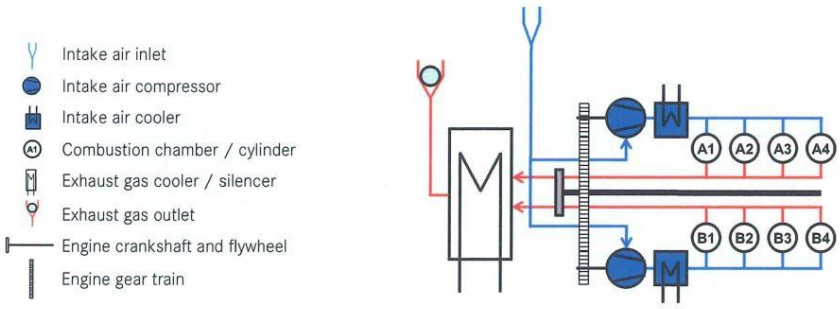

Figure 6: Air flow in engine with mechanically driven supercharger[53]

2.1.2. Single stage turbocharging

In contrast with the supercharging system, single stage turbocharger systems are mechanically uncoupled from the engine. The power required to drive the compressor is obtained from a turbine driven by the hot exhaust gases. Figure 7 shows a typical configuration of a turbocharger system. The turbine is mechanically connected to the compressor to transfer the energy obtained from the exhaust gasses. This form of charging also aims to increase the specific power of the diesel engine, but it obtains its energy from the exhaust gasses which are normally expelled into the air. Basically, waste energy is recovered to drive the compressor and therefore increasing charge air pressure does not require any form of mechanical energy. Since the engine has more air available, the specific power can be increased and since mechanical and heat losses increase slower, the overall efficiency of the engine increases.

The dynamic response of the engine is influenced by installing a turbocharger system. The charge pressure of the turbocharger depends on the rotating speed of the compressor, which depends on the amount of air supplied to the turbine. At low engine speed, the amount of exhaust gas available to the turbine will be low. Therefore, available charge pressure from the compressor will be limited. The turbocharger is a dynamic system itself and has inertia. Therefore, the supplied charge air pressure on acceleration will lag behind the charge air pressure at steady state operation of the engine. This results in less air in the cylinder available for combustion, giving concerns for thermal overloading of the diesel engine as explained in Section 3.6.4.

2.1.3. Series turbocharging

Further increase in specific power and efficiency of the single stage turbocharged engine can be achieved by adding an extra turbocharger in series with the initial turbocharger. The goal of series turbocharging is to increase the charge air pressure even more to achieve higher specific power and an higher efficiency. The stages of series turbochargers can either operate as one system or as separate systems. If individual chargers can be phased in or phased out, the system is classified as a combination of series and sequential turbocharging. Similar to parallel-sequential turbocharging, phasing in and out of the different chargers is an important aspect of combined series and sequential turbocharging.

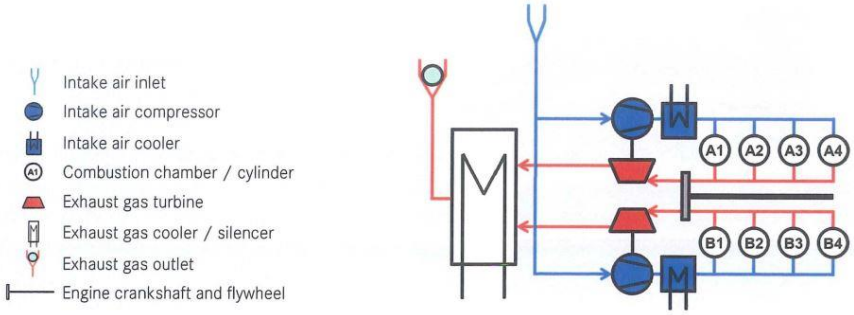

Figure 7: Air flow in an engine with a single stage turbocharger [53]

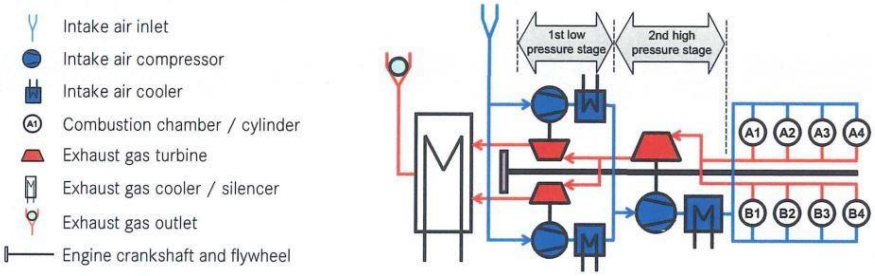

Figure 8: Air flow with two-stage turbocharging [53]

In general, according to [18], series turbocharging has several advantages compared to single stage turbocharging:

- Due to multiple stage compression, a higher charge air pressure can be realised, increasing the mean effective pressure values of the engine. Charge air pressure can be increased until peak pressure limits of the engine are reached.
- An improved charging efficiency, even at unchanged charge pressure, since the efficiencies of the compressor and turbine increase with a lower pressure ratio in a single stage as confirmed by Galindo et al. [10]. Additionally, the total efficiency can be further increased with an intercooler between the two compressors to cool the charge air between the compressor stages.
- Wider compressor and turbine maps enhance the opportunities to optimize the charge unit to the engine operating range.
- Due to higher charge air pressure the Miller process during valve overlap improves, reducing the charge air temperature by means of in cylinder expansion of the charge air, ultimately leading to efficiency improvements [6].
- The increase of indicated mean effective pressure of the gas exchange process can be as high as 6 percent of the total mean effective pressure, improving the efficiency of the engine [6].

Nevertheless the disadvantages of the system are significant:

- As seen in Figure 4 acceleration behaviour of the series turbocharger is usually worse in comparison with a single charger, since two rotors have to be accelerated with the same exhaust gas energy [18]. This could be solved by sequentially engaging the different charge stages, although this increases the complexity of the system even more.

- The second charger requires a larger installation space and imposes a significant weight increase of the system.
- Increased thermal inertia of the exhaust system, which can be a challenge for exhaust gas after treatment systems due to heatloss and temperature control[18].

2.1.4. Parallel-sequential turbocharging

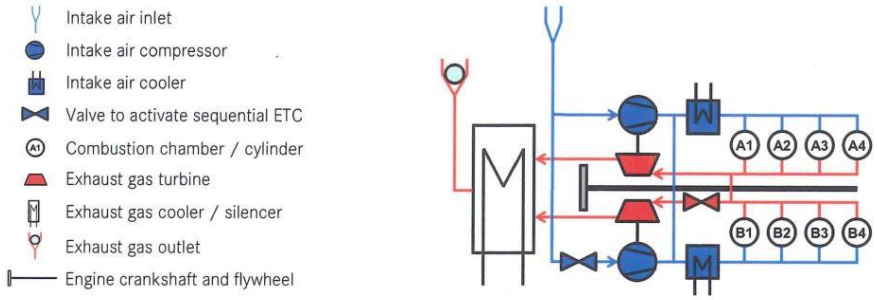

Figure 9: Air flow with sequential turbochariging [53]

The goal of sequential turbocharging is to have a stable charge air pressure at different engine speeds. Supplied with a more constant boost pressure, the operating envelope of the engine can be widened as seen in Figure 4. A single turbocharger design is always a trade off between good transient response, compressor efficiency, turbine efficiency, and operation range. This trade off can be avoided by switching multiple turbochargers in parallel. During low flow rate the smallest turbocharger is operated, as soon as the turbocharger starts to get choked the second charger is phased in. The amount of chargers in a system is theoretically unbounded, and although systems with five chargers are known [24] systems with two chargers are more common aboard ships.

Parallel-sequential turbocharging offers several advantages as dicussed in Zhang et al. [56]:

- The turbochargers can have an operating envelope at which compressor efficiency and turbine efficiency is high.
- By changing the switching strategy the performance of the turbochargers can be optimized for different purposes e.g. quick acceleration of the engine by a delayed switch to more turbochargers, high efficiency by switching for optimal charger efficiency.
- Transient response will be improved given that with an increasing number of chargers the size of the chargers, and thus the inertia, will decrease.
- The engine operation envelope will be widened as seen in Figure 4.

The disadvantages of the system are minor and mainly caused by the increase in complexity of the system:

- Increase in technical complexity and amount of parts.
- Implement complex control strategies to prevent oscillatory behaviour of the turbochargers.
- If unequal sized chargers are used to optimize for acceleration or partload performance, the maximum boost level is limited by the smallest charger [56].

During operation the different turbocharger units are phased in and out depending on the operating state of the engine. Phasing in and out of the different turbocharger units is an important aspect of sequential turbocharging. As stated above much effort is required in creating a controller which determines the point at which a charger is phased in or out.

2.1.5. Hybrid turbocharging

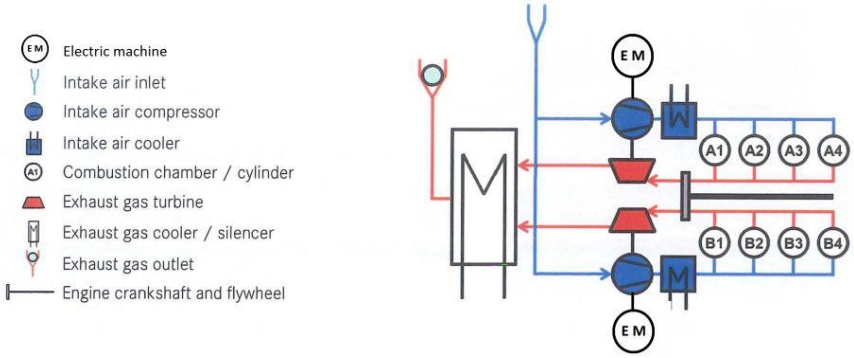

Figure 10: Air flow with hybrid turbocharging [53]

Hybrid turbochargers consist of a conventional turbocharger with an electric machine connected to the main shaft as seen in Figure 11. The electric machine can both work in generator mode, subtracting power from the turbocharger or in motor mode, adding power to the turbocharger. The concept resembles a single charger and a super charger in one concept. The goal of hybrid turbocharging is similar to that of sequential turbocharging: improving efficiency and supplying constant charge pressure to the engine independent of the engine operating point.

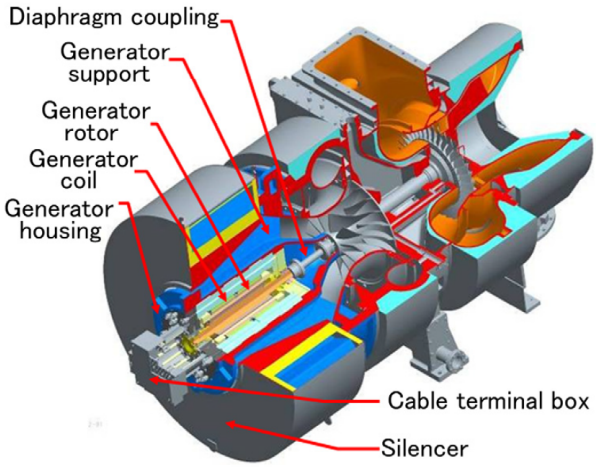

Figure 11: Cut away view of a hybrid turbocharger [41]

Hybrid turbocharging offerings the following advantages:

- Increase in charge air pressure over the complete operating envelope of the engine.
- Inertia characteristics of the turbocharger can be reduced significantly by power input the electric machine. However, the inertia of the system increases as a result of the inertia added by the electric machine.
- Electrically controlling the speed of the turbocharger gives more flexibility in the matching. Therefore, the matching of the turbocharger can be optimized more, for example for efficiency at the nominal operating point or for acceleration performance.

The disadvantages are mainly due to the electrification of the system:

- Costly due to a high speed (10.000+ rpm) electrical machine.
- A bi directional converter has to be installed in order to add and subtract power from the turbocharger. These are expensive, and take space and weight.

Hybrid turbocharging in marine applications is quite novel today. Extensive research has been done by Mitsubishi heavy industries [19][20][25][41]. Shiraishi et al. [25] studied the energy savings which can be achieved through electric-assist turbocharging on marine diesel engines not only in models [19] but also in a test set-up. The modelling has been performed with an in-house code [19] of Mitsubishi heavy industries, which made it impossible to investigate the modelling strategies. However, information with respect to test set-up is available. A 660 kilowatt four stroke engine from Akasaka Diesels limited was used to perform the verification test. The result are shown in Table 1 and show a considerable improvement on fuel consumption. Shiraishi et al. also compared the particulate concentration in the exhaust gases at start up of the engine with and without electrical assistance of the turbocharger. The results are shown in Figure 12. However, the graphs are not quantified which makes it difficult to draw conclusions. The particulate concentration in the exhaust gases of the engine with electrical assisted turbocharger shows a lower peak value, but the area under the graphs suggest the emission is almost the same. Furthermore, it is remarkable that after t=45 seconds the particulate concentration looks higher with electrical assisted turbocharger. It is suspected that the scale of the graphs is not equal, although the lines suggest otherwise. Shiraishi et al. concluded that the hybrid turbocharger was able to reduce fuel oil consumption and black smoke emission at start-up. Unfortunately, this can not be checked.

	Assist electric power (Output ratio to engine [%])	Turbocharger speed (rpm)	Boost pressure (bar)	Fuel reduction (%)	Net fuel reduction (%)
25% Load (184 kW)	0 kW	14611	0.2	-	-
	1.3 kW (0.70%)	16000	0.25	2.7	2
	5.3 kW(2.90%)	18000	0.32	5.7	2.8
38% Load (258 kW)	0 kW	19240	0.37	-	-
	3.5 kW (1.40%)	21000	0.45	4.1	2.7
	5.9 kW (2.30%)	21810	0.49	4.2	1.9

Table 1: Change in fuel consumption ratio with hybrid turbocharger [25]

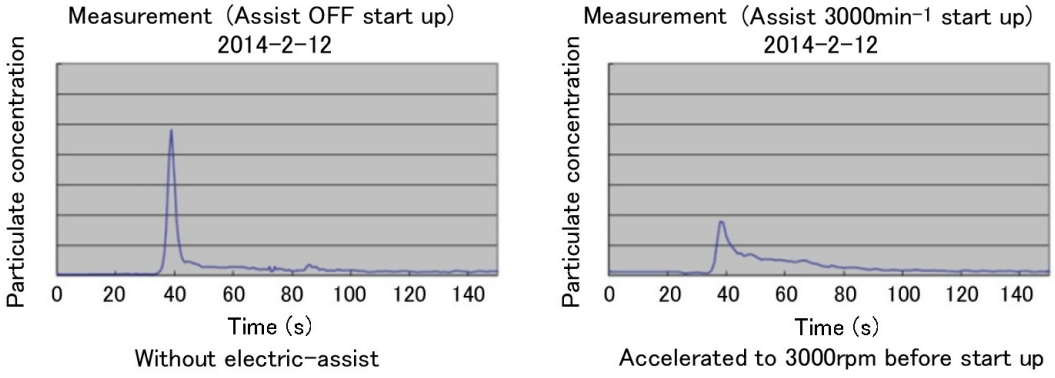

Figure 12: Particulate concentration in exhaust gas with and without electrically assisted turbocharging [25]

2.1.6. Variable turbine geometry

The matching of a turbine to the engine and compressor is always a trade-off. At low engine speeds only a low mass flow is entering the turbine, requiring a small effective turbine area in order to produce the work required by the compressor. The effective area is usually larger, causing the so called 'turbo lag'. However, for high-speed engine operating points, a turbine with a larger effective area is required to cope with the large mass flow from the engine in order to avoid choke. A variable turbine geometry (VTG) is applied in order to widen the operating

envelope of the turbine. By implementing a variable turbine geometry the conditions for flow entry into the turbine can be varied as seen in Figure 13. By varying the effective flow area the turbocharger is able to achieve high boost pressure at low engine speeds, improving the dynamic behaviour of the engine. At high engine power, the high volume flows can be achieved with comparatively good turbine efficiency.

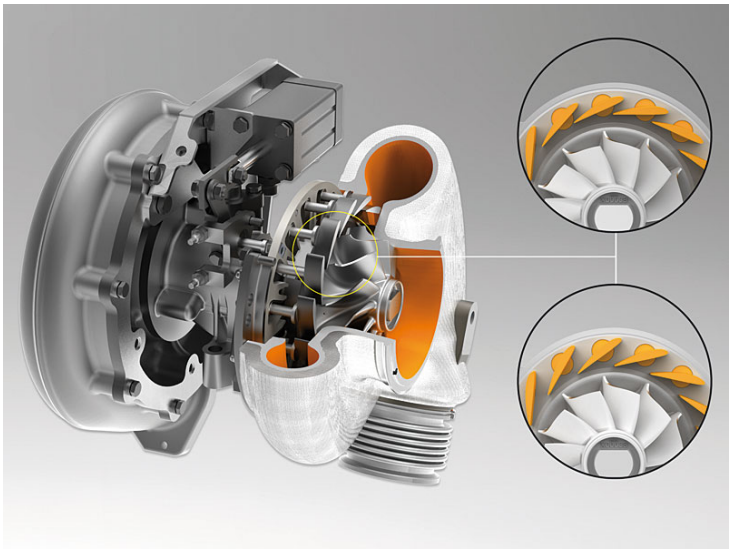

Figure 13: Turbocharger with a variable geometrie [24]

Variable turbine geometry offers the following advantages:

- By varying the effective flow area the dynamic behaviour of the engine can be improved.
- Improving the efficiency of the turbine in off design conditions.
- System size and piping on the engine does not increase.

The disadvantages are mainly due to the increased complexity of the turbine system:

- Since the system consist of a lot of moving parts, the system is difficult to manufacture in comparison with normal turbines.
- Variable geometry mechanism can cause reliability challenges, the system is much more sensitive for fouling due to particular matter in the exhaust gases.
- A control system that can deal with non linearities is necessary in order to use the systems potential.

2.1.7. Waste gate, Bypass and Blow off valves

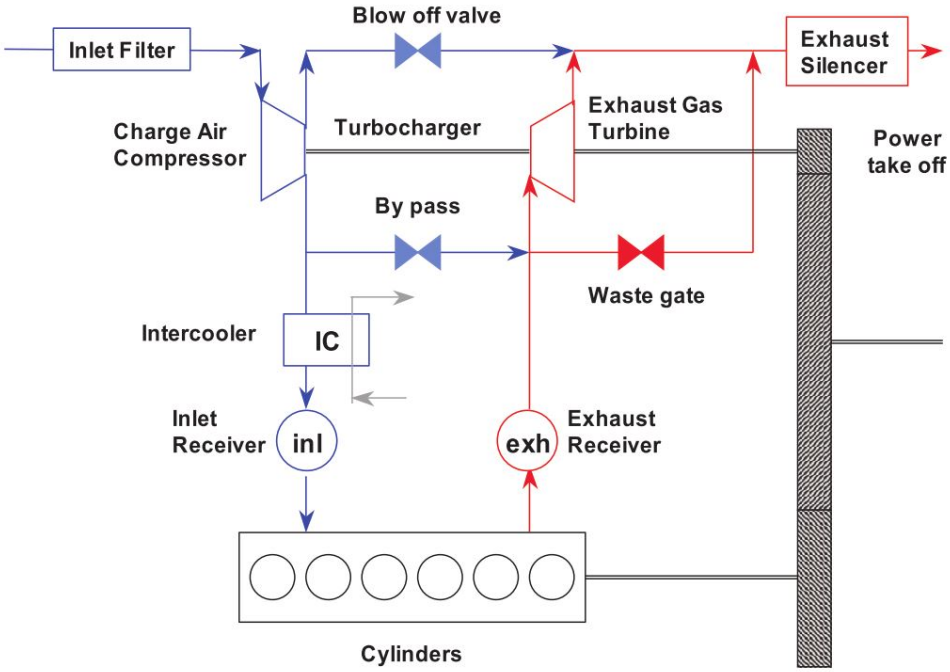

Figure 14: Air flow with wastegate turbocharging [46]

As mentioned earlier and stated by Jensen et al. [21] the trade-off in turbocharger matching is for either an optimum efficiency at full load or good transient performance. A waste gate is applied to match the engine with a smaller turbocharger then required for full load conditions, improving transient and low load performance. In order to avoid over speed or maximum pressure of the engine, a waste gate is opened at higher loads to blow off some of the exhaust gasses without going through the turbine. A waste gate is simple and cost effective. Therefore, it is widely used in marine applications. However, the cost of the better performance in transient and low load operations, is that at full load: charge pressure will drop in comparison with a full load matched charger.

A bypass valve is used in the opposite way, and often in combination with a sequential turbocharging layout. After switching from one to two turbochargers, exhaust gas pressure is sometimes too low to drive the turbocharger. Therefore, flow from the compressor is lead directly into the turbine bypassing the engine as depicted in Figure 14. Therefore, the pressure in the inlet receiver drops moving the compressor away from the surge line.

2.1.8. Multiple turbo

Especially in marine applications engines with more than one turbocharger are common. In the automotive industry these configurations are sometimes called as Bi or Twin turbocharging, referring to the amount (two) of turbochargers. In Figure 7, where the configuration was classified as a single charged concept, two chargers are installed, each feeding its own bank of cylinders. Effectively each bank of cylinders has his own charger. Hence, this could also be classified as a Bi turbocharged engine. However, in marine applications this is usually not done because engines often have more than one turbocharger. The advantage of applying multiple chargers instead of one large charger is that the inertia of the smaller chargers is much lower. Therefore, increasing the dynamic performance of the engine.

2.1.9. Turbo-compounding

In turbo-compounding, the goal is to extract more power from the exhaust gas flow. This power is fed back to the main shaft. Turbo-compounding can be done electrically or mechanically, on the initial turbocharger or via an extra power turbine. As explained by Aghaali et al. [3] various configurations are possible. If even more effort is done to recover energy, rankine cycles can be installed in order to gain the last left over energy from the exhaust flow, however this falls under the category waste heat recovery. An extenive overview of wast heat recovery technologies can be found in [44],[43].

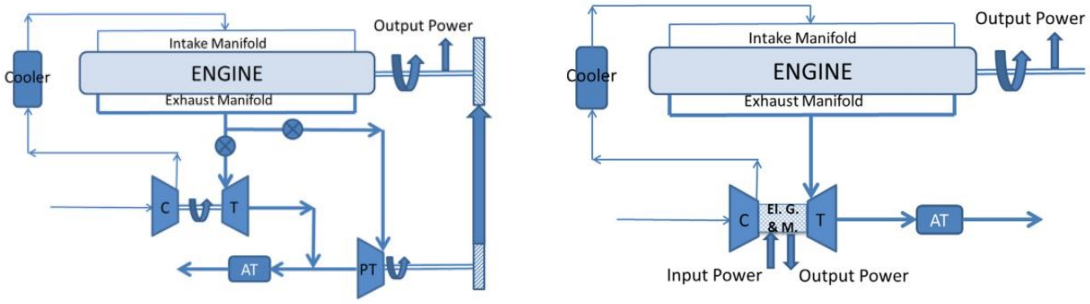

(a) Mechanical turbo-compounding (b) Electric turbo-compounding

Figure 15: Examples of turbo-compounding [3]

2.2. Classification of charge air configurations

The classification of charge air configurations is not straightforward. Part of the confusion is caused by manufacturers, especially in the automotive branch where fancy names as 'Bi turbo' are introduced in order to boost sales. However, it does not help that some systems are so complicated that a system classification is difficult, or maybe to complicated to use. A good example is the MTU 1163 as seen in Figure 16 which is equipped with five turbocharger groups which can be engaged sequentially, each consisting of 2 turbochargers in series. MTU calls this two-stage sequential turbocharging, but this could also be explained as a two-stage charger, which sequentially uses the first and the second stage. It al comes down to the fact that different configurations can be used combined as stated by Stapersma [46].

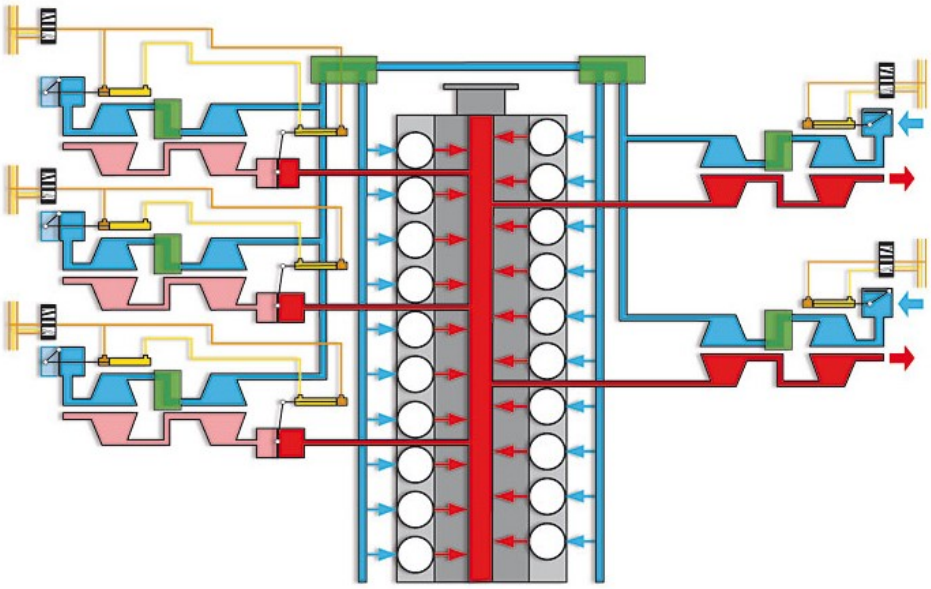

Figure 16: MTU 1163 engine equipped with 2-series,5-parallel,sequential turbocharging [24]

In order to avoid confusion about the turbocharger configuration a straightforward classification would be helpful. When classifying turbocharging concepts, as in many other engineering subjects, the resemblance with an electric circuit can be made. This thesis proposes a sort of mechanical-electrical analogy, although not so extensive. The aim of the classification is that its simple, unambiguous and also clear for people who are not familiar with the classification.

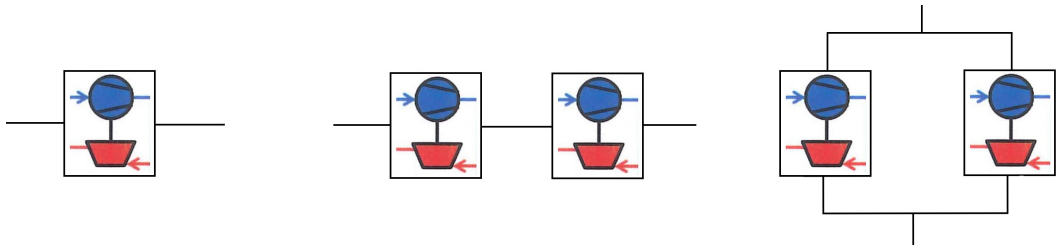

(a) Single turbocharging (b) Series turbocharging (c) Parallel turbocharging

Figure 17: Different turbocharger configurations

First the position of the chargers with respect to the other chargers in the system is determined, in principle this can be a *single*, *series* or *parallel* configuration. Then, in order to indicate the number of chargers a prefix is added. For example, if two chargers are connected in series the configuration is called: two-series turbocharging, now often indicated as two-stage turbocharging. Further for each type of configuration an additional series of *number-configuration-technologie* is added to the name of the complete charger configuration. In order to indicate whether the chargers are switched sequential, are supported by an electric motor or fitted with variable turbine geometries a suffix is added. Although the suffixes as proposed here are limited to *sequential*, *VTG* and *hybrid* other suffixes are possible. If a turbocharger is fitted with more then one additional technology all are mentioned in the name.

Summarized in formula form:

$$\underbrace{number}_{1,2,3..} - \underbrace{configuration}_{single,\ series,\ parallel} - \underbrace{technology}_{sequential,\ hybrid,\ VTG} \tag{2.1}$$

For example, the MTU 1163 as seen in Figure 16 will be classified as a: 2-series - 5-parallel-sequential turbocharging configuration.

Two important parts of a turbocharger configuration are excluded from classification: the addition of blow off valves, by passes and waste gates is not included. Because numerous different configurations of valves and bypasses can be made, including them in the classification would make it too complex. Furthermore, the size of the chargers is not included despite the fact that especially dynamic performance is very sensitive to turbocharger size.

2.3. Conclusion

After analysing the charger concepts described above the motivations to install a specific configuration are clear. Series, parallel-sequential and hybrid turbocharge concepts offer better performance in terms of charge pressure at part load and pressure ratio in comparison to non or single turbocharged diesel engines. Therefore, Series, parallel-sequential and hybrid turbocharge concepts allow for better control of the air excess ratio. The air excess ratio influences the efficiency, thermal loading and emissions of the diesel engine [45].

For fast naval combatants a wide operating envelope of the engine is very important to be able to carry out a big variety of tasks under any conditions. This can be supported by an example of an operational profile of a fast naval combatant as shown in Appendix A.1. From the various charge air configurations series turbocharging mainly aims to increase the charge pressure.

Parallel-sequential turbocharging and hybrid turbocharging will presumably widen the operating envelope of the diesel engine considerably. The hybrid turbocharger will have the advantage that it can rely on an external energy source to boost the turbocharger, probably achieving the best results when accelerating. The downside of this charger is that more equipment aboard is necessary, and space aboard ships is limited. The parallel-sequential turbocharger has to rely solely on energy in the exhaust therefore performing slightly worse with respect to lag in comparison with the hybrid turbocharger. For both systems it can also be seen that the complexity of the charge systems increases quite severely in comparison to single charged engines and supercharged engines. This requires the use of complex control systems to operate the systems and raises questions about reliability issues. Nevertheless the advantages of parallel sequential and hybrid turbocharging look promising. Especially the improved charge air pressure at part load can result in a better efficiency, less emissions, a wider operating envelope and improved acceleration performance. Therefore, Parallel-sequential turbocharging and hybrid turbocharging are investigated further.

3

Simulation

In this section a simple Mean Value First Principle (MVFP) diesel engine model is investigated. The model is under continuous development at the department of marine engineering of the TU Delft. Two versions of the simple diesel model will be investigated. First, a model in which the turbocharger is modelled as a power balance as seen in Figure 23 is investigated. This model is commonly known as the Diesel-A model at the TU Delft. Second, a model in which the turbocharger is modelled by means of the equations of motion as seen in Figure 24 is investigated. Both models will be explained and compared after which an advice regarding the application is given.

3.1. Modelling approach

In order to investigate the effect of different turbocharger configurations on the measures of effectiveness of a ship, a simulation model is required. The choice of model is not evident since complexity, accuracy, and computational time have to be considered.

To approach the modelling in a structured way, the methods of Vrijdag et al. [54] were used. They propose a systematic approach towards the modelling, verification, calibration and validation of a ship propulsion simulation. The approach is depicted in Figure 18.

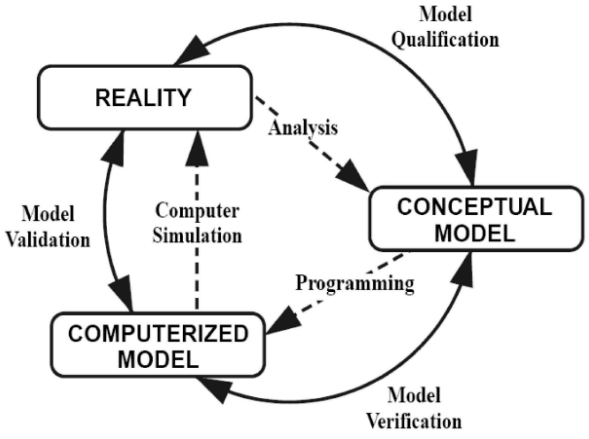

Figure 18: Development cycle of a simulation model as proposed by Vrijdag et al. [54]

The qualification will be discussed in Section 3.2, in which the model choices are explained. The Verification and Calibration will be discussed in Section 4.11.2 in which the results of two different models are compared. Finally, the validation based on a measurement campaign at sea will be discussed in Section 5.3.1.

3.2. Qualification

Vrijdag et al. [54] defines qualification as the determination of adequacy of the conceptual model to provide an acceptable level of agreement for the domain of the intended application.

Therefore, the simulation goals should determine the derivation of the conceptual model from reality. Although this seems straightforward, according to Vrijdag et al. [54] modellers are often tempted to use legacy codes that were developed earlier, sometimes by others, with other goals in

mind, which can easily lead to non-adequate computer codes. At the TU Delft various propulsion models have been developed for example by: Vollbrandt [52], Kalikatzarakis [22], Schulten [40], and Geertsma et al.[11]. An example of a propulsion model is depicted in Figure 19.

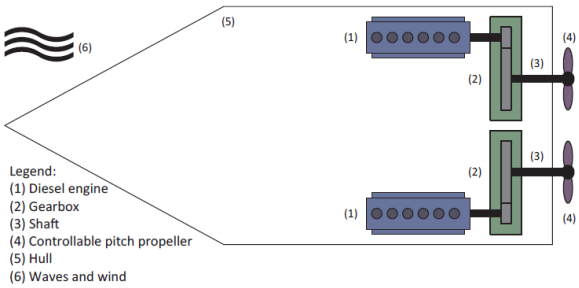

(a) Typical mechanical propulsion system layout for a naval vessel.

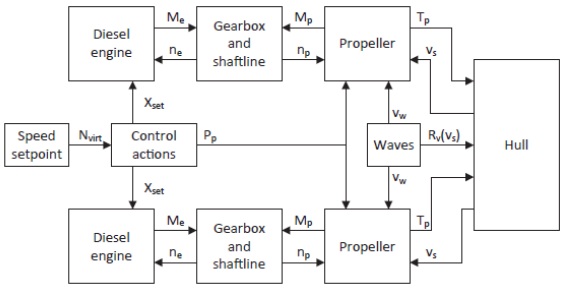

(b) Schematic presentation of the model of a mechanical propulsion system

Figure 19: Propulsion model as proposed by Geertsma et al. [11]

The model choice in this case, has to correspond with the goal of this research. Which is the main question as proposed in Section 1.

- Can the efficiency and performance of diesel hybrid configurations aboard fast naval combatants be improved by applying advanced charge air configurations?
- Is it possible to model advanced charge air configurations by means of a simple mean value diesel engine model?

The aim of this research focusses on the dynamic performance of the diesel engine and the effect of various charge air configurations on the performance of the diesel engine. Ultimately, the performance of the diesel engine affects the performance of the ship. The correlation between the diesel engine and the ship's performance was not investigated deeply. In this thesis we decided to only model the diesel engine and the charge air configurations extensively. The other components as depicted in Figure 19a were not incorporated.

Requirements:

- Create a model containing the following sub-models: engine, turbocharger.
- Accuracy of the turbocharger model should be such that the effect of advanced turbocharger configurations can be investigated.
- The turbocharger model has to be able to perform power take off and power take in.
- Accuracy of the diesel engine model should be such that thermal overloading limits of the diesel engine can be checked.

Selecting the right modelling method is always a trade off between accuracy and computational power, therefore different models have been developed. According to Loonstijn [31] models for simulating engine performance can be divided in two categories: empirical models which use mathematical expression to describe the processes related to engine performance and analytical models which use expressions that are derived from physical processes. Schulten et al. [39] remarks that at deeper level of analytical models some empirical modelling is inevitable and therefore every diesel model is a combination of analytical and empirical modelling.

In order to select the right engine model the trade off between accuracy and computational power as well as complexity for the user has to be considered. The most convinient way to do this is to determine the amount of physical aspects of the models. Geertsma et al. [12] categorised diesel engine models according to the level of dynamics and physical detail.

This work consists of a comparative study of the effects of different charge air configurations on the diesel engine performance. Therefore, an accurate prediction of the fuel consumption, charge air pressure and temperatures of the engine are required. Geertsma et al. [12] used a MVFP diesel engine model to investigate the performance of a single charged diesel engine. Validation showed that the MVFP diesel engine used by Geertsma et al. was able to predict fuel consumption, charge air pressure and temperature of a single charged diesel engine within ±5% accuracy. For comparative studies into propulsion concepts, this is satisfactory. As already revealed in the research questions, it would be valuable to see if this approach can also be adapted for more advanced charge air configurations. In MVFP modelling the engine is constructed by coupling different engine processes as sub models. This results in a model which is not computational intensive. Also, the model can usually be calibrated with data form the Factory Acceptance Test (FAT) of the engine and the project guide. A schematic overview of the model is depicted in Figure 20. The model consists of an engine model including a turbocharger model.

3.3. Overall model

As depicted in Figure 20 the overall model can be divided in two main components: the engine which will be discussed in this section and the turbocharger which will be discussed in Section 4.

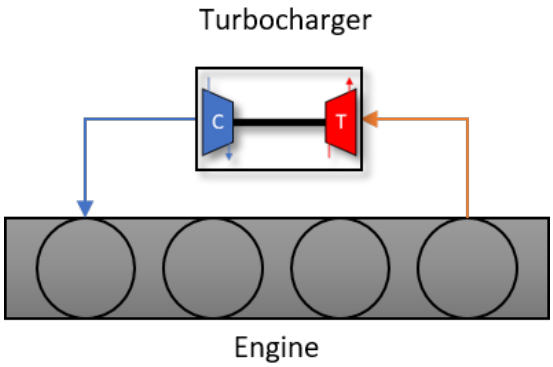

Figure 20: Overview of the overall model

Schulten et al. [39] proposed to model the various engine components as control volumes which can either resemble a volume or a resistance, as seen in Figure 21. The volume element acts as an integrator resolving the in and outflow to determine the state of the volume. The resistance element resolves the mass flow as a function of pressure difference over the element by means of the momentum equation.

The coupled elements form an electrical RC-type of network as seen in Figure 22. If advanced turbocharging strategies are investigated, the most important blocks are: compressor, inlet receiver, cylinder, outlet receiver, and turbine. These blocks directly influence the turbocharger since they form the connection of the gas flow from compressor to turbine.

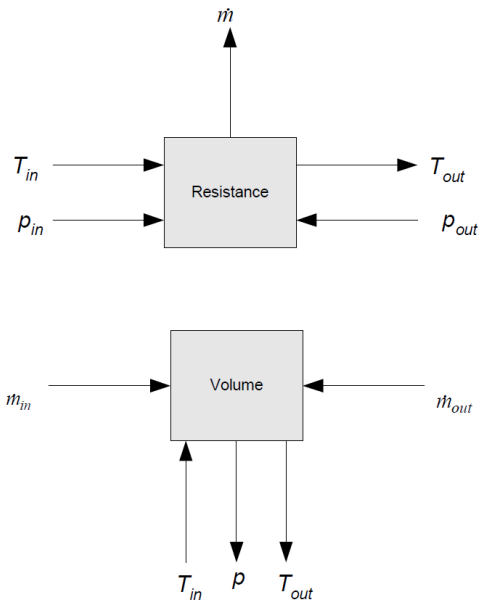

Figure 21: Volume and Resistance element [39]

These two basic elements have the following functions:

- Resistance element: Calculate the mass flow through the element as a function of the pressure difference over the element.
- Volume element: Calculate the internal state properties of the element as a function of the mass and energy leaving and entering the element.

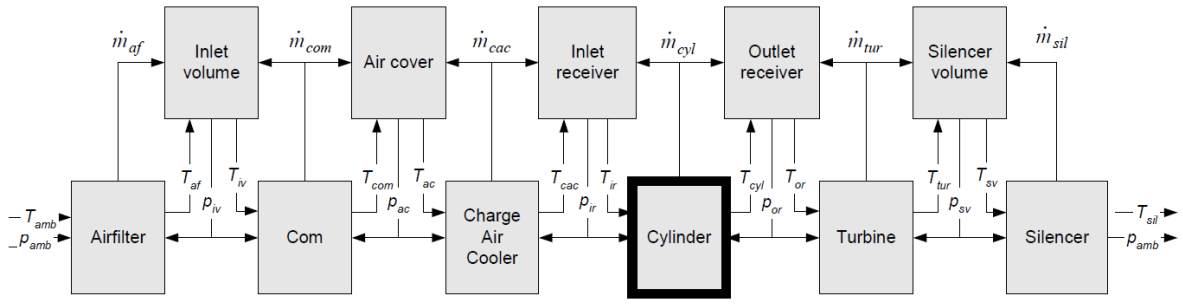

Figure 22: Volume and Resistance network [39]

3.4. Mean value first principle diesel model

The model as proposed by Geertsma et al. [12] was further improved by Loonstijn [34] who added a more detailed gas exchange. The model consists of four submodels: A compressor (COM) which also functions as an inlet receiver, a cylinder (CYL) sub model, an outlet receiver (OR) and a turbine (TUR) as depicted in Figure 23.

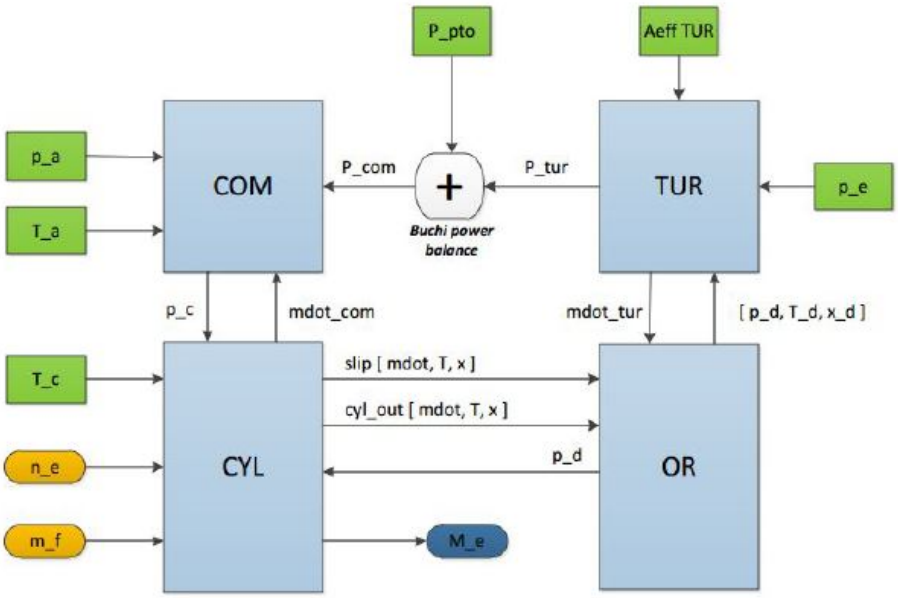

Figure 23: A schematic representation of a simple MVFP diesel engine model with a power based turbocharger [34]

In order to meet the specifications as described in the Section 3.2 about qualification, various modifications were added to the model proposed by Loonstijn [34]. The modifications to the turbocharger model, which includes the COM, TUR and power balance block are discussed in Section 4.

The initial approach to model the hybrid turbocharger included an electrical machine and a controller. In order to couple the electric machine to the turbocharger, a more physical model based on the equations of motion was proposed. However, due to the model structure of the model as proposed by Loonstijn [34] it was not possible to implement a motion based turbocharger.

Therefore, instead we chose to use a more structered modelling approach. The modular hierachical and causal modelling pradigm as proposed by Colonna et al. [7] provides a solid basis to a more structured model. The equations implemented in the modules follow from physical relations and conservation laws in the lumped parameter form. Bilateral coupling in combination with the causality principle are applied to obtain a solving system of algebraic and differential equations characterized by a low index [7].

In order to comply with the model paradigm an inlet receiver was added to the model. The model structure of the modified model is depicted in Figure 24.

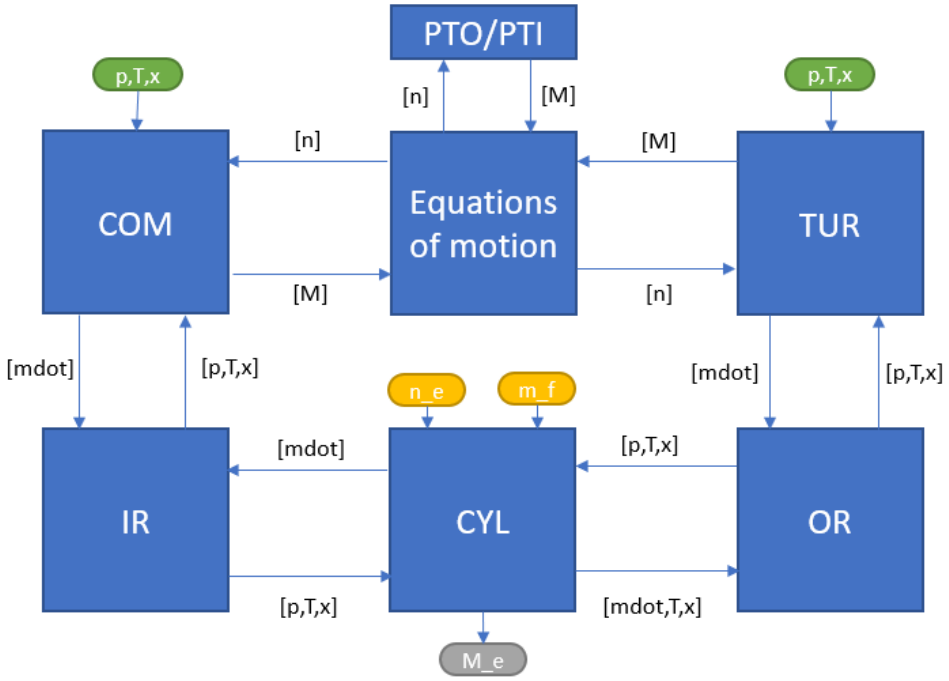

Figure 24: A schematic representation of a simple diesel model with an equation of motion based turbocharger

In the following sections, the inlet receiver, cylinder and outlet receiver sub model will be briefly discussed. The compressor, turbine and equations of motion model will be discussed in Section 2.

3.5. Inlet receiver

The inlet receiver form the connection between the compressor and the cylinder inlet. Therefore, the inlet receiver is based on two mass flows. Mass flow enters from the compressor and leaves to the cylinder. Conservation of mass applies and therefore it is possible to construct a mass balance:

$$\dot{m}_{IR} = \dot{m}_{in} - \dot{m}_{out} \tag{3.1}$$

where $\dot{m}_{in}$ and $\dot{m}_{out}$ are the mass flows in [kg/s] entering and leaving the inlet receiver.

$$m_{IR} = \int \dot{m}_{IR} \cdot dt \tag{3.2}$$

It is assumed only pure air is coming from the compressor and it can be treated as a perfect gas. Further, heat pickup from the inlet receiver wall is neglected. Then the first law of thermodynamics for an open system is introduced (3.3).

$$\begin{aligned} \frac{d}{dt} E_{cv} = \dot{Q} - \dot{W}_{cv} + \sum_{i}^{\#inlet} \dot{m}_i \cdot \left[h_i + \frac{v_i^2}{2} + g z_i \right] \\ - \sum_{j}^{\#outlet} \dot{m}_j \cdot \left[h_j + \frac{v_j^2}{2} + g z_j \right] \end{aligned} \tag{3.3}$$

Where E_{cv} is the energy in the control volume [kJ], $\dot{Q}$ is the heat flow in [kJ/s], $\dot{W}_{cv}$ is the work performed by the control volume [kJ/s], h is the enthalpy per unit mass [kJ/kg].

Finally, the actual pressure and temperature of the inlet receiver can be calculated by applying the ideal gas law and the calculated values for the mass in the inlet receiver:

$$T_{IR} = \int dT_{IR} \cdot dt \tag{3.4}$$

$$p_{IR} = \frac{\dot{m}_{IR} \cdot R_{air} \cdot T_{IR}}{V_{IR}} \tag{3.5}$$

Where p is the pressure in the inlet receiver in [Pa], R_{air} is the universal gas constant $= 8,31446 JK^{-1}mol^{-1}$. T is the temperature in the inlet receiver in [K] and V the volume of the inlet receiver.

3.6. Cylinder model

The cylinder model consists of the cylinder process and the gas exchange as depicted in Figure 25. The cylinder process is represented by a six point seiliger cycle and is modelled in the seiliger sub model. As in the inlet receiver, the gas is treated as a perfect gas with a homogeneous composition. The Gas exchange is modelled in the air swallow, gas disposal and Zinner blow down sub model. A schematic overview of the cylinder model is depicted in Figure 26.

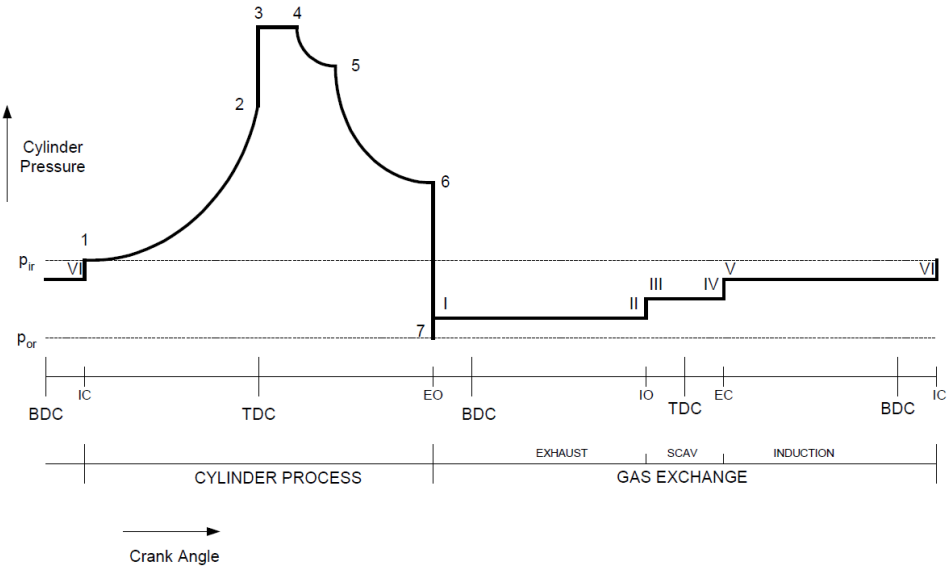

Figure 25: Diesel process as proposed by Schulten et al. [39]

- **Polytropic compression** 1 - 2: Air is compressed in the cylinder, at the end of the compression stroke fuel is injected and combustion starts.
- **Isochoric combustion** 2 - 3: The second stage of the seiliger cycle consists of isochoric combustion, since there is no volume change performed work is zero by definition.
- **Isobaric combustion** 3 - 4: The third stage of the seiliger cycle consist of isobaric combustion, work is performed and it is assumed that the pressure is constant.
- **Isothermal combustion** 4 - 5: The fourth stage of the seiliger cycle consist of isothermal combustion, work is performed and it is assumed that temperature is constant.
- **Polytropic expansion** 5 - 6: The sixth stage of the seiliger cycle constist of Polyctropic expansion,
- **Blowdown** 6 - 7: The exhaust valve opens, the gasses in the cylinder blow down because the pressure in the cylinder (p_6) is higher than the pressure in the outlet receiver (p_{or}). Some gases remain in the cylinder and continue their expansion.
- **Exhaust** I - II: The piston moves up and forces most of the exhaust gases out.
- **Scavenging** III - IV: The open connection (valve overlap) and the pressure difference between inlet and outlet receiver, initiates the flow of scavenge gases through the cylinder.
- **Induction** V - VI: Fresh air is drawn into the cylinder by the downward movement of the piston.

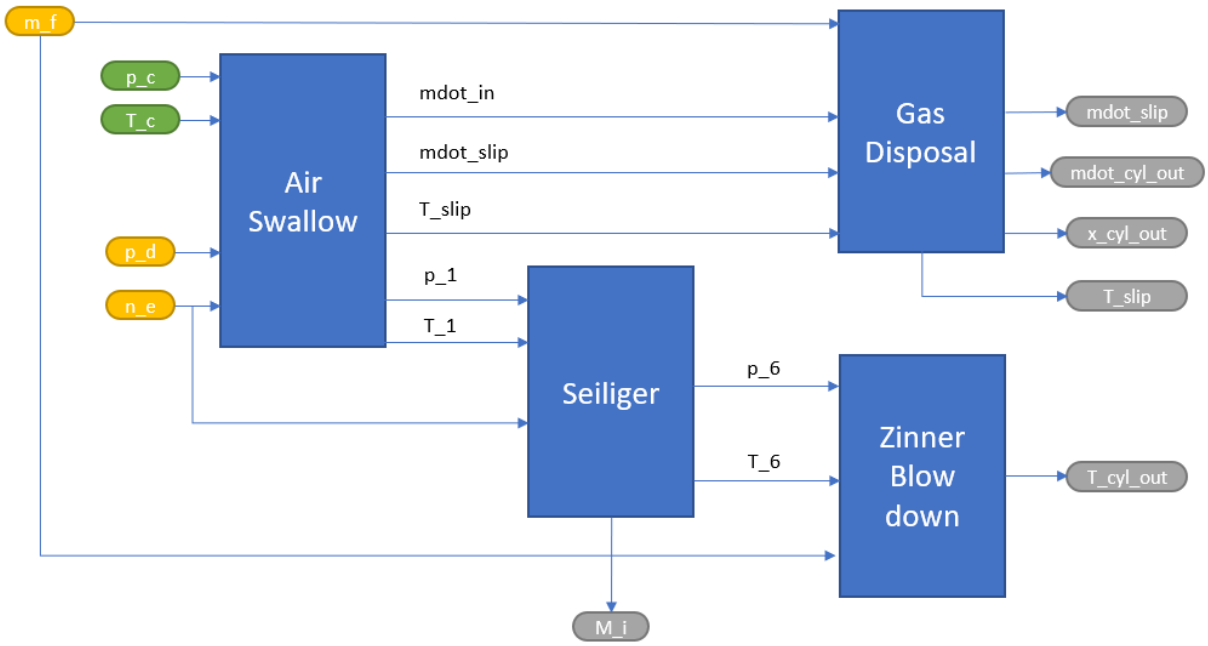

Figure 26: Schematic overview of the cylinder model

3.6.1. Air swallow

The air swallow sub model determines the mass flow of fresh air which goes into the cylinder. The air swallow sub model will be discussed according to the work of Loonstijn [34] with the theoretical background from Stapersma [45],[46].

Table 2: Inputs and Outputs of the air swallow sub model

Airswallow			
Inputs:		*Outputs:*	
T_c	Charge temperature [K]	$\dot{m}_{in}$	Total mass flow into engine [kg/s]
p_c	Charge pressure [Pa]	$\dot{m}_{slip}$	Slip mass flow [kg/s]
p_d	Outlet receiver pressure [Pa]	T_{slip}	Slip mass flow temperature [K]
n_e	Engine speed [hz]	p_1	Trapped pressure [Pa]
		T_1	Trapped temperature [K]

The total mass flow into the engine consist of the induction mass flow and the scavenge mass flow.

$$\dot{m}_{in} = \dot{m}_{ind} + \dot{m}_{sc} \tag{3.6}$$

Where $\dot{m}_{ind}$ is the induction mass flow [kg/s] and $\dot{m}_{sc}$ is the scavange massflow in [kg/s]. For a turbocharged engine, according to Stapersma [46] [6.52] the induction mass can be calculated using the ideal gas law.

$$\dot{m}_{ind} = \frac{p_c \cdot (V_{IC} - V_{EC})}{R_{air} \cdot T_{ind}} \tag{3.7}$$

Where p_c is the pressure in the inlet receiver, V_{IC} the cylinder volume [m^3] at inlet valve closure, V_{EC} the volume [m^3] of the cylinder at exhaust valve closure and T_{ind} the induction temperature in [K]. To find the induction mass flow for the entire engine, the induction flow per cylinder is multiplied by the firing frequency.

$$\dot{m}_{ind} = m_{ind} \cdot \left(\frac{i \cdot n_{eng}}{k} \right) \tag{3.8}$$

Where i is the number of cylinders in the engine, k the number of revolutions per cycle, and n_{eng} the engine speed in [Hz].

The mass flow into the cylinder passes the cylinder inlet port and valve and therefore the temperature of the gas increases. The indcution temperature was calculted as follows [46] [6.30]

$$T_{ind} = T_c + \epsilon_{INL} \cdot (T_{INL} - T_c) \tag{3.9}$$

Where T_c is the intlet receiver temperature [K], ϵ_{INL} the heat exchange effectiveness [-] and T_{INL} the temperature of the inlet port in [K].

In order to calculate the scavenge mass flow, the nozzle equation as explained by Stapersma [46] [6.120] was used.

$$\dot{m}_{sc} = i \cdot A_{sc,eff} \cdot \left(\frac{p_c}{\sqrt{R_c \cdot T_c}} \right) \cdot \Psi(\pi_{sc}) \tag{3.10}$$

Where Ψ is the non dimensional flow coefficient and $A_{sc,eff}$ the effective scavenge area of the cylinder in $[m^2]$.

The non dimensional flow coefficient Ψ can be calculated for choking and non-chocking conditions:

$$\Psi(\pi_{sc}) = \sqrt{1 - \frac{1}{\pi_{sc}}} \quad for: \quad \pi_{sc} < 2 \tag{3.11}$$

Where π_{sc} is the pressure ratio over the cylinder during scavenging

$$\Psi(\pi_{sc}) = \sqrt{1 - \frac{1}{\pi_{sc}}} \quad for: \quad \pi_{sc} \geq 2 \tag{3.12}$$

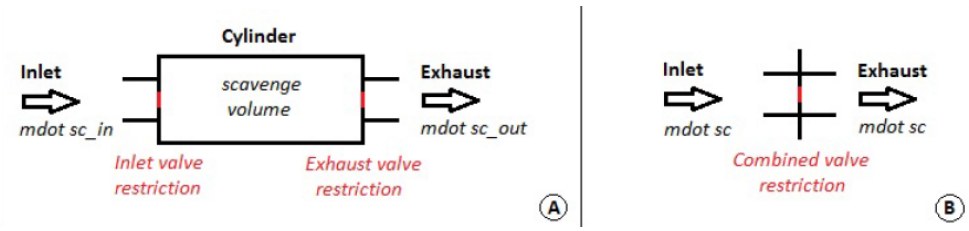

Figure 27: a) Filling and emptying model. b) nozzle equation model [32]

In the model of the scavange flow, some important simplifications were made as explained by Loonstijn [32]. First the scavenge efficiency was constant and second the trapped scavenge temperature was equal to the induction temperature. Also, the scavenge volume was not represented by a volume element based on the first law of thermodynamic, but as a combination of two flow restrictions as seen in Figure 27. These simplifications are discussed by Stapersma [46] [6.3] and result in Equation (3.10).

In [32] Loonstijn proposes to expand the scavenge model in order to make this specific diesel model suitable for the modelling for two stroke engines, where scavenging plays an important role. However, since it was expected that the improvements for a four stroke engine are limited the implementation was not investigated here.

The induction mass flow and the scavenge mass flow determine the total mass flow for the engine and can be calculated according to Equation (3.6).

The trapped mass can be calculated with Equation 3.13 according to Stapersma [46].The trapped mass is the mass that is actually 'trapped' in the cylinder just before combustion and takes part in the combustion.

$$m_1 = \frac{p_1 \cdot V_1}{R_1 \cdot T_1} = \frac{p_c \cdot V_{IC}}{R_{air} \cdot T_1} \tag{3.13}$$

in order to determine the trapped mass, the trapped temperature and the trapped pressure are required. The trapped temperature can be calculated as a result of mixing of fresh air from the inlet receiver and trapped scavenge air, Stapersma [46, 6.57]:

$$T_1 = \frac{1}{\frac{1}{T_{ind}} \cdot \frac{(V_{IC} - V_{EC})}{V_{IC}} + \frac{1}{T_{sc-tr}} \cdot \frac{V_{EC}}{V_{IC}}} \tag{3.14}$$

If the simplification $T_{ind} = T_{sc-tr}$ is applied, this results in $T_1 = T_{ind}$, and therefore:

$$m_1 = \frac{p_c \cdot V_{IC}}{R_{air} \cdot T_{ind}} \tag{3.15}$$

then similar to Equation (3.8) the trapped mass per cylinder was multiplied by the firing frequency which results in:

$$\dot{m}_1 = m_1 \cdot \left(\frac{i \cdot n_{eng}}{k} \right) \tag{3.16}$$

In order to find the amount of fresh air in the cylinder, the scavenge efficiency has to be taken into account. In the model, this is taken as a constant value of 1.0 since the model only considers 4 stroke diesel engine with significant air slip [45, 2.117].

$$\eta_{sc} \equiv \frac{m_{fresh}}{m_1} \tag{3.17}$$

The slip mass flow can now be determined:

$$\dot{m}_{slip} = \dot{m}_{in} - \eta_{sc} \cdot \dot{m}_1 \tag{3.18}$$

Where η_{sc} is the scavenge efficiency, m_{fresh} the mass off fresh air in [kg], and $\dot{m}_{slip}$ the flow [kg/s] slipping trough the cylinder.

Finally the slip flow temperature is set equal to the induction temperature, assuming no further heat pickup occurs during scavenging.

$$T_{slip} = T_{ind} \tag{3.19}$$

Further, in order to determine the slipratio s_{sl} for the model, an iterative loop is used. The approach is to increase the slip factor until the outlet receiver temperature at the nominal point is correct.

3.6.2. Seiliger

The seiliger sub model consist of a 6 point seiliger cycle and an heat release sub model. The six point seiliger is shown in Figure 28 and discussed in the work of Stapersma [45].

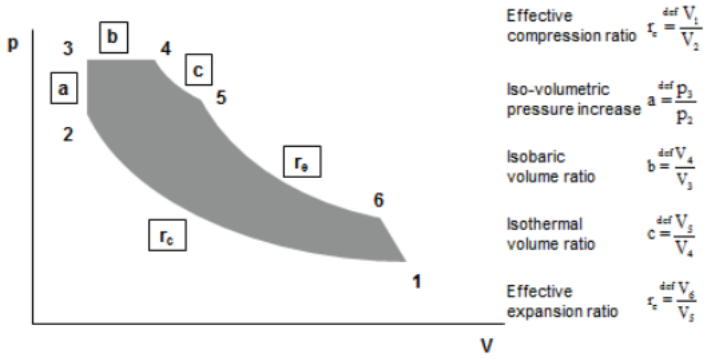

Figure 28: Six point seiliger cycle [45]

Table 3: Seiliger cycle equations [45]

Seiliger stage	**Volume** V	**Pressure** p	**Temperature** T	**Specific work** w	**specific Heat** q
Compression 1-2	$\frac{V_1}{V_2} = r_c$	$\frac{p_2}{p_1} = r_c^{\kappa_a}$	$\frac{T_2}{T_1} = r_c^{(\kappa_a - 1)}$	$w_{12} = \frac{R_a(T_2 - T_1)}{\kappa_a - 1}$	–
Isochoric combustion 2-3	$\frac{V_3}{V_2} = 1$	$\frac{p_3}{p_2} = a$	$\frac{T_3}{T_2} = a$	–	$q_{23} = c_{v,a}(T_3 - T_2)$
Isobaric combustion 3-4	$\frac{V_4}{V_3} = b$	$\frac{p_4}{p_3} = 1$	$\frac{T_4}{T_3} = b$	$w_{34} = R_a(T_4 - T_3)$	$q_{34} = c_{p,a}(T_4 - T_3)$
Isothermal combustion 4-5	$\frac{V_5}{V_4} = c$	$\frac{p_4}{p_5} = c$	$\frac{T_5}{T_4} = 1$	$w_{45} = R_a T_4 \ln c$	$q_{45} = R_a T_4 \ln c$
Expansion 5-6	$\frac{V_6}{V_5} = \frac{r_{eo} r_c}{bc}$	$\frac{p_5}{p_6} = \frac{p_5}{\left(\frac{r_{eo} r_c}{bc}\right)^{n_{exp}}}$	$\frac{T_5}{T_6} = \frac{T_5}{\left(\frac{r_{eo} r_c}{bc}\right)^{n_{exp}-1}}$	$w_{45} = \frac{R_a(T_6 - T_5)}{(n_{exp} - 1)}$	–

3.6.3. Heat release

The heat release is described according to the summary found in the work of Geertsma et al. [12]. The heat release model represents the heat release in kJ/kg during isochoric q_{23} , isobaric q_{34} and isothermal q_{45} combustion as represented by the six point seiliger cycle.

$$q_{23} = X_{cv}(t) \cdot \frac{m_f(t) \cdot \eta_q(t) \cdot \eta_{comb} \cdot h^L}{m_1(t)} \tag{3.20}$$

$$q_{34} = (1 - X_{cv}(t) - X_{ct}(t)) \cdot \frac{m_f(t) \cdot \eta_q(t) \cdot \eta_{comb} \cdot h^L}{m_1(t)} \tag{3.21}$$

$$q_{45} = X_{ct}(t) \cdot \frac{m_f(t) \cdot \eta_q(t) \cdot \eta_{comb} \cdot h^L}{m_1(t)} \tag{3.22}$$

where η_q is the heat release efficiency, X_{cv} and X_{ct} are the amounts of heat released at constant volume and temperature respectively, η_{comb} is the combustion efficiency and h^L is the lower heating value of fuel at ISO conditions [kJ/kg].

The percentage of heat lost is assumed inversly related to engine speed n_e [Hz]:

$$\eta_q(t) = 1 - (1 - \eta_{q_{nom}}) \cdot \frac{n_{e_{nom}}}{n_e(t)} \tag{3.23}$$

In order to determine the heat release efficiency $\eta_{q,nom}$ for the model, an iterative loop is used. The approach is to decrease the heat release efficiency until the nominal cycle work of the model is correct for the nominal point.

The heat released during constant volume combustion is considered to increase linearly with engine speed:

$$X_{cv}(t) = X_{cv_{nom}}(t) + \frac{n_e(t) - n_{e_{nom}}}{n_{e_{nom}}} \cdot X_{cv_{grad}} \tag{3.24}$$

The released during constant temperature combustion is considered to increase proportional to fuel injection:

$$X_{ct}(t) = X_{ct_{nom}}(t) \cdot \frac{m_f(t)}{m_{f,nom}} \tag{3.25}$$

3.6.4. Air excess ratio

The air excess ratio λ of the engine is defined as the ratio of total fresh air in the cylinder to the minimum amount of fresh air required for combustion [47]. The air excess ratio is determined by the air swallow characteristics of the engine. For four stroke diesel engines with significant airslip the scavage efficiency can be assumed untiy [45][Ch. 2, p. 55]. Therefore, the air excess ratio equals the pseudo air excess ratio and can be defined as follows:

$$\lambda = \frac{m_1}{m_f \cdot \sigma_f} \tag{3.26}$$

where σ_f is the stoiciometric air to fuel ratio of the fuel (14.5), m_f is the mass of fuel [kg] injected and m_1 is the trapped mass of air [kg] at the start of compression. The trapped mass at the start of compression is mainly determined by the charge air pressure:

$$m_1 = \frac{p_1 \cdot V_1}{R_a \cdot T_1} \tag{3.27}$$

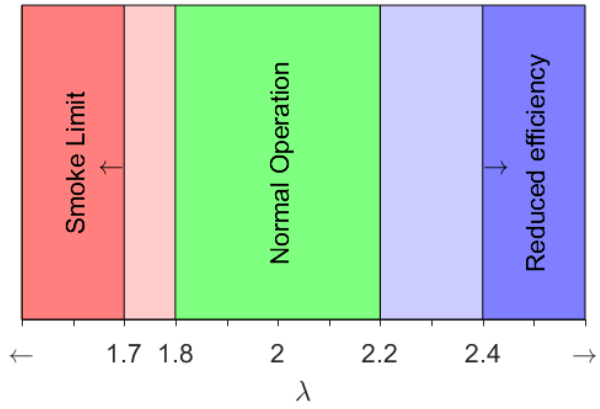

Figure 29: Lambda values as recommended by Stapersma [45]

The air excess ratio is bounded by certain limits as depicted in Figure 29. On the left side there is the smoke limit which is dictated by a lower boundary. Below this boundary there is insufficient air to burn the injected fuel completely. For diesel engines the smoke limit lies at around $\lambda = 1.5 \sim 1.7$ according to Stapersma [45]. On the right side the upper limit is bounded by the temperature of the end phase of combustion as seen in Figure 30. If the temperature becomes to low, the combustion is incomplete and unburned hydrocarbons remain. According to Stapersma [45], normal values of λ range from 1.8 to 2.2.

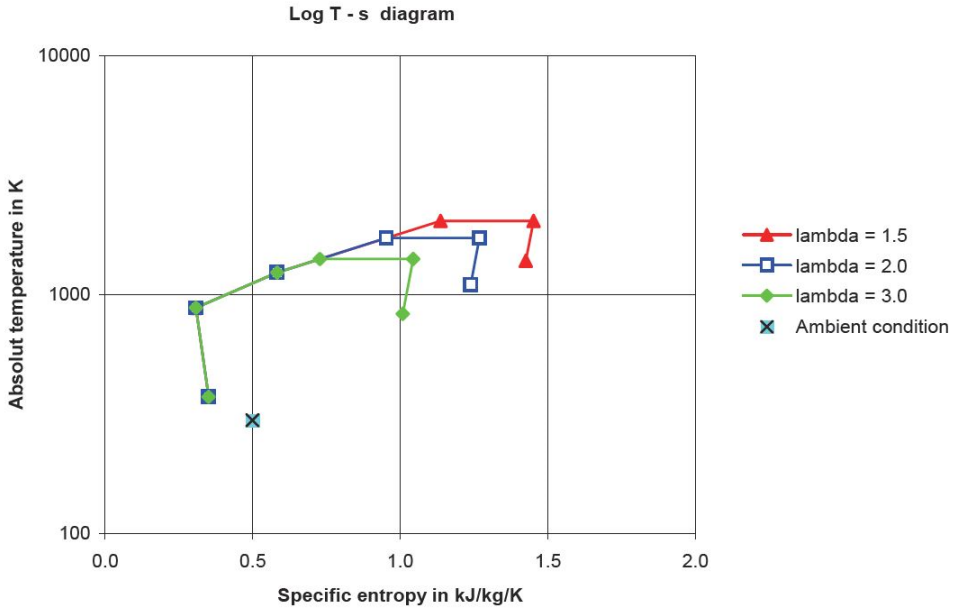

Figure 30: Effect of air excess ratio in T-s diagram [45]

Thermal loading

The air excess ratio is an important indicator for the thermal loading of the engine as discussed in [38]. If the air excess ratio drops below a certain level, the temperatures in the cylinder rise as depicted in Figure 30. As a consequence, the temperatures in the combustion chamber and exhaust system significantly exceed the permissible range which can lead to piston burn-off, cracks in the cylinder head, valve and turbocharger damage [53].

3.6.5. Gas disposal

Gas Disposal			
Inputs:		*Outputs:*	
$\dot{m}_{in}$	Mass flow into engine [kg/s]	$\dot{m}_{slip}$	Slip mass flow [kg/s]
$\dot{m}_{slip}$	Slip mass flow [kg/s]	$\dot{m}_{cyl\_out}$	Mass flow out of the cylinder [kg/s]
$\dot{m}_f$	Fuel mass flow [kg/s]	x_{cyl_out}	Air mass fraction in cylinder out flow [kg/s]

Table 4: Inputs and outputs of the gas disposal sub model

The analysis of the gas disposal sub model is comparable with the approach of the air swallow sub model. The model will be discussed according to the work of Loonstijn [34] with the theoretical background from Stapersma [46].

$$\dot{m}_{cyl\_out} = \dot{m}_{in} + \dot{m}_f - \dot{m}_{slip} \tag{3.28}$$

If the amount of fuel injected in the cylinder and the amount of fresh air trapped in the cylinder are known the air excess ratio (3.26) can be calculated. Based on the air excess ratio, the fraction of air in the gas leaving the cylinder is determined:

$$x_{cyl\_out} = 1 - \frac{1}{\lambda} \tag{3.29}$$

$$\lambda = (\lambda^*) \cdot \frac{1}{\eta_{sc} \cdot \eta_{pu}} = \left(\frac{\dot{m}_{in} - \dot{m}_{slip}}{\dot{m}_f} \cdot \frac{1}{\sigma_f} \right) \cdot \frac{1}{\eta_{sc} \cdot \eta_{pu}} \tag{3.30}$$

Where η_{pu} is the ratio of combustion air to trapped mass [-], η_{scav} is the scavenge efficiency, and η_{bld} is the polytropic expansion coefficient.

3.6.6. Zinner blowdown

After opening of the exhaust valve the hot exhaust gases are expelled to the outlet receiver. The blowdown was represented according to Zinner [57] and is also described by Stapersma [46]. The blow down temperature can be calculated as follows:

$$T_{bld} = \left(\frac{1}{n_{bld}} + \frac{n_{bld} - 1}{n_{bld}} \cdot \frac{p_d}{p_6} \right) \cdot T_6 \tag{3.31}$$

The polytropic expansion coefficient n_{bld} allows for heat transfer to the cylinder wall, exhaust valve and inlet duct. The resulting temperature for the outlet receiver is a result of the mixing of different mass flows and will be discussed in the next section.

In order to get an estimator for the thermal loading of the diesel engine as explained by Sapra et al. [38] the temperature of the exhaust valve as proposed by Grimilius et al. [16] is also calculated in the Zinner blow down sub model.

$$T_{ev,est} = \frac{T_6 + r \cdot T_1}{1 + r} \tag{3.32}$$

with:

$$r = s^{0.8} \cdot \left[\frac{T_1}{T_6}\right]^{0.25} \cdot \left[\frac{EC - IO}{IO - EC}\right]^{0.2} \tag{3.33}$$

Where $T_{ev,est}$ is the estimated exhaust valve temperature [K] and r the heat transfer ratio, s is the scavenge factor.

the connection to the Zinner blow down is the polytropic expansion coefficient, which allows for the heat transfer from the blow down gasses to the exhaust valve.

3.7. Outlet receiver

The outlet receiver forms the connection between the cylinder outlet and the turbine inlet. Therefore, the outlet receiver is based on two mass flows. The mass flow which leaves the cylinder and the mass flow which enters the turbine. The working principle of the outlet receiver is almost identical to the inlet receiver. However, there is one big difference. For the inlet receiver, the assumption that the air flowing into the inlet receiver consist of pure air was made. For the outlet receiver, this assumption does not hold. The mass flow going into the inlet receiver consist of exhaust gas. Exhaust gas contains two components in this model. The gas that took part in the combustion and the gas that 'slipped' through the cylinder during scavenging. The latter is called slip flow and consists of pure air. The combustion air and the slip flow mix in the outlet.

The pressure, temperature, and mass can now be calculated using the same procedure as for the inlet receiver.

$$\dot{m}_{OR} = \dot{m}_{cyl\_out} + \dot{m}_{slip} - \dot{m}_{tur\_in} \tag{3.34}$$

$$T_{OR} = \int dT_{OR} \cdot dt \tag{3.35}$$

$$p_{OR} = \frac{\dot{m}_{OR} \cdot R_{air} \cdot T_{OR}}{V_{OR}} \tag{3.36}$$

3.8. Conclusion

First a model based with a buchi based power balance to model the turbochager was investigated. In order to couple the electric machine to the turbocharger, a more physical model based on the equations of motion was proposed. However, due to the model structure of the model as proposed by Loonstijn [34] it was not possible to implement a motion based turbocharger. Therefore, it was decided to turn to a more structured model. The modular hierachical and causal modelling pradigm as proposed by Colonna et al. [7] provides a solid basis to a more structured model. In order to comply with the model paradigm an inlet receiver was added to the model. In terms of turbocharger modelling the difference between the approaches is significant. However, in terms of the engine part of the model the revisions are minor.

4

Turbocharger model

In this section the modelling approach of the turbocharger will be discussed. Two approaches have been investigated: First, a method based on the Büchi equation and a power balance which are discussed in Section 4.2 and 4.3. Secondly a method based on the equations of motion of a turbocharger is investigated in Section 4.4. This method required a general model for off-design performance of a single stage turbomachine as proposed by Stapersma [48] and discussed in Section 4.6.

Power balance

$$\pi_{com} = \left\{ 1 + \beta \cdot \delta \cdot \chi \cdot \eta_{\mathrm{TC}} \cdot \tau \cdot \left(1 - \frac{1}{\pi_{tur}^{\frac{\gamma_{de}-1}{\gamma_{de}}}} \right) \right\}^{\frac{\gamma_{air}}{\gamma_{air}-1}}$$

Equations of motion

$$M_{TC} = \alpha_{TC} \cdot I_{TC}$$

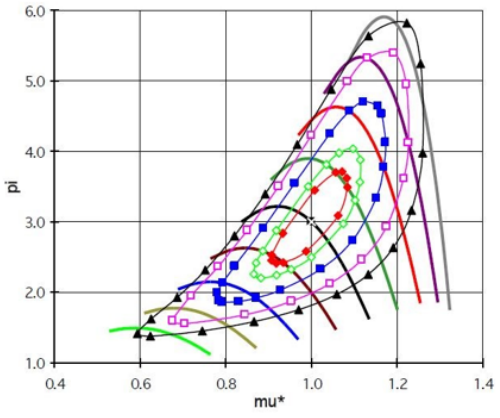

Figure 31: Modelling approaches

4.1. Compressors and Turbines

Modelling of the turbocharger is usually done by dividing the turbocharger into its basic components as seen in Figure 32: a turbine driving a compressor. The sub systems are then modelled separately and coupled by means of conservation laws. For engine modelling various methods of compressor and turbine modelling are used.

Figure 32: Turbocharger schematic

A common way to model the compressor and turbine is via empirical methods. The mass flow, pressure, speed and efficiency parameters are acquired from the manufacturer of the turbocharger and loaded into the engine model as a lookup table. This is an accurate method because the data from the manufacturer is usually test bench data and therefore resembles the actual compressor or turbine. The data can be presented in a compressor or turbine map as seen in Figure 33.

Another method to model the compressor and turbine is to model compressor or turbine char-

acteristics. This can be done with a model based on dimensionless parameter (4.1) (4.2) groups as described by van Buijtenen et al. [49].

$$\nu = \frac{n \cdot D}{\sqrt{R \cdot T_{in}}} \quad \text{and} \quad \pi = \frac{p_{out}}{p_{in}} \tag{4.1}$$

$$\mu = \frac{m \cdot \sqrt{R \cdot T_{in}}}{p_{in} \cdot D^2} \quad \text{and} \quad \eta \tag{4.2}$$

Various models have been proposed as for example: Jensen et al. [21], Stapersma [48] et al. These type of models are called mean-line models [31].

Then there are more simple methods based on the fundamental thermodynamics and fluid dynamics. Examples are: Compressor and turbine models based on the first law of thermodynamics as described by Moran et al. [36].

If advanced turbocharging strategies are used, the model is extended by coupling various components in series or parallel or by incorporating additional components.

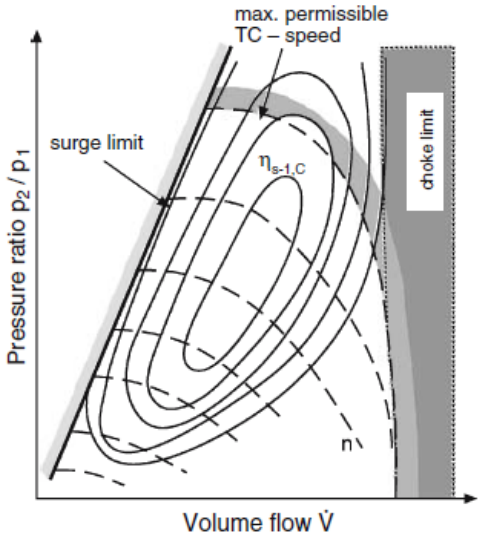

Figure 33: Principle map limitations of radial compressors: surge, speed and choke limit[18]

Turbine: For modelling purposes, turbines are often treated in the same way as compressors. The same dimensionless parameter groups as presented by van Buijtenen et al. [49] for the compressor can be applied to the turbine. As with the compressor this type of model needs experimental data to form the turbine map.

Surge: At the surge limit, operating point of the compressor enters an 'unstable' area where the balance between mass flow and pressure gradient across the compressor is unfavourable. In this area a disturbance causing the mass flow to decrease results in a pressure drop. If the downstream air pressure does not fall quick enough it will lead to reverse flow in the compressor. As the pressure levels out, the compressor picks up again and the cycle is repeated. This cycle of events is called surge. Surge results in pressure waves and vibrations in the complete flow system. [49].

Choke: The choke limit is characterized by the fact that the mass flow in the compressor or turbine reaches sonic speed. Usually this is at narrowest area of the inlet diffuser. The mass flow cannot be further increased, even by increasing the compressor speed.

In the model only choking in the inlet is taken into account which for a compressor only takes place at high speeds and mass flow. At increasing mass flow along the lower constant speed curves the outlet pressure and temperature become low, forcing the outlet mass flow to choke [48]

4.2. Compressor Büchi model

Compressor Büchi model			
Inputs:		*Outputs:*	
T_a	Compressor inlet temperature [K]	p_c	Charge pressure [Pa]
p_a	Compressor inlet pressure [Pa]		
$\dot{m}_{com}$	Mass flow trough compressor [kg/s]		
P_{com}	Available compressor power [W]		

Table 5: Inputs and outputs of the Büchi compressor model

The Büchi compressor model is based on the Büchi equation (4.3), essentially stating $w_{com} = w_{tur}$. It is a very convenient way to model the turbocharger because it is simple, the model can easily be adapted to more advanced configurations and the amount of inputs are limited and usually available in the FAT data of an engine as explained by Geertsma et al. [12].

$$\pi_{com} = \left\{ 1 + \beta \cdot \delta \cdot \chi \cdot \eta_{\mathrm{TC}} \cdot \tau \cdot \left(1 - \frac{1}{\pi_{tur}^{\frac{\gamma_{de}-1}{\gamma_{de}}}} \right) \right\}^{\frac{\gamma_{air}}{\gamma_{air}-1}} \tag{4.3}$$

Where β is the power correction factor, δ is the fuel addition factor, χ ratio of specific heats of air and exhaust gas, τ is the temperature ratio and γ the specific heat ratio.

A schematic overview of the charge air and exhaust system of an engine is given in Figure 34. This scheme will be used as 'convention' to explain the models unless stated otherwise.

The pressure and temperature ratio over the compressor are as follows:

$$\pi_{com} = \frac{p_b}{p_a} \tag{4.4}$$

$$\tau_{com} = \frac{T_b}{T_a} \tag{4.5}$$

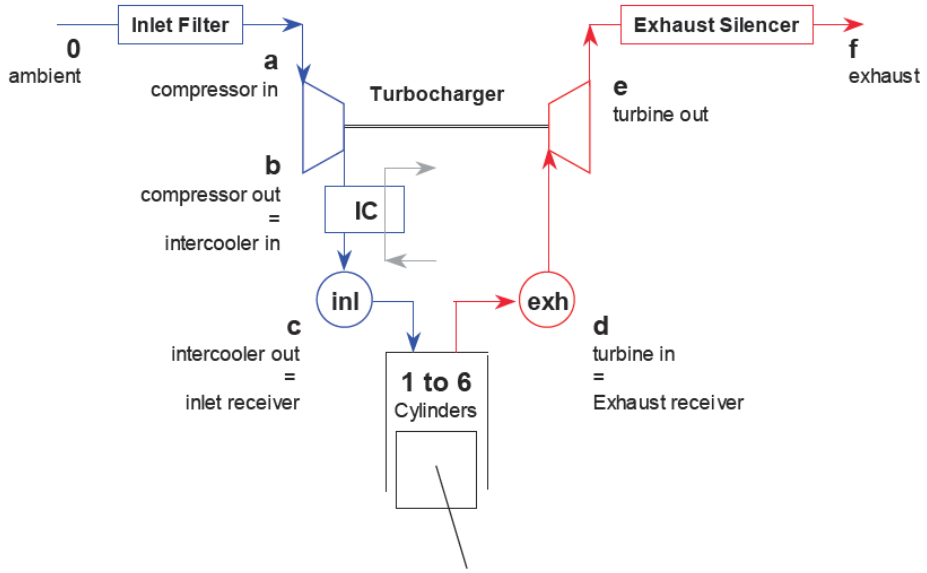

Figure 34: Turbocharger overview for modelling [46]

If the first law is applied on the compressor, neglecting heat losses and working with perfect gas, the work of a compressor can be expressed in a temperature change:

$$w_{com} = h_b - h_a = c_{p,ab} \cdot (T_b - T_a) \tag{4.6}$$

in which $c_{p,ab}$ is the mean specific heat between the compressor inlet 'a' and the real outlet condition 'b', currently this is 'simplified' to a constant $c_{p,a}$, which gives an error of around three percent, which is quite significant. Therefore it might be more convenient to either use the mean value $c_{p,ab}$ based on the nominal operating point of the compressor. To make the $c_{p,ab}$ value dependent on compressor outlet temperature.

To allow for flow losses isentropic efficiency is introduced and the compressor specific work input is then:

$$w_{com} = \frac{c_{p,ab} \cdot T_a}{\eta_{is,com}} \cdot \left(\pi_{com}^{\frac{\gamma_{ab}-1}{\gamma_{ab}}} - 1 \right) \tag{4.7}$$

The isentropic outlet temperature can be calculated if the inlet and outlet temperature of the compressor are known, by applying equation (4.8). The isentropic efficiency is estimated by a a fit function based on the FAT data points.

$$\eta_{is,com} = \frac{T_{is,b} - T_a}{T_b - T_a} \tag{4.8}$$

$$T_{is,b} = T_a \cdot \tau_{is,com} \tag{4.9}$$

$$\tau_{is,com} = \pi_{com}^{\frac{\kappa-1}{\kappa}} \tag{4.10}$$

Formula (4.8), (4.9) and (4.10) are applied to determine the compressor states in the FAT points, after which the Matlab function fit is used to determine curve through the data points and define

the istentropic efficiency of the compressor at all states between zero and nominal pressure ratio. The resulting function is plotted in Figure 35.

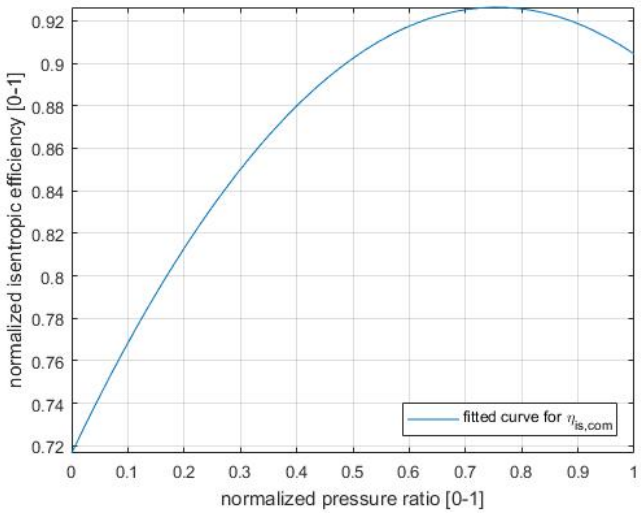

Figure 35: Isentropic efficiency for compressor, fitted on FAT points

For T_b the FAT data of the MAN 28/33 was used, due to the fact that the FAT data of the W26 only consisted the inlet receiver temperatures and pressures. Both engines are fitted with the same turbocharger namely the ABB TPL-65 A-30.

Effectively, now $\eta_{is,com} = f(\pi_{com})$ the isentropic efficiency is assumed to be a function of pressure alone. However, a compressor map will show that the efficiency is clearly also a function of mass flow and rotational speed, this will be further explained in the section about compressor maps.

4.3. Power balance

The power balance model was proposed by Loonstijn [34]. The power balance block as depicted in Figure 23 consist of a simple power balance as depicted in Figure 36:

$$P_{com} = P_{tur} + P_{PTI} \tag{4.11}$$

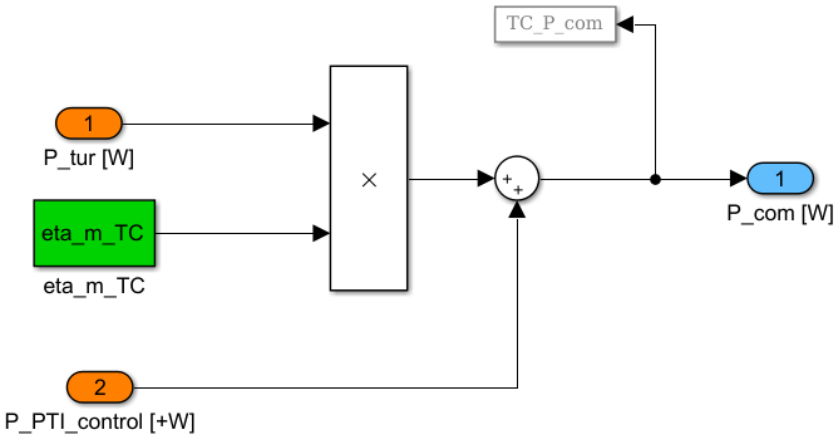

Figure 36: Simulink model of the power balance based model

The power balance directs power from the turbine to the compressor. A constant mechanical loss for the bearing friction is taken into account of 1%. Also, power take off (PTO) or power take in (PTI) is added to the power balance.

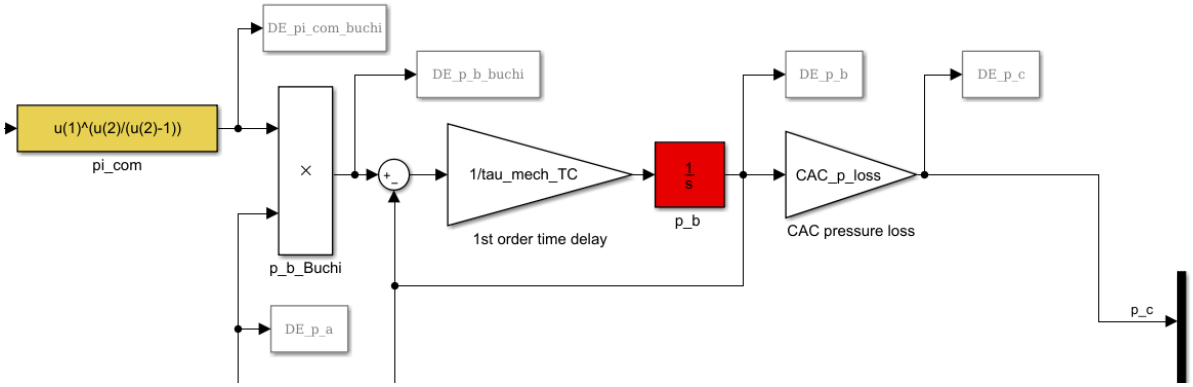

Figure 37: Simulink model of the power balance based compressor

The power available for the compressor then enters the compressor sub model. The formulas are explained in Section 4.2. However, the formulas are only valid if the Büchi equation (4.3) can be applied. Which means, the compressor and the turbine have to be in dynamic equilibrium. In order to solve this, a first order time delay is used.

First the pressure ratio according to the Büchi balance (4.3) is calculated:

$$p_{c,buchi} = p_a \cdot \pi_{com,buchi} \tag{4.12}$$

Then the first order time delay is used to determine the actual charge air pressure as depicted in Figure 37. This allows for an imbalance between the compressor and turbine during acceleration an deceleration. The 'delayed' pressure is then integrated over time as seen in Equation 4.13

$$p_c = \int \frac{1}{\tau_{TC-mech}} \cdot \pi_{com,buchi} \cdot dt \tag{4.13}$$

If the model overview in Figure 23 is inspected it can be seen that the compressor represents a volume element. Although, physically, a compressor resembles a resistor element. This is solved by the mechanical time constant $\tau_{TC-mech}$. The mechanical constant accounts not only for the imbalance between the compressor and the turbine, it functions as 'volume' for the inlet receiver. Also, the constant represents the physical inertia of the turbocharger itself which causes the 'turbo lag'. These parameters all cause a delay in the charge air pressure, but are not physically coupled.

4.4. Equations of motion model

The equations of motion block as depicted in Figure 24 consists of a simple equation of motion as described by e.g. Hibbler et al. [17]:

$$M_{TC} = \alpha_{TC} \cdot I_{TC} \tag{4.14}$$

Where M_{TC} is the torque, α_{TC} is the angular acceleration and I_{TC} is the moment of inertia with:

$$M_{TC} = M_{tur} - M_{com} \pm M_{PTI} \tag{4.15}$$

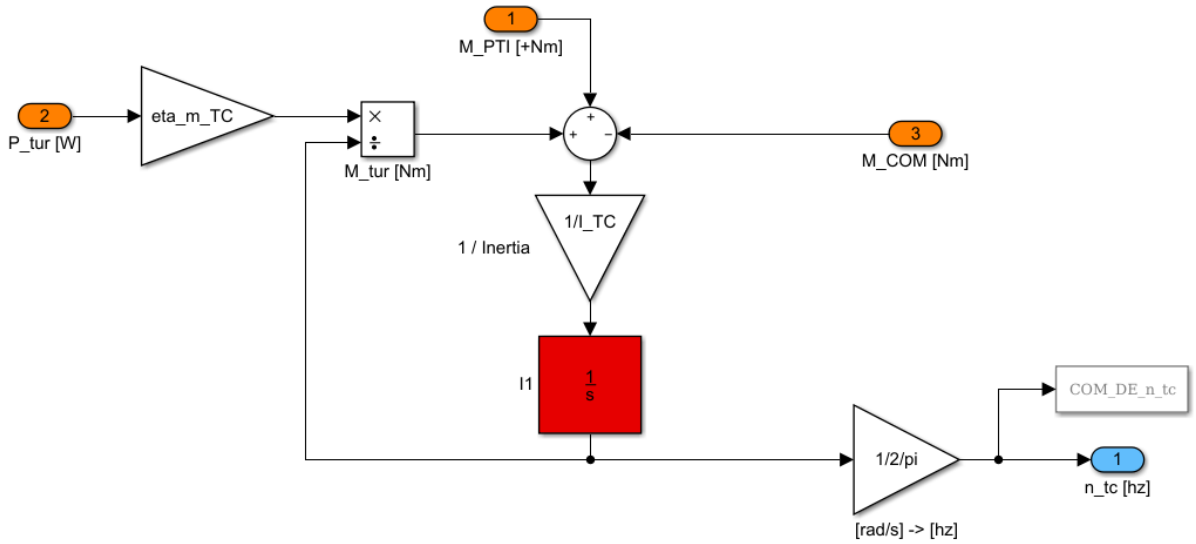

Figure 38: Simulink model of the equation of motion based model

The torque block consists of a torque balance. First the torque requested from for the compressor is subtracted from the torque delivered by the turbine. Also, torque as result of an electric machine performing power take off (PTO) or power take in (PTI) is added to the torque balance. A constant mechanical loss for the bearing friction is taken into account of 1%. The resulting torque of the turbocharger is calculated. The resulting torque is then used to calculate the compressor angular acceleration according to newton's second law:

$$\alpha_{TC} = \frac{M_{TC}}{I_{TC}} \tag{4.16}$$

which is then integrated with respect to time to obtain the angular speed of the turbocharger [rad/s]

$$\omega_{TC} = \int \alpha_{TC} \cdot dt \tag{4.17}$$

Since the model is a first principle model, the model also holds if the compressor and turbine are not in dynamic equilibrium.

4.5. Compressor map model

If the turbocharger model is based on the equations of motion, a correlation for mass flow and rotational speed for the compressor has to be found. During literature the so called Diesel B-minus model was encountered, a combination of the diesel A and B model, both developed at the TU Delft. This model approach features a diesel model, in which the turbocharger is based on maps instead of the Büchi balance. This approach has been investigated by Loonstijn [33], Loonstijn implemented a compressor model proposed by Jensen et al. [21] Jensen et al. proposed a mass flow model based on dimensionless head parameter ψ, Mach number Ma and mass flow rate ϕ.

The compressor is expressed in terms of a dimensionless head parameter ψ as defined in equation (4.18):

$$\psi = \frac{c_{p,a} \cdot T_a \cdot \left(\pi_{com}^{\frac{\kappa-1}{\kappa}} - 1 \right)}{0.5 \cdot U_{com}^2} \qquad \text{with} \quad U_{com} = \pi \cdot d_{com} \cdot n_{tc} \tag{4.18}$$

where d_{com} is the diameter of the compressor in [m]. The dimensionless flow rate ϕ_{com} is defined in equation(4.19) and is used to express the mass flow rate.

$$\phi_{com} = \frac{\dot{m}_{com}}{\rho_0 \cdot \pi/4 \cdot d_{com}^2 \cdot U_{com}} \tag{4.19}$$

The dimensionless head parameter ψ can be expressed as function of the dimensionless flow rate ϕ and the Mach number.

$$M_a = \frac{U_{com}}{\sqrt{\kappa \cdot R \cdot T_{in}}} \tag{4.20}$$

$$\psi = \frac{K_1 + K_2 \cdot \phi_c}{K_3 - \phi_c} \qquad \text{with} \quad K_i = k_{i1} + k_{i2} \cdot M_a \tag{4.21}$$

The compressor efficiency is expressed as function of dimensionless flow rate and the inlet Mach number. Jensen et al. found the efficiency has a second order dependence on ϕ for any given Mach number. The coefficients a_i where found to have a dependence as stated in equation (4.22)

$$\eta = a_1 \cdot \phi^2 + a_2 \cdot \phi + a_3 \qquad a_i = \frac{b_{1,i} + b_{2,i} \cdot M_a}{b_3 - M_a} \qquad i = 1, 2, 3 \tag{4.22}$$

Loonstijn concluded after matching the model to an actual compressor map of a MAN 34NA/S turbocharger that the model gives a good approximation in the lower speed ranges but at higher speed ranges the accuracy declines. He suggest the accuracy has to be investigated further. The results of the compressor matched by Loonstijn are depicted in Figure 39b.

However, Jensen et al. did an experiment to validate the compressor model, and concluded that for this particular experiment in the speed range below 160000 rpm the agreement between predicted an experimental pressure ratio is within a two percent bandwidth. Above 160000rpm, the agreement deteriorates, which Jensen et al. attribute to the Mach number in this region which exceeds 1.1 apparently changing the character of the flow. It is likely that the phenomenon encountered by Jensen et al. was choke. Jensen et al. did not mention surge or choke limits in their paper, therefore presumably choke and surge where neglected. Despite the limited amount of explanation about his methods, the results are impressive.

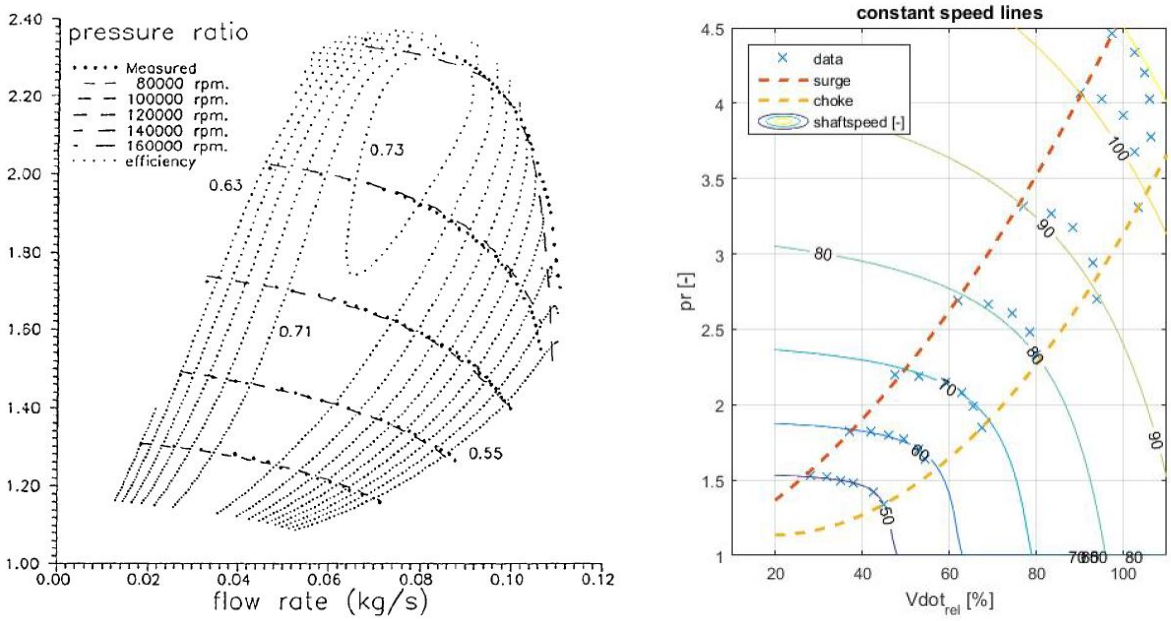

(a) Map produced by Jensen et al.[21]

(b) Map produced by Loonstijn[33]

Figure 39: Compressor maps produced by the method as proposed by Jensen et al. [21]

4.6. A general model for off-design performance of a single stage turbomachine

Another method for general compressor maps has been proposed by Stapersma of the TU Delft and is described in: A general model for off-design performance of a single stage turbomachine [48].

Stapersma proposes a compressor model based on four shape parameters to fit the single stage characteristic of a turbomachine. His goal was to create a model which was mathematically simple an reversible with respect to as many in and output variables as possible.

The four shape parameters can be divided into 2 groups, the parameters ψ_0 and M_{a0} that control the constant speed curves and the parameters x and y that control the shape of the efficiency lines. Together with the pressure ratio, mass flow, rotational speed and nominal efficiency in the nominal point these parameters used to construct the compressor model. An example of a resulting compressor map can be seen in Figure 40.

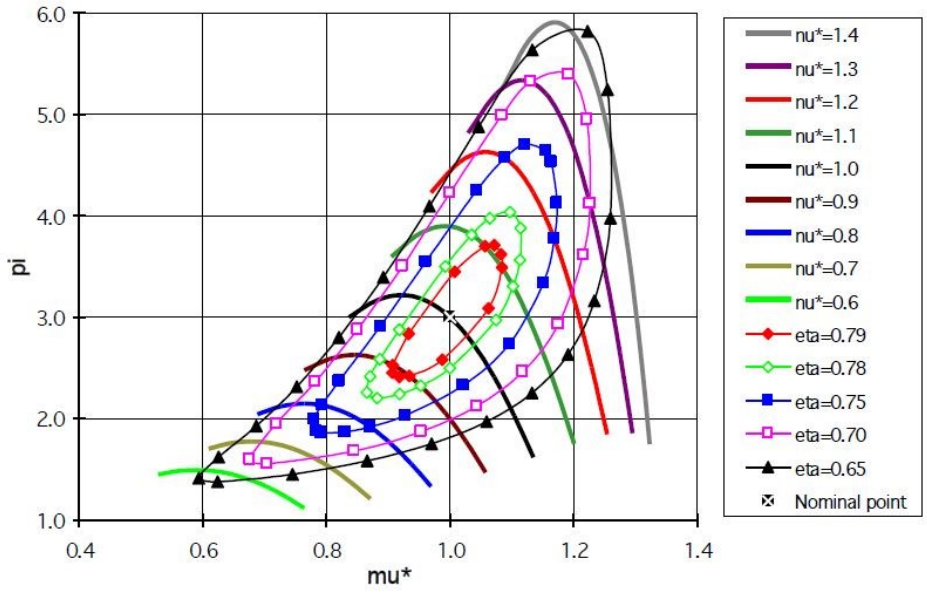

Compressor characteristic: Pressure ratio as a function of corrected mass flow along lines of constant corrected rotorspeeds for a single stage compressor with ψ_o = +0.4, x = 3.0, y = 1.0, Ma_0 = 0.5, π_o = 3 and η_o = 0.8; lines of constant isentropic efficiency included

Figure 40: General compressor map as proposed by Stapersma [48]

Stapersma described the compressor model extensively in [48], all the mathematical equations including a sensitivity analysis are explained in detail. Therefore, only the resulting equations and relevant parameters will be discussed.

First the four shape parameters will be discussed, further down in the derivation of the model these are used to find a solution for the flow coefficient (4.30).

The assumption that the enthalpy function can be assumed as a linear function of the flow coefficient at the inlet stage leads to:

$$a = 1 - \frac{1}{\psi_0} \tag{4.23}$$

where ψ_0 is the enthalpy coefficient.

Changing the flow coefficient the angle of attack of the fluid relative to the rotor will change, having effect on the losses and hence on the efficiency. If an parabolic curve is assumed and the pressure coefficient is non zero at zero flow we find a parameter b:

$$b = -x \cdot \frac{1}{\psi_0} \tag{4.24}$$

x determines the gradient of the efficiency along the constant speed of the compressor map.

Losses also depend on rotational speed in term of a Reynolds and a Mach effect, which is captured in the d parameter:

$$d = -y \cdot \psi_0 \cdot sign(\psi_0) \tag{4.25}$$

y determines the gradient of the efficiency along the back-bone of the compressor map.

In order to take into account the Mach number and gas dynamics (compressibility effects) the q parameter or compressibility parameter is introduced, which tells us something about the nominal Machnumber in the machine.

$$q = \frac{\frac{\kappa - 1}{2} \cdot Ma_0^2}{1 + \frac{\kappa - 1}{2} \cdot Ma_0^2} \tag{4.26}$$

Now Stapersma chooses a value for the enthalpy coefficient ψ_0 which determines the steepness of the constant speed curves. He does this according to the work of Gordon Wilson, 1984. However this process is not described in detail, Stapersma suggest compressors can divided into three groups: Highly, medium, and lightly loaded compressors, each have a range of enthalpy coefficients. How this classification is motivated, and how for example highly loaded is defined is unclear. Presumable the pressure ratio plays an important role here. Then a value for M_{a0} is chosen, M_{a0} also plays a role in the steepness of the constant speed curves, especially in the regions of higher mass flow and rotor speed.

Because of the structure of the diesel engine model with the motion based turbocharger, as explained in the Section 3.4 the model inputs chosen are pressure ratio and rotational speed of the turbocharger. Further, a nominal point needs to be determined, by definition this is the point of of optimum efficiency.

Table 6: Inputs and outputs of the compressor map model

Compressor map model			
Inputs		*Outputs*	
T_{in}	Compressor inlet temperature [K]	T_{out}	Compressor outlet temperature [K]
p_{in}	Compressor inlet pressure [Pa]	$\dot{m}$	Mass flow trough compressor [kg/s]
p_{out}	Compressor outlet pressure [Pa]		
n	Compressor speed [Hz]		

The relative rotorspeed and relative inlet temperature

$$n^* = \frac{n}{n_0} \quad \text{and} \quad T_{in}^* = \frac{T_{in}}{T_{in,0}} \tag{4.27}$$

determine the relative value of the non-dimensional rotor speed ν^* and pressure ratio:

$$\nu^* = \frac{n^*}{\sqrt{T_{in}^*}} \quad \text{and} \quad \pi = \frac{p_{out}}{p_{in}} \tag{4.28}$$

which together with the pressure ratio enables us to define a pressure coefficient ϵ^* :

$$\epsilon^* = \frac{1}{\nu^{*2}} \cdot \frac{\left(\pi^{\frac{\kappa-1}{\kappa}} - 1\right)}{\left(\pi_0^{\frac{\kappa-1}{\kappa}} - 1\right)} \tag{4.29}$$

and the flow coefficient ϕ^* from:

$$\epsilon^* = 1 + a \cdot (\phi^* - 1) + b \cdot (\phi^* - 1)^2 + d \cdot (\nu^* - 1)^2 \tag{4.30}$$

In order to find a solution for the flow coefficient we rewrite the equation to:

$$\phi^* = \frac{-B - \sqrt{B^2 - 4 \cdot A \cdot C}}{2 \cdot A} \tag{4.31}$$

With:

$$\begin{aligned} A &= b \\ B &= a - 2 \cdot b \\ C &= 1 - \epsilon^* - a + b + d \cdot (\nu^* - 1)^2 \end{aligned} \tag{4.32}$$

With the flow coefficient ϕ^*, non dimensional rotor speed ν^* and compressibility parameter q known the Mach number in the machine can be calculated:

$$\begin{aligned} M_a^* &= \phi^* \cdot \nu^* \cdot \sqrt{\frac{1-q}{1 - q \cdot (\phi^* \cdot \nu^*)^2}} \\ \Rightarrow \quad M_a &= M_a^* \cdot M_{a0} \end{aligned} \tag{4.33}$$

Then non dimensional mass flow μ^* is calculated:

$$\mu^* = \frac{M_a^*}{\sqrt{(1-q) + q \cdot {M_a^*}^{2\frac{\kappa+1}{\kappa-1}}}} \tag{4.34}$$

which gives us the possibility to take choke effects (at the entrance of the compressor) into account by limiting the M_a^* value:

$$\begin{aligned} M_{a,max}^* &= \sqrt{\frac{\kappa - 1}{2} \cdot \frac{1-q}{q}} \\ M_a^* > M_{a,max}^* \quad &\Rightarrow \mu^* = \quad \mu^*(M_{a,max}^*) \end{aligned} \tag{4.35}$$

Choke: In the model only choking in the inlet is taken into account which for a compressor only takes place at high speeds and mass flow. At increasing mass flow along the lower constant speed curves the outlet pressure and temperature become low, forcing the outlet mass flow to choke; the point where this occurs could be calculated but this has not been done yet [48, pp. 59].

The relative inlet pressure and relative inlet temperature are defined as follows:

$$p_{in}^* = \frac{p_{in}}{p_{in,0}} \quad \text{and} \quad T_{in}^* = \frac{T_{in}}{T_{in,0}} \tag{4.36}$$

Then, the mass flow can be expressed as:

$$\begin{aligned} \dot{m^*} &= \frac{\mu^* \cdot p_{in}^*}{\sqrt{T_{in}^*}} \\ \text{gives:} \quad \dot{m} &= \dot{m^*} \cdot \dot{m}_0 \end{aligned} \tag{4.37}$$

$\dot{m}$ as function of rotational speed was the parameter required to construct the motion based turbocharger model. However, in order to find the other output T_{out} and the efficiency, we will continue.

the enthalpy coefficient ψ^* is then:

$$\psi^* = 1 + a \cdot (\phi^* - 1) \tag{4.38}$$

with a from equation (4.23)

This makes it possible to determine the temperature ratio τ over the compressor and the temperature at the oulet:

$$\begin{gathered} \tau = 1 + \psi^* \cdot \nu^{*2} \cdot (\tau_0 - 1) \\ \text{gives:} \quad T_{out} = \tau \cdot T_{in} \end{gathered} \tag{4.39}$$

Finally the efficiency can be obtained:

$$\begin{gathered} \frac{\eta_c^*}{\eta_t^*} = \frac{\eta^*}{\psi^*} \\ \text{gives:} \quad \eta = \eta^* \cdot \eta_0 \end{gathered} \tag{4.40}$$

With these formulas and parameters the compressor map as seen in Figure 40 can be constructed.

4.7. Conclusion on compressor models

Three methods of compressor modelling were investigated. A power balance based on the Büchi equation and two methods to construct a general compressor map. The power balance based on the Büchi equation is a very simple and straightforward way of modelling the turbocharger. The map approaches require more theoretical knowledge of turbo machinery and are harder to implement. In order to adapt the MVFP diesel engine model for a motion based turbocharger, a speed dependent compressor model was required. The power balance approach is not suitable for this. Therefore, it was decided to put effort in the map approaches. This should be regarded as a tool to accomplish the main questions of the thesis instead of a goal on its own. Since the model as proposed by Stapersma [48] is detailed described, this one is chosen to be investigated further.

4.8. Compressor Map Matching

In order to match the compressor map to an engine, speed, pressure and mass flow data is required. Usually, the FAT data of an engine doesn't contain all of this data. However, if extensive emission and fuel consumption data is available in the FAT dataset it is possible to calculated the mass flow of air through the compressor. Unfortunately, emission data was not included in the FAT data sets available at the defence materiel organisation. Therefore this data was collected during a measurement campaign. The data used for the compressor matching has been measured aboard a Zeven provinciën-class frigate. The details about the measurement campaign can be found in Section 5.

4.8.1. Design space

The compressor map matching starts with choosing the four design parameters and a nominal point. The nominal point is *by definition* the point of optimum efficiency. This point does not have to be the design point. In order to chose a nominal point, the data acquired aboard Zr. Ms. De Ruyter as seen in Figure 41 was examined.

Stapersma [48] proposes a range of values for the the design parameters as discussed in Section 4.6.

Table 7: Model parameters as proposed by Stapersma [48]

Model parameters	Range
ψ_0	0.3 - 0.5
x	2 - 4
y	0.3 - 1.5
Ma_0	0.4 - 0.7

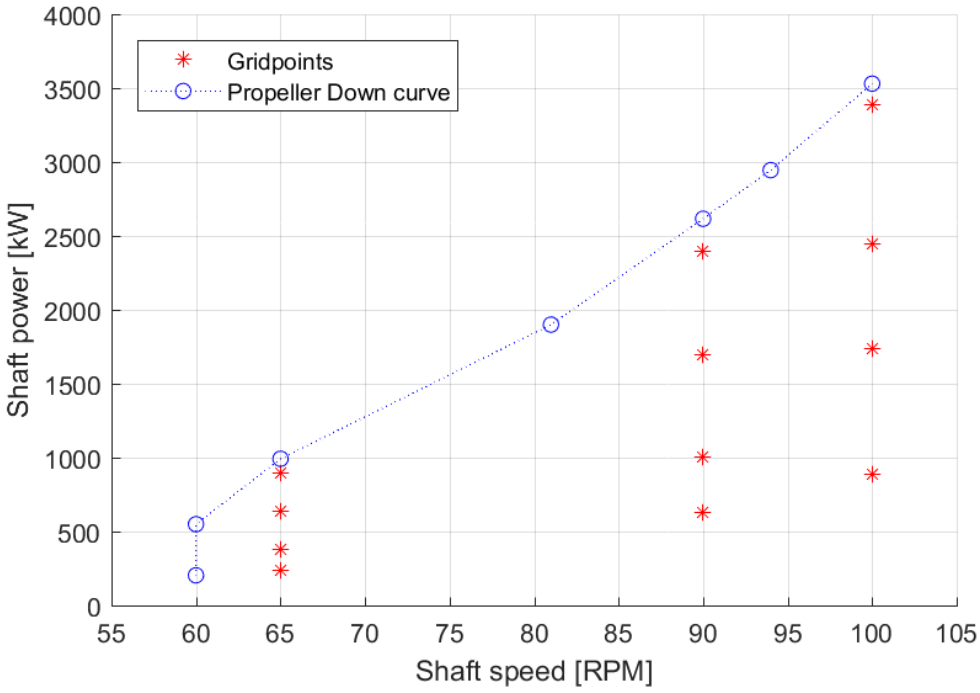

Figure 41: Data set from measurements aboard Zr. Ms. De Ruyter May, 2017

A convenient way to find design parameters is to use an optimization algorithm as described in Papalambros et al. [37]. This optimization problem is quite simple so a simple method was

used. In order to find a set design parameters Matlab was used to calculate an extensive set of possible combinations. The result for each set of parameters was compared with the measured data using the normalized mean squared error as shown in equation (4.41).

$$NMSE = \sum_{i=1}^{n} \left(\frac{\dot{m}_{model(i)} - \dot{m}_{measured(i)}}{\dot{m}_{measured(i)}} \right)^2 \tag{4.41}$$

An example of the optimization results can be found in Figure 42. For each set of design parameters the NMSE of the dataset is shown. The graphs show that some of the parameters converge to an interior minimum characterised by the parabolic shape of parts of the NMSE function. It can also be seen that some parameters converge to the boundaries, indicating that the optimum is on the boundary of the design space.

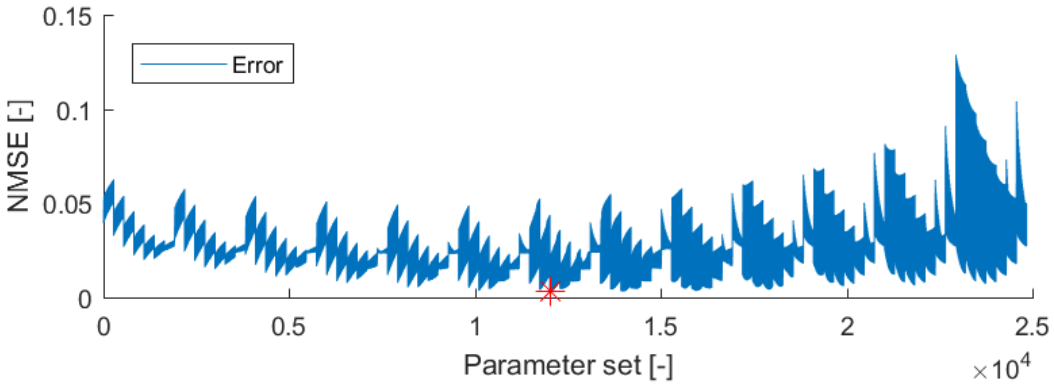

Figure 42: Propeller curve model: $\psi_0 = 0.6, M_{a,0} = 0.50, x = 2.00, y = 0.30 \quad matchpoint = 5$

After the optimization procedure, the design parameters which result in the smallest NMSE are used as input for the compressor model to see how the model performs. First a single dataset is used as model input, and then as input for the optimization algorithm. The results for the propeller curve can be seen in Figure 43.

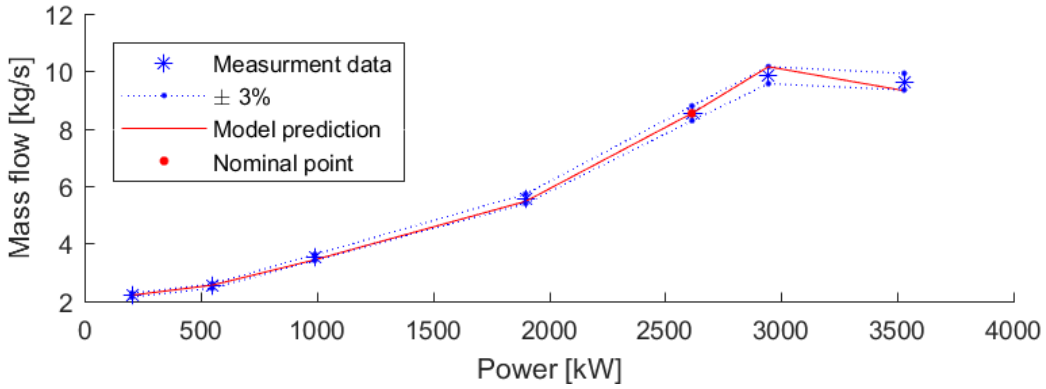

Figure 43: Propeller curve model: $\psi_0 = 0.6, M_{a,0} = 0.50, x = 2.00, y = 0.30 \quad matchpoint = 5$

The model predictions are within a three percent bandwidth from the measured data. The nominal point is indicated with a red dot. Since the compressor has to supply the required airflow at nominal engine load the nominal point was estimated to be the upper mass flow regions. Further, at the last three data points the engine was running in two turbocharger operation mode. Therefore, in order to match the compressor the mass flow of these points was divided by two. After matching, the predicted values from the model were multiplied by two to make a comparison with the measurements.

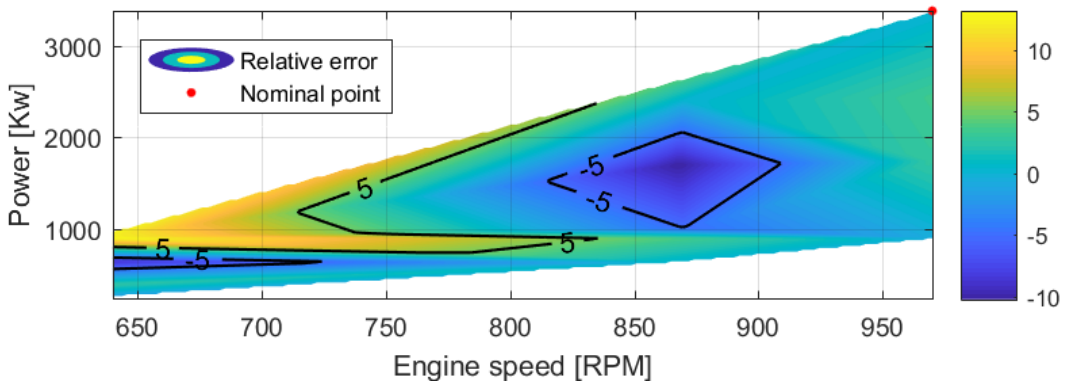

(b) $\psi_0 = 0.30, M_{a,0} = 0.6, x = 2.00, y = 0.30 \quad matchpoint = 3, 4$

Figure 44: Matching results of the compressor for various nominal points

The procedure for the propeller curve can be repeated for a grid of measurement points as indicated by the stars in Figure 41. The advantage of a grid is that the data points are wider spread, therefore the matching procedure should give better results. Further, the data gives information about the compressor performance when the engine is not operated at the propeller curve.

The results for the grid data can be seen in Figure 44. As by the propeller curve the nominal point is estimated to lay in the upper right region of the grid, since the compressor has to supply the air flow at nominal engine load. Further, the data between the measurement points is linear interpolated in order to construct a complete map. Linearisation will probably introduce an error because the mass flow is not actually linear depended of power or engine speed. For example, the horizontal increase in relative error just below 1000 kW shaft power is presumably an effect of the linearisation. Also the diamond shaped minus five percent boundary is presumably an effect of the linearisation. However, the error due to the linearisation process are not transferred to the actual model. Although, as an result of the introduced error a non optimal set of parameters could be chosen for the model.

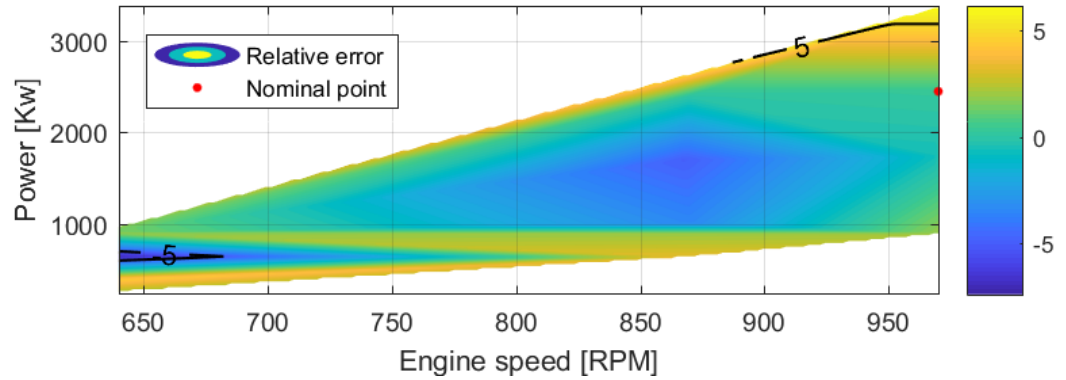

(a) $\psi_0 = 0.30, M_{a,0} = 0.55, x = 2.00, y = 0.70 \quad matchpoint = 3, 3$

These results give confidence that is is possible to match a compressor map on a limited amount of ship data. However, also a compressor map was available from the W26 engine as depicted in Figure 45.

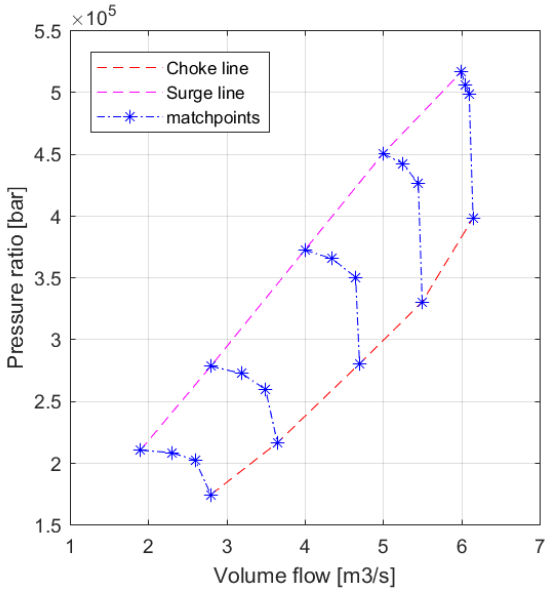

Figure 45: Compressor map reading form the actual compressor of the W26

These let to the matching as depicted in Figure 46. It can be seen that the matching more off on the right side of the map, this is presumably caused by the small spread of the data points at high flow rates.

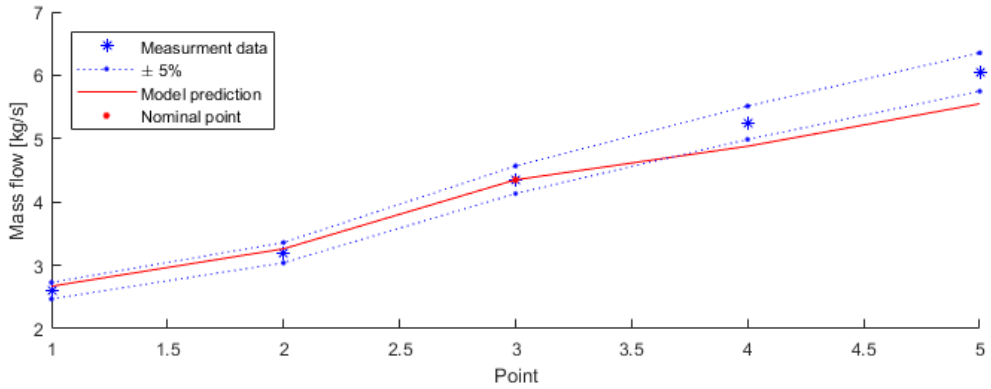

Figure 46: Propeller curve model: $\psi_0 = 0.9, M_{a,0} = 0.30, x = 2.00, y = 1.30 \quad matchpoint = 3$

4.8.2. Conclusion on the map matching

The matching of compressor map with a compressor model is a time consuming process. If more effort and research is put into the matching process it might be possible to match the compressor model even better than it is now. Further, the measurements aboard an actual ship, on an actual engine are also a challenge as explained in Section 5. Despite these barriers, it was possible to match the compressor model to the measured data mostly within a five percent error. The results are slightly influenced by the fact that limited data points are available to construct a complete map. This was solved by linearly interpolating the measurement data over the map which clearly introduces errors. Further, it was seen that during the optimization procedure a few parameters converged to the boundaries of the design space. It would be interesting to investigate how the current boundaries are motivated and whether it is feasible to broaden the design space. Summarizing, the compressor model performers reasonably good and the objective of implementing a compressor model was to acquire a tool to investigate various charge air concepts. This objective is accomplished with the annotation that the optimization process, the choice of the nominal point and the matching parameters is only superficially investigated.

Because the measurement results were questionable at some points, it was decided use the actual compressor map to match the general compressor map. The results as presented in Figure 46 were implemented in the compressor model.

4.9. Turbine model

The turbine plays a crucial role in the turbocharger by supplying the power to drive the compressor. The turbine is driven by exhaust gases leaving the cylinders consisting of the mass flow of reacted air which entered the engine plus the mass of the added fuel. Similar to the approach of the compressor modelling, the turbine can be modelled based on a map or by means of a mass and energy balance. The turbine is moddeled as an simplified swallow characteristic as proposed by Stapersma [46] and seen in equation (4.42). The assumption that ψ only depends on pressure can be justified by taking a look at Figure 47. It can be seen that compressor speed hardly plays a role in the swallow capacity.

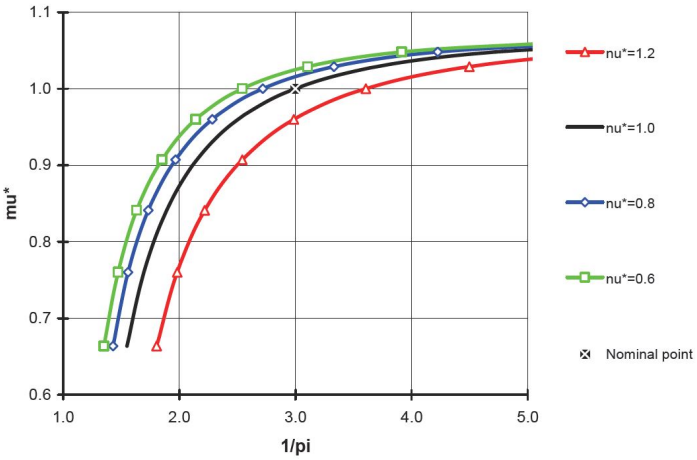

Figure 47: Turbine swallow characteristic [46]

Further, in order to allow for STC or VGT to be modelled, the effective are $A_{tur,eff}$ can be varied by means of equation (4.43) as explained by Geertsma et al. [13]. $A_{tur,eff}$ is changed in accordance with the number of turbochargers engaged relative to the number of turbocharger engaged at nominal speed. $A_{tur,eff}$ is determined with the nominal performance value and the pressure in the exhaust receiver as proposed in work of Geertsma et al. [12].

$$\dot{m}_{tur} = A_{tur,eff} \cdot \frac{p_{or}}{\sqrt{R_{or} \cdot T_{or}}} \cdot \psi(\pi_{tur}) \tag{4.42}$$

$$A_{tur,eff} = A_{tur,eff,relative} \cdot A_{tur,eff,normal} \tag{4.43}$$

where $A_{tur,eff}$ is the effective turbine area in $[m^2]$ and ψ the flow coefficient. from here the turbine characteristic can be simplified further to the mass flow formula for isentropic flow through a nozzle as proposed by Dixon [8]:

$$\psi = \sqrt{1 - \left(\frac{1}{\pi_{tur}}\right)^{f}} \qquad with: f = 2 \tag{4.44}$$

The specific power model is using a constant isotropic efficiency and thermodynamic relations for poly tropic expansion. The turbine exit temperature T_{ex} is determined from the exhaust receiver temperature T_d, using the isentropic turbine efficiency $\eta_{tur_{is}}$ and specific heat loss q_{hl} in kJ/kg, as described by Geerstma et al. [12]:

$$T_{ex_{is}} = T_d \left(\frac{p_{ex}}{p_d}\right)^{\left(\frac{\kappa_g - 1}{\kappa_g}\right)} \tag{4.45}$$

$$T_{ex_{id}} = T_d + \eta_{tur_{is}}(T_{ex_{is}} - T_d) \tag{4.46}$$

The isentropic turbine efficiency $\eta_{tur_{is}}$ is determined as:

$$\eta_{tur_{is}} = \frac{T_{ex_{id}} - T_d}{T_{ex_{is}} - T_d} \tag{4.47}$$

The specific heat loss q_{hl} is considered to be linearly dependant on the power of the turbine:

$$q_{hl} = P_{tur} \cdot \eta_{hl,nom}, \tag{4.48}$$

where $\eta_{hl,nom}$ the heat loss coefficient is taken as a constant. Geertsma et al. [12] has found a better way to implement this, however, this was not implemented in the model.

With the heat loss known, the turbine exhaust temperature T_{ex} can be calculated:

$$T_{ex}(t) = T_{ex_{id}} - \frac{q_{hl}}{c_{p_g}} \tag{4.49}$$

where $T_{ex_{is}}$ is the isentropic turbine exhaust temperature, and $T_{ex_{id}}$ is the ideal turbine exhaust temperature, including turbine losses without heat loss.

Wit the turbine outlet temperature known, the specific work of the turbine yields:

$$w_{tur} = \cdot c_{p_g} \cdot (T_d - T_{ex_{id}}) \tag{4.50}$$

Finally, combining the mass flow and the specific work the turbine power can be calculated:

$$P_{tur} = \beta \cdot \dot{m}_{tur} \cdot w_{tur} \tag{4.51}$$

where β is the Zinner pulse correction factor as described by [46, 8.30]

4.10. Hybrid turbocharger

In this work a hybrid turbocharger is defined as a turbocharger with an electric machine coupled to the main shaft as seen in Figure 48. Hybrid turbochargers can be used for different proposes. The electric machine can work in generator mode, subtracting power from the turbocharger (PTO) or in motor mode, adding power to the turbocharger (PTI). The objective of PTO is to subtract additional energy from the exhaust gases. For example, to supply energy to the electric grid of the ship. The objective of PTI is to diminish the turbo 'lag' to improve transient behaviour and to increase the charge air pressure for the engine.

Figure 48: hybrid turbocharger schematic [14]

Hybrid turbochargers are part of the bigger group electrified turbocharger as depicted in Figure 49. This work scopes at concept (d). This was driven by the goal of improving the efficiency of the propulsion system and also the acceleration performance. This is not possible with concepts (a), (b) since these can only recover energy via the electric machine. Concept (c) is classified as electric supercharging and is therefore less interesting on the point of efficiency. Further, concept (e) was rejected because of the high power transfers in the turbocharger of marine diesel engines. This would result in complex en expensive system.

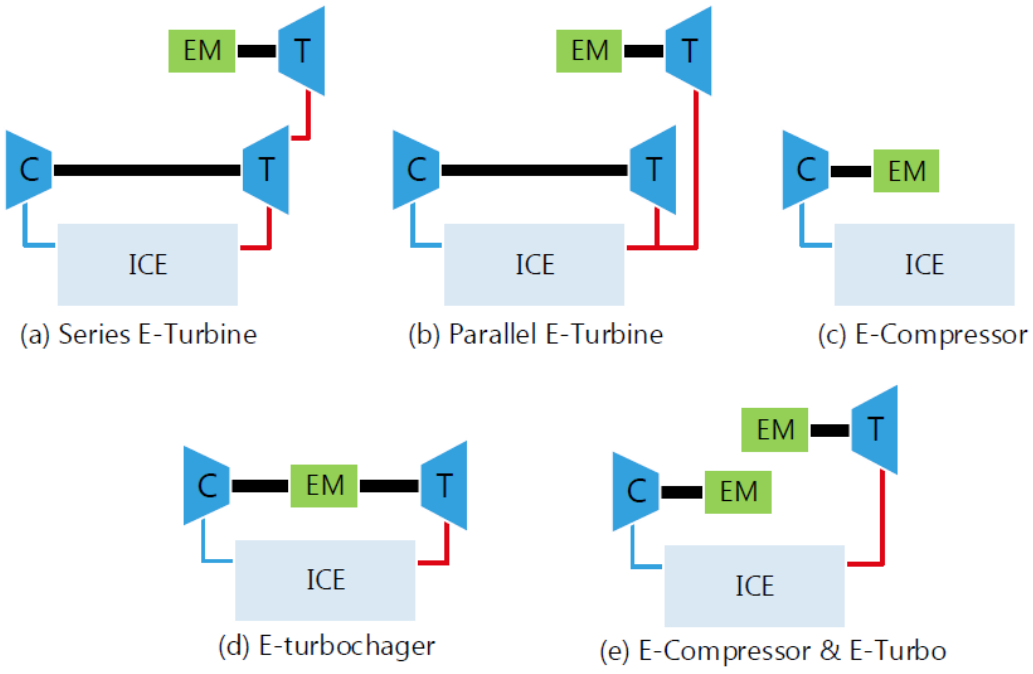

Figure 49: Electrified turbocharger configurations as investigated by [4]

As explained in Sections 4.3 and 4.4 the turbocharger is modelled as a power balance or based on the equations of motion. In order to implement the electric machine an extra power or torque input was added to the system as depicted in Figure 50. The system boundary for modelling the hybrid turbocharger is defined by the red dotted line. This means the electric machine is not modelled as an dynamic system. The interaction between the mechanical turbocharger and the electric machine is a very interesting topic, but in this research the emphasis lays on the overall performance of the configuration. In the overall performance of the system, the interaction between the electric machine and turbocharger can probably be neglected because of their relative small contribution in the overall performance.

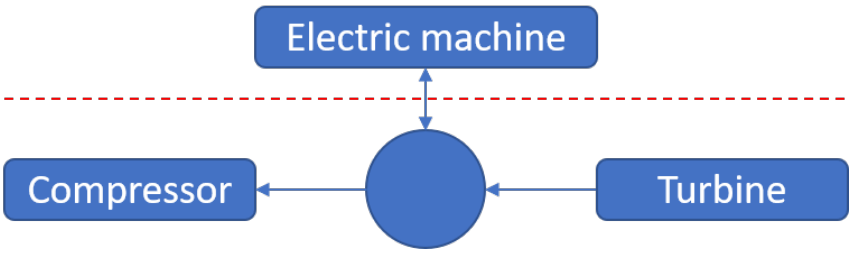

Figure 50: Electric machine turbocharger coupling

Since the electric machine dynamics are not taken into account, the system can be modelled as a control system for the power input to the power balance as seen in Figure 51.

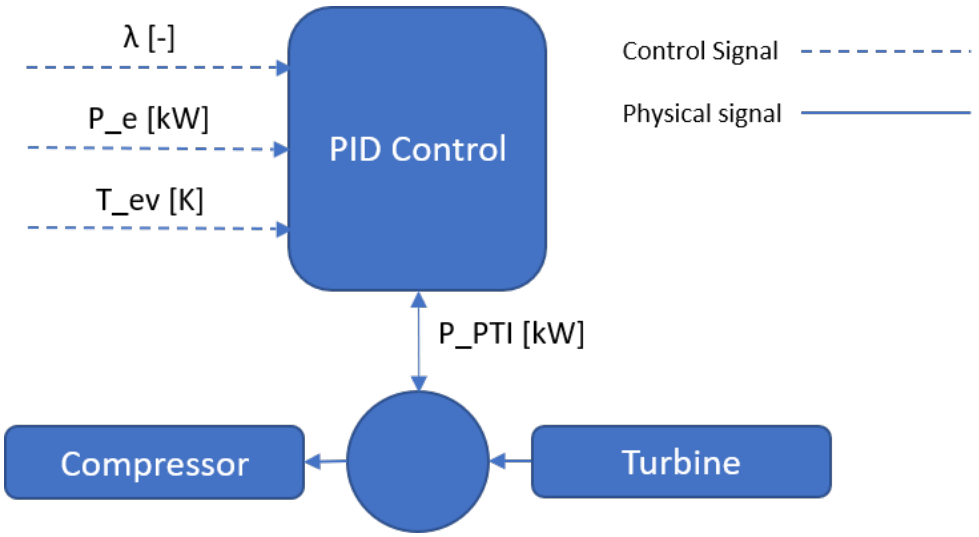

Figure 51: Control system

The control system uses 3 signals to determine the power input or output off the hybrid turbocharger.

- Air excess ratio λ [-]
- Exhaust valve temperature T_{ev} [K]
- Engine power P_e [kW]

The output of the system is P_{PTI} [kW] which can be either positive or negative.

The controller itself consists of a PID controller as depicted in Figure 52 and described by Franklin et al. [9]

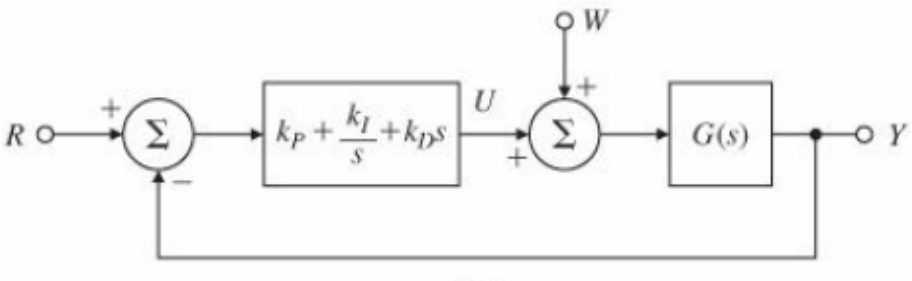

Figure 52: Schematic of a PID controller [9]

The air excess ratio as discussed in Section 3.6.4 is the leading control parameter. Normal operating value for the air excess ratio of a diesel engine are between 1.8 and 2.2. Therefore, it was decided to set the objective value for the air excess ratio to $\lambda = 2$. If the air excess ratio is above $\lambda = 2$, the system will take off power (PTO) from the turbocharger. If the value is under $\lambda = 2$ the system will supply power to the turbocharger (PTI).

In order to determine the nominal power of the electric machine connected to the hybrid turbocharger first the power through the normal turbocharger is investigated as seen in Figure 53.

It can be seen that almost 1800 kW is transferred from the turbine to the compressor in the nominal point. Based on the work of Shiraishi et al. [42] a machine with 200 [kW] nominal power was selected. This is about 10% of nominal turbo power and 5% of nominal engine power. The nominal power of the hybrid turbocharger was compared to the power of the non-hybrid turbocharger as depicted in 53b. It can be seen that ratio of power available from the hybrid turbocharger to the the power produced by the turbine is significant, especially at low engine loads.

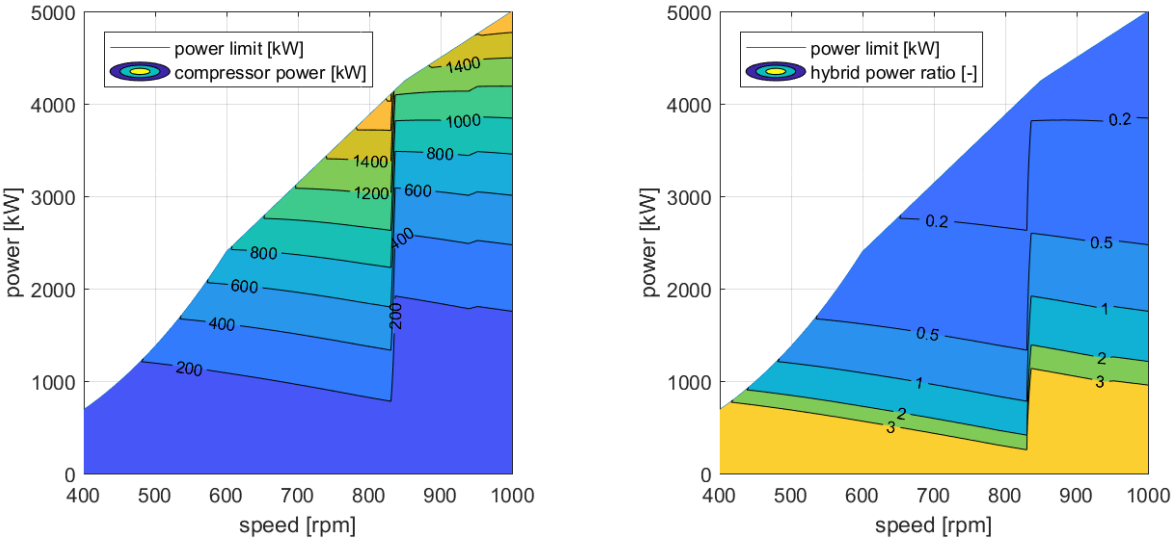

(a) Power transferred from the exhaust to the inlet via the turbocharger W26

(b) Ratio of additional power available from hybrid turbocharger

Figure 53: Power transferred from the exhaust to the inlet via the turbocharger W26

Since the speed of the particular turbocharger on the W26 is around 30.000 rpm at the nominal point the question raises whether these types of electric machines are feasible. The awnser was found in the work of Borisavljevic et al.[5] who investigated existing high speed electric machines in 2010. From Figure 54 is can be seen that an electric machine of 200 [kW] brake power and 30000 is feasible.

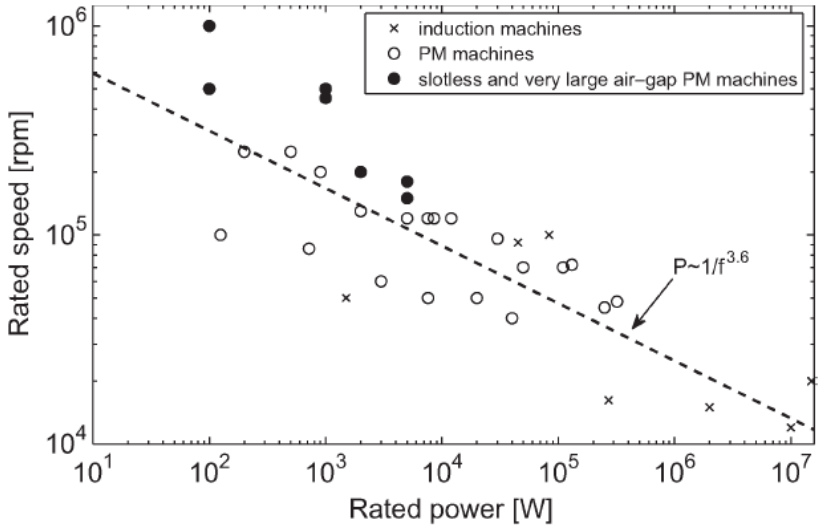

Figure 54: Diagram of rated speeds and powers of existing high-speed machines [5]

4.10.1. Power management

The power subtracted or supplied by the hybrid turbocharger can have different sources as depicted in Figure 55. The power from the hybrid turbocharger can be added to the propulsion shaft (a). It can be stored in a battery to be used later when power take in is required (b). Or it can be fed to the electric grid of the ship to be used as hotel load (c).

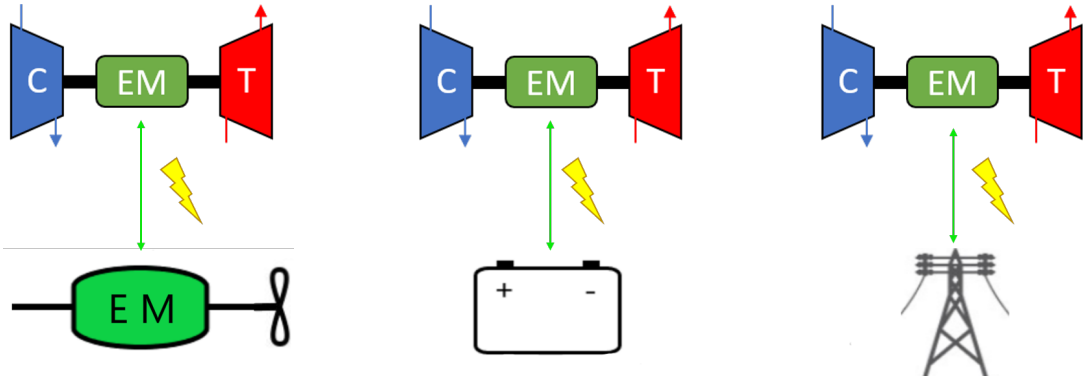

(a) Turbo Compounding (b) Battery storage (c) Use for hotel load

Figure 55: Different energy strategies

For the take in power it was assumed that is was either generated by the generators for the hotel load at 195 [g/kwh] or by the diesel engine at the fuel consumption point the diesel is using at the specific moment the power is required. Further a 10% electric loss for the converters, cables and the electric machine itself was taken into account.

4.11. Comparison between Büchi an Map turbocharger model

4.11.1. Calibration procedure

The calibration procedure for the W26-STC engine was based on the same method as the compressor map matching. A start value for the used parameters was determined either by FAT data, the project guide, physics theory or estimated. Then a number of simulations were performed while systematically changing a parameter set. The set which resulted in the smallest error was then determined. This was used a 'tool' during calibration, at the end the parameters were selected by hand.

This resulted in the parameters given in Table 8.

Table 8: W26 case study diesel engine model parameters from project guide (PG), physics theory (P), FAT data (F) or estimate (E).

Diesel engine parameter description	**value**	**source**
nominal engine power $P_{e_{nom}}$	5000 kW	PG
nominal engine speed $n_{e_{nom}}$	16.7 rev/s	PG
number of cylinders i_e	16	PG
number of revolutions per cycle k_e	2	PG
bore diameter D_B	0.26 m	PG
stroke length L_S	0.32 m	PG
crank rod length L_{CR}	0.64	PG
crank angle after TDC, inlet closure α_{IC}	225 °	PG
crank angle after TDC, exhaust open α_{EO}	107 °	[40]
nominal spec. fuel consumption $m_{bsfc_{nom}}$	206.01 g/kWh	F
geometric compression ratio ε_c	15.8	[40]
cylinder volume at state 1 V_1	0.0162 m^3	PG
nominal pressure at state 1 $p_{1_{nom}}$	3.72e^5 Pa	PG
maximum cylinder pressure $p_{max_{nom}}$	185e^5 Pa	F
isentropic compressor efficiency $\eta_{is,com}$	0.83	F
temperature after the intercooler T_c	323 K	F
temperature of the inlet duct T_{inl}	423K	E
intercooler pressure loss ratio	0.05	E
parasitic heat exchanger effectiveness ε_{inl}	0.02	E
turbocharger time constant τ_{TC}	7.9 s	E
turbocharger inertia I_{TC}	0.18 kgm^2	[40]
gas constant of air R_a	287 J/kgK	P
specific heat at constant volume of air $c_{v,a}$	717.5 J/kgK	P
specific heat at const. pressure of air $c_{p,a}$	1005 J/kgK	P
specific heat at const. p of exhaust gas $c_{p,g}$	1100 J/kgK	P
isentropic index of air κ_a	1.4	P
isentropic index of the exhaust gas κ_g	1.353	P
lower heating value of fuel h^L	42700 J/kg	PG
stoichiometric air to fuel ratio σ_f	14.5	PG
polytropic exponent for expansion n_{exp}	1.38	E
polytropic exponent for blowdown n_{bld}	1.35	E
nominal mechanical efficiency $\eta_{m_{nom}}$	0.85	E
constant volume portion gradient $X_{cv_{grad}}$	-0.2761	E
constant temperature portion $X_{ct_{nom}}$	0.1104	E
ambient pressure p_{amb}	1e^5 Pa	PG
ambient temperature T_{amb}	318 K	PG

4.11.2. Calibration results

After calibration the diesel engine model was compared with the FAT data. The model is run at the power and speed settings corresponding to the FAT. The results are depicted in Figure 56 and 57. Both the Büchi model and the equation of motion based model were investigated.

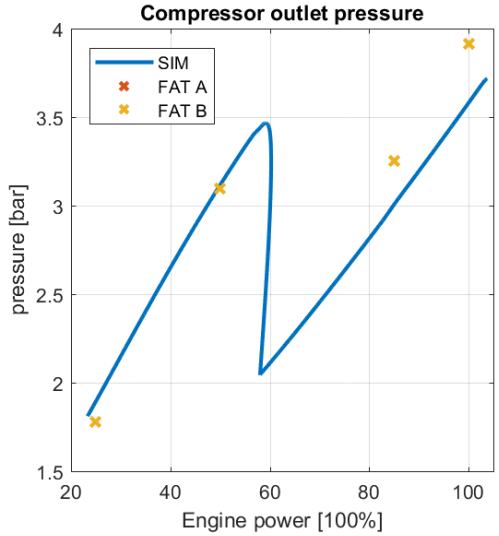

(a) Büchi based model - Compressor outlet pressure [bar]

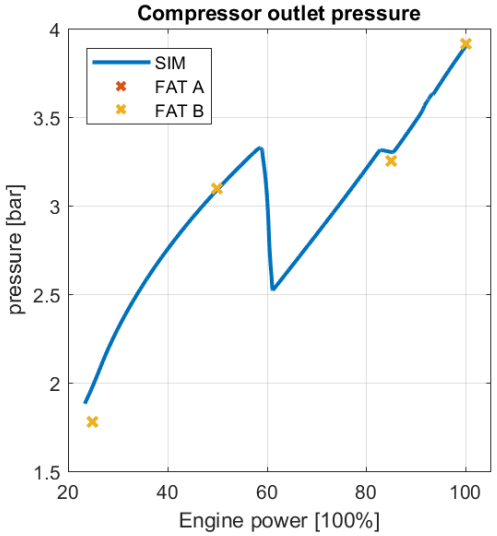

(b) Motion based model - Compressor outlet pressure [bar]

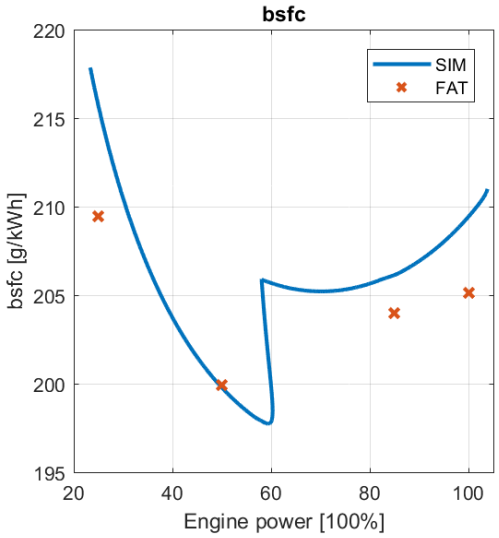

(c) Büchi based model - Fuel consumption [g/kwh]

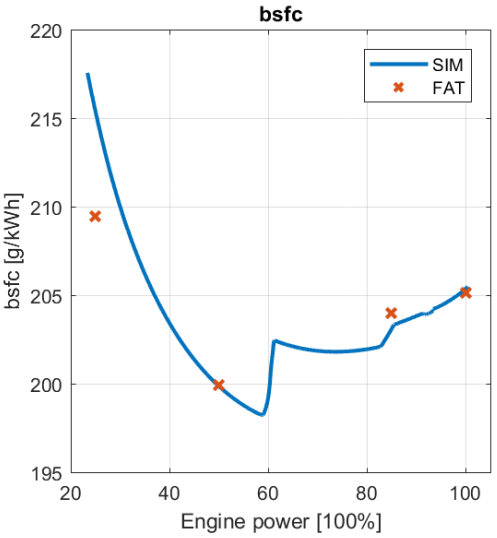

(d) Motion based model - Fuel consumption [g/kwh]

Figure 56: Model predictions of the bsfc [g/kWh] and charge pressure [bar] the Büchi based model (left) and motion based model (right)

For the charge air pressure it can been seen that the motion based model clearly gives the best results. Especially the closure of the bypass valve around 80% power is captured much better. This can probably be explained by the more physical correct model as explained in Section 3 and Section 4. Further, it can be seen that the model prediction of the charge air pressure of the Büchi based model is below the FAT data after switching from one to two turbochargers. Therefore, it can be concluded that in terms of charge air pressure prediction the map based approach is preferred.

The fuel consumption prediction of both models is well within 5%. Again, the map based model seems to capture the closure of the bypass valve better. Both models perform satisfactory.

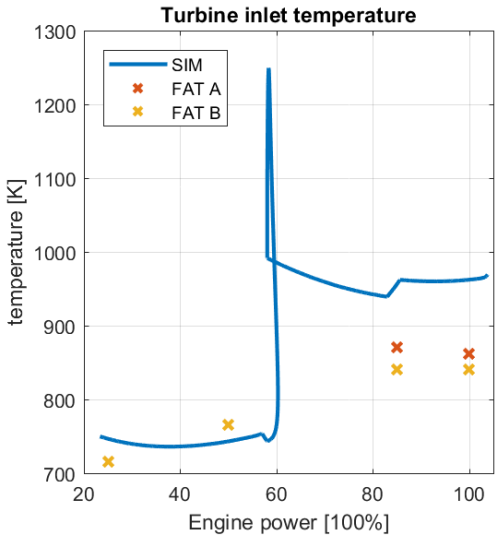

(a) Büchi based model - Turbine inlet temperature [K]

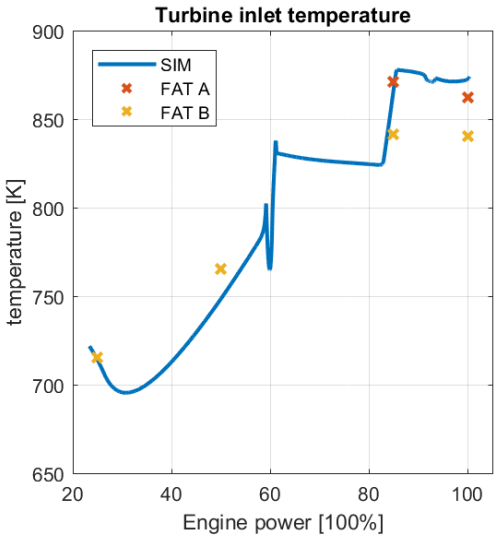

(b) Motion based model - Turbine inlet temperature [K]

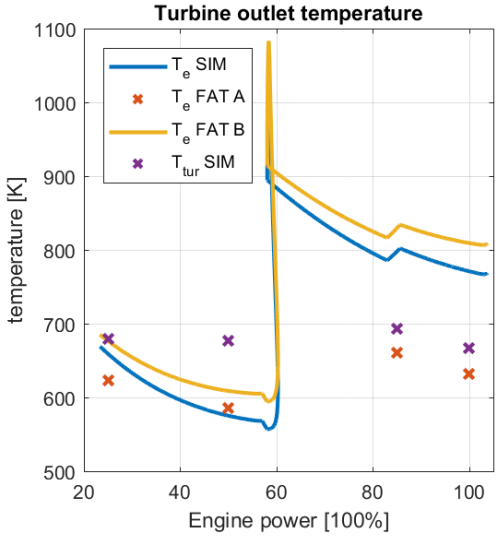

(c) Büchi based model - Turbine outlet temperature [K]

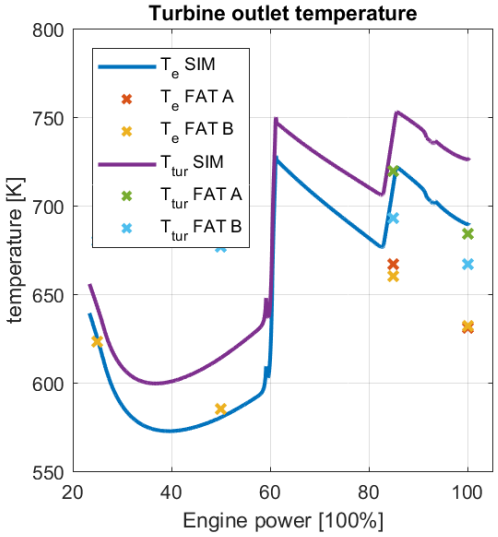

(d) Motion based model - Turbine outlet temperature [K]

Figure 57: Model predictions Turbine inlet and outlet temperature [K]

In Figure 57 the validation results of the turbine are depicted. The turbine validation was difficult because the FAT data did not consist of any pressure measurements before the turbine. Therefore, is was not possible to verify the model predictions for the turbine inlet pressure. It is interesting to see that the model predictions of the Büchi model for the turbine outlet temperature are over estimated in two turbocharger operation. This is probably the cause of the underestimation of the charge air pressure.

4.12. Conclusion

Compressor models

Three methods of compressor modelling were investigated. A power balance based on the Büchi equation and two methods to construct a general compressor map. The power balance based on the Büchi equation is a very simple and strait forward way modelling the turbocharger. The map approaches require more theoretical knowledge of turbo machinery and are harder to implement. In order to adapt model for torque input on turbocharger shaft, speed dependent compressor

model was required. The power balance approach is not suitable for this. Therefore, it was decided to put effort in the map approaches. This should be regarded as a tool to accomplish the main questions of the thesis instead of a goal on its own. Since the model as proposed by Stapersma [48] is detailed described, this one is chosen to be investigated further.

Map matching

The matching of compressor map with a compressor model is a time consuming process. If more effort and research is put into the matching process it might be possible to match the compressor model even better than it is now. Further, the measurements aboard an actual ship, on an actual engine are also a challenge as explained in Section 5. Despite these barriers, it was possible to match the compressor model to the measured data mostly within a five percent error. The results are slightly influenced by the fact that limited data points are available to construct a complete map. This was solved by linearly interpolating the measurement data over the map which clearly introduces errors. Further, it was seen that during the optimization procedure a few parameters converged to the boundaries of the design space. It would be interesting to investigate how the current boundaries are motivated and whether it is feasible to broaden the design space. Summarizing, the compressor model performers reasonably good and the objective of implementing a compressor model was to acquire a tool to investigate various charge air concepts. This objective is accomplished with the annotation that the optimization process, the choice of the nominal point and the matching parameters is only superficially investigated. Because the measurement results were questionable at some points, it was decided use the actual compressor map to match the general compressor map. The results as presented in Figure 46 were implemented in the compressor model.

Calibration

Given the limited amount of FAT data that was available it can be concluded that the Calibration results are satisfactory. Both models track the bsfc within 5% of the FAT data. For the charge air pressure, the buchi power balance model is slightly off on two turbocharger operation. This should be taken into account when validation the model with measurement results. For the turbine it was difficult to draw conclusions because the pressure ratios over the turbine were not included in the FAT data. In conclusion it is expected that both the motion based model and the buchi based model give a good prediction for the overall configuration. However, if the turbocharger dynamics play an important role, it is advised to use the motion based turbocharger model.

5

Measurements Zeven provincien-class

Theoretical models are very useful, but it is important to keep track off how good they represent the real world. In this section, a measurement campaign held aboard a ship of the Royal Netherlands Navy will be analysed.

5.1. Introduction

In may 2017 Zr. Ms. De Ruyter was scheduled to take part in an emission measurement campaign. This offered the opportunity to expand this campaign with a extensive measurement of the diesel propulsion system in order to validate model predictions for the propulsion plant.

Zr. Ms. De Ruyter is equipped with an CODOG configuration as seen in Figure 59. The propulsion plant consists of two shaft lines, each consisting of a Wartsila W26-STC diesel engine, a Rolls Royce Spey SM 1A gasturbine and a gearbox.

During a week at the north sea, various measurement runs were performed. A large amount of data was collected, however, only the data which was used for validation of the measurements will be presented here.

Figure 58: Zeven provinciën class frigate Zr. Ms. De Ruyter of the Royal Netherlands Navy [23]

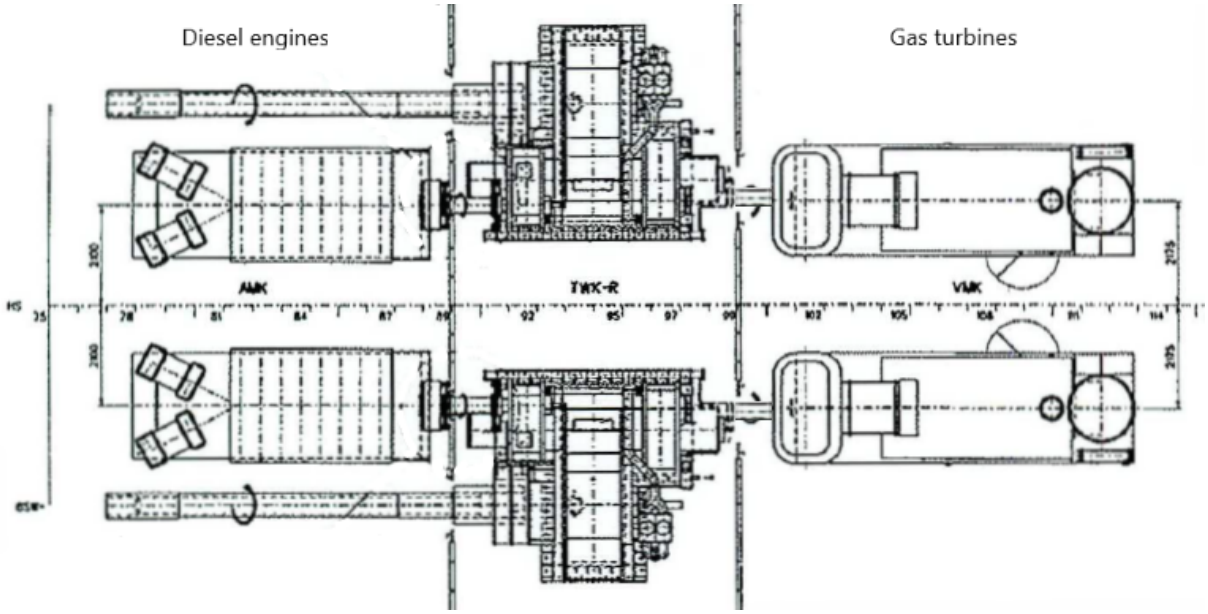

Figure 59: Configuration of Zr. Ms. De Ruyter

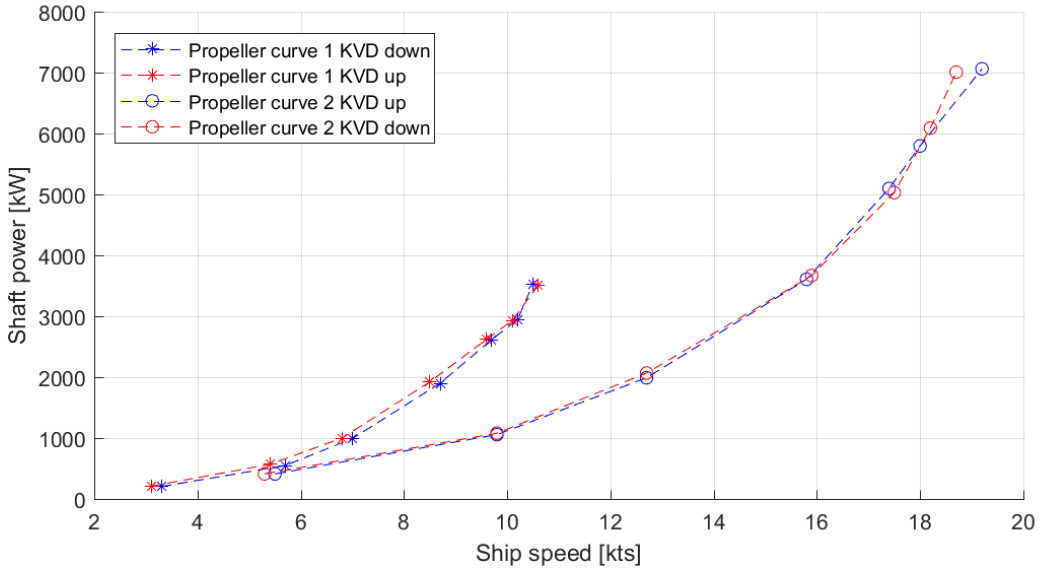

(a) Propeller curves

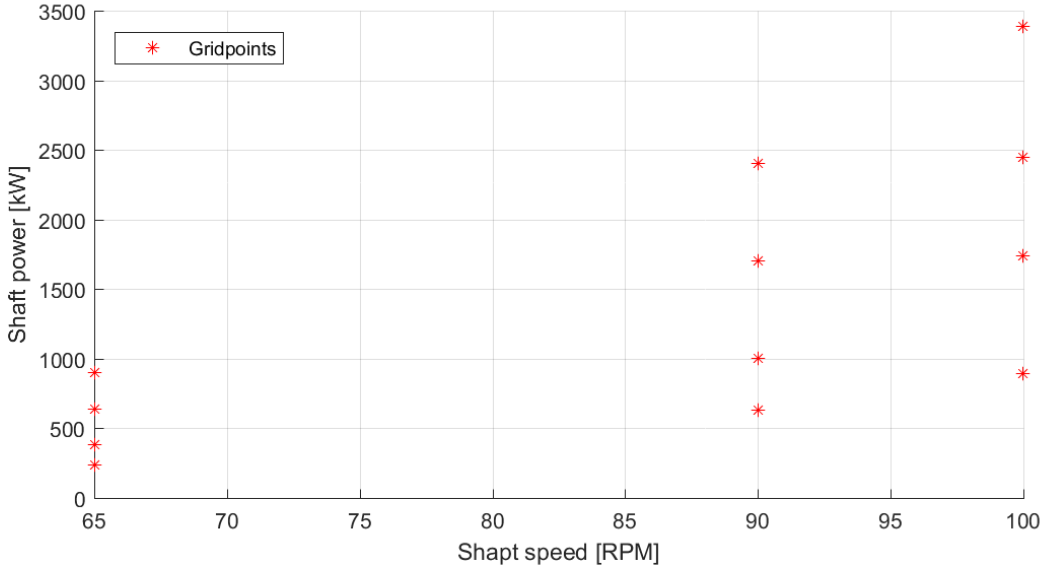

(b) Grid points

Figure 60: Measurements aboard Zeven Provincien class, May 2017

Figure 60 shows the measurements on the propeller curve and the grid points. The propeller curve measurement was measured in upward direction and in downward direction. Two propeller curves have been measured, with one shaft line engaged and with both shaft lines engaged. Between each measurement point the system was given 15 minutes to stabilize before the measurements were actually taken. The stable state was determined by observation of the fuel rack position and the torque fluctuation in the propeller shaft. Further, a grid was measured by taking control of the propulsion system in 'hand electric mode' which enables the operator to set the pitch of the propeller and shaft speed instead of using a combinator curve.

5.2. Measurement equipment

In this section the measurement equipment used aboard Zr. Ms. De Ruyter will be discussed briefly.

Fuel flow measurements

The fuel flow measurements were performed with an Coriolis mass flow meter. The meters are permanently installed aboard. Both the fuel feed and the return feed is measured resulting in the fuel consumption in $[kg/hr]$. The measuring principle is based on the controlled generation of Coriolis forces.

(a) Proline Promass 40E

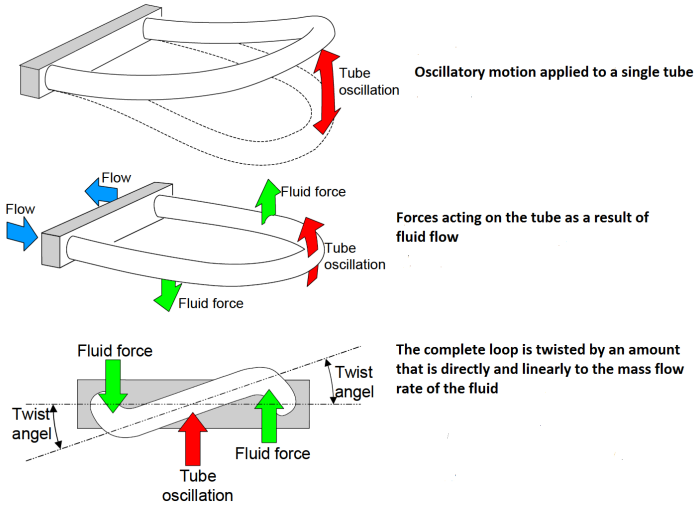

(b) Coriolis effect [1]

Figure 61: Mass flow measurement equipment

5.2.1. Emission measurements

Emission measurements are performed using the Horiba PG-350E portable gas analyser. The sampling is performed with a M & C PSP4000 gas sample probe. The probe was placed in the exhaust channel after the turbine. The measurement of NO is done using a Fluid Modulation and Chemiluminescence type Analyser. The NO is oxidized to an excited state ($NO_2^\star$) of NO_2 by a reaction with ozone O_3. The change to its ground state radiates light which can be measured.

$$NO + O_3 \rightarrow NO_2^\star + O_2$$
$$NO_2^\star \rightarrow NO_2 + light$$

In the low concentrations of NO found in the flue gasses, the radiated light is proportional to the NO concentration. To measure NO_x, the NO_x is first converted to NO. The analyser can at any time only measure NO or NO_x. The concentrations of CO and SO_2 are measured using a 'fluid modulation and infrared absorption'-type analyzer. Molecules consisting of different atoms can absorb infra-red rays in a specific wavelength region. The absorption of infra-red light corresponds with the concentration. The amount of transmitted light is attenuated by the amount absorbed and reaches the detector. [30]

5.2.2. Torque and power measurements

The torque and speed of both propeller shafts were measured as depicted in Figure 62. The measuremnts were taken by an external company: Techno Fysica B.V. The torque was measured by use of strain gauges. Strain gauges deform as a result of the applied torque on the shaft. The shaft speed was measured by an optical sensor, which counts a marker on the shaft. The system saves the speed an torque measurements separate and then calculates the power transferred by

the shaft. The measurements are sampled with 100 $[Hz]$ and are averaged over 10 samples. The measurement has a precision higher than 98.5% according to Techno Fysica B.V. [29]

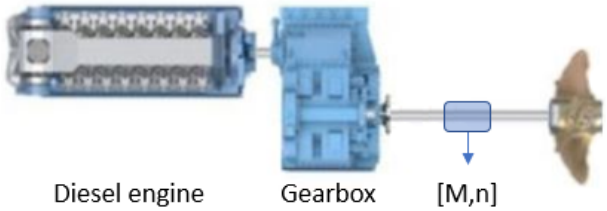

Figure 62: Torque en speed measurement aboard Zr. Ms. De Ruyter [52]

5.3. Validation

Validation is defined as the process of determining the degree to which a model is an accurate representation of the real world from the perspective of the intended uses of the model. [54]

In order to compare the model predictions with the measurement results the model has to be adapted slightly. First of all, the power measurements where performed on the propeller shaft as explained in Section 5.2.2. Therefore, the losses induced by the gearbox and the shaft bearings have to be taken into account. For the Zeven provinciën class, the losses are calculated by the shipyard that build the ship (Schelde groep) and can be found in Appendix A.2.

Further, the operating envelope of the W26-STC is incorporated in the diesel model as explained in Figure 63.

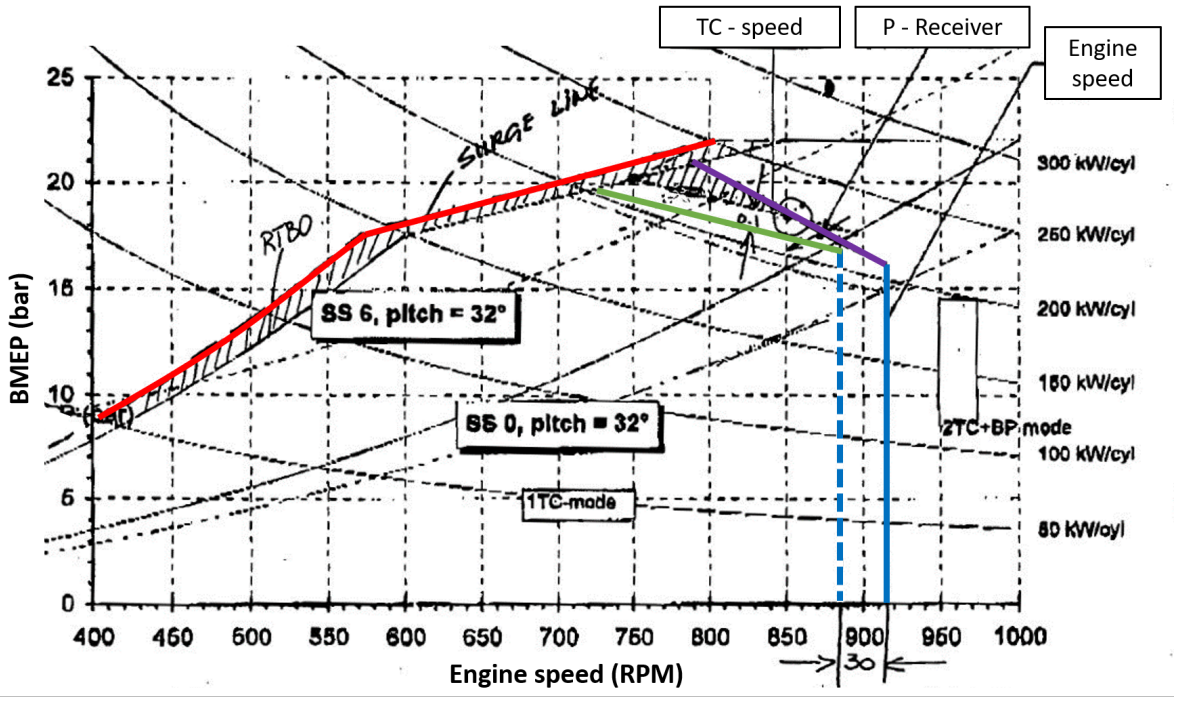

Figure 63: Operating envelope of Zr. Ms. De Ruyter

The operating envelope of the W26-STC as installed aboard the Zeven provincien class frigates is depicted in Figure 63. The switching parameters for the single or two turbocharger operation are engine speed, inlet receiver pressure and turbocharger speed. In order to avoid excessive switching hysteresis for switching is taken into account. However, from operational experience it is known that currently the control of the switching is not sufficient to use the operating envelope freely.

Further it can be seen that up till 600 rpm the air limit is bounded by the air limit curve which is taken here as a third power between 400 and 600 rpm. Between 600 rpm and 850 rpm the engine follows a boundary which is also determined by the air limit (surge). From 850 rpm to 1000 rpm the engine is limited on maximum torque. Also, the combinator curve for seastate 0 and 6 and pitch 32 deg can be seen.

5.3.1. Validation results

Fuel consumption [g/kWh]

Figure 64 shows the operating envelope with the model predictions for the break specific fuel consumption in [g/kWh]. Also, seven measurement points along the propeller curve are drawn in. At these seven measurement points the break specific fuel consumption predicted by the model is compared with the break specific fuel consumption as measured aboard Zr. Ms. De Ruyter.

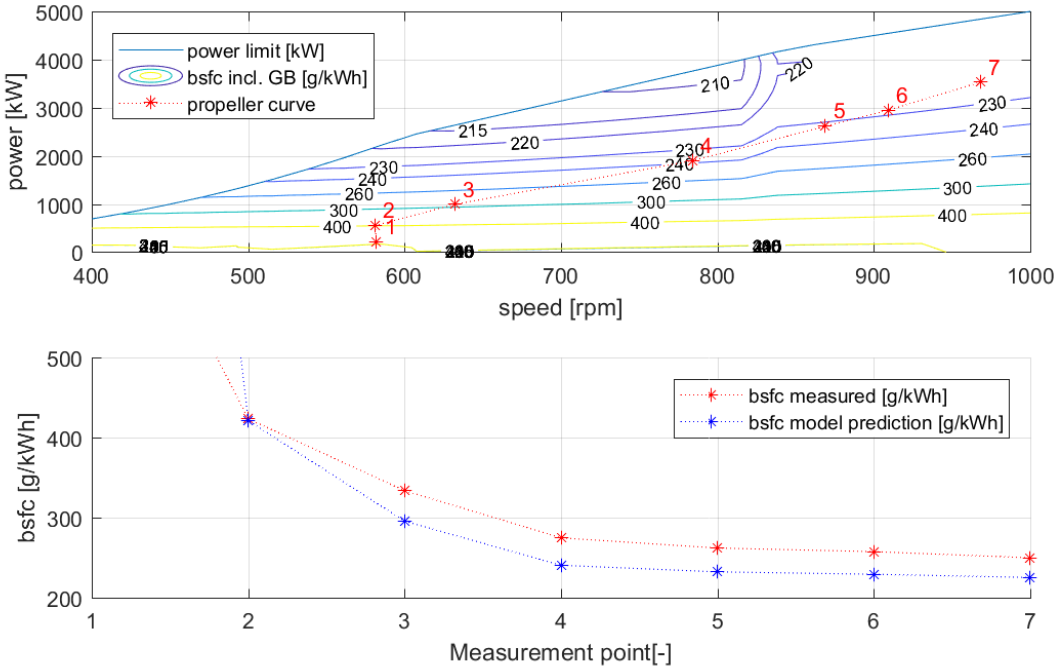

Figure 64: Bsfc [g/kWh] including gearbox and shaft losses

The first measurement point was taken just after coupling the diesel engine to the gearbox, meaning that only 204 kW of propulsion power was delivered to the propeller. Since the losses to effective power ratio is so high at this point, the bsfc is very high at around 1500 g/kWh. For convenience of the plot, point one is left out. Then, it can be seen that the bsfc at point two is in good accordance with the model prediction. From point two onwards the model has an offset of at point 3 off 38 [g/kWh] decreasing to 25 [g/kWh] at point 7. Which is quite significant.

The problem in investigating this error starts with the measurements itself. The power delivered by the engine was measured on the shaft between the gearbox and the propeller. Therefore, gearbox losses and shaft losses are included in the measurement. Although taken into account in the model, these losses add an extra uncertainty, especially because the gearbox is arranged to deliver the 18 MW of the gas turbines to the propeller shaft. The connection between the diesel engine and the gearbox is made of carbon fibre material and therefore, the material is not isotropic. The measurement method as used on the propeller shaft is therefore not applicable and it was not possible to measure the power output of the engine directly.

Another cause of the offset could be a measurement error in the fuel mass flow measurement. The fuel mass flow measurement results seem consistent as seen in Figure 65b however, this doesn't exclude a constant deviation due to a calibration offset.

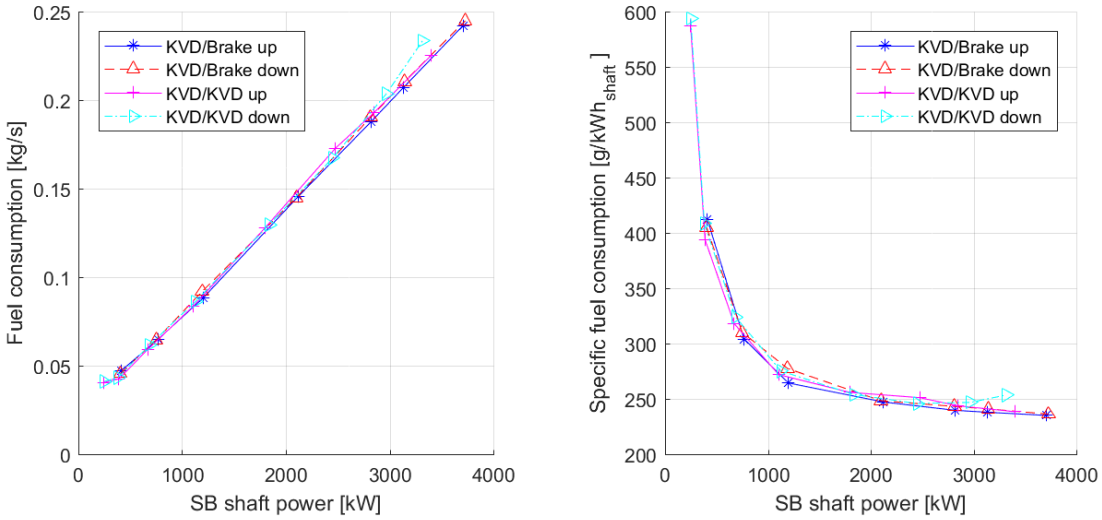

(a) Fuelflow [kg/s] (b) Bsfc [g/kWh]

Figure 65: W26-STC fuel measurement

Another aspect that has to be taken into account is the calibration data. The diesel engine model was calibrated on the FAT data, which is measured at the factory site before engine delivery. This specific engine is almost 20 years old. Although not further investigated, it is assumable that the engine does not meets its initial specifications any more. The performance degradation of diesel eninges can be associated with wear and fouling during operation. Kökkülünk et al. [28] did measurements aboard bulk carrier M/V Ince Inebolu which is fitted with a 6.5 MW two stroke diesel engine. Kökkülünk et al. [28] measured a total performance degradation of 20.9% which let to a bsfc increase of 26.74 [g/kWh]. The cause of the degradation was divided in two groups: the difference in measurement conditions with respect to the FAT data. For example, a higher ambient temperature or a change in injection timing. The second group is contributed to wear, ageing, deterioration and mechanical problems. The first group can be solved by periodic maintenance or a change in measurement conditions. The second group, is more permanent en could only be (partly) resolved by an very extensive maintenance overhaul. Both groups presumably played a role in the measurements aboard Zr. Ms. De Ruyter.

Concluding, the cause of the deviation could be a measurement error. However, it is likely that the calibration versus actual engine parameters played a big role. Also, the performance degradation of various components of either the shaft line or the engine are suspected to contribute. Unfortunately, it was not possible to pinpoint the exact cause.

Mass flow of air [kg/s]

Figure 66 shows the model prediction and measurement results for the mass flow of air through the engine. Three measurement sets are shown: first the calculation based on volume flow of O2 [%] and the calculation based on volume flow of CO2 [%] as proposed by Stapersma [47]. Also, the readings from the compressor map based on the measured inlet receiver pressure and turbocharger speed.

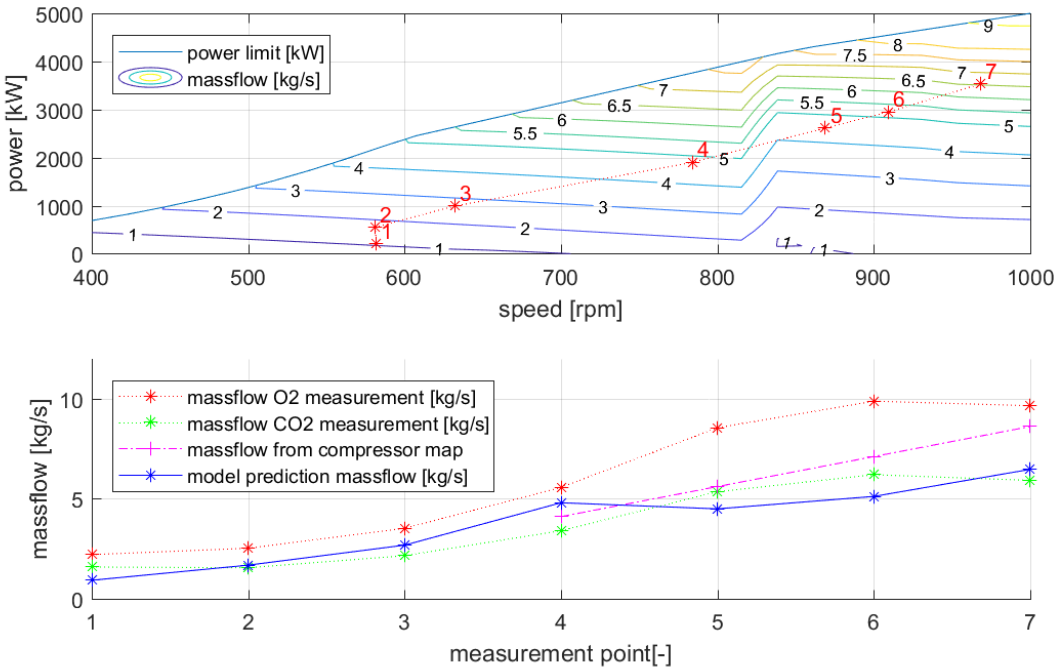

Figure 66: Mass flow [kg/s] through the engine

As seen in Figure 67 the measurements with regards to the O2 method and the CO2 method gave different results. The measured data for the volume flow of O2 and C02 is not so precise, especially the data sets measured on one engine operation have a big offset. Figure 67a and 67b show two outliers at 1000 kW shaft power. However, if these are removed, the data set on two engines is quite consistent. Further, a steep drop in O2 flow and a steep rise in CO2 flow can be seen. The sudden change in O2 and CO2 flow can be contributed to the opening en closing of the bypass valve on the engine. Due to addition of fresh air before the turbine, the volume flows of O2 and C02 change.

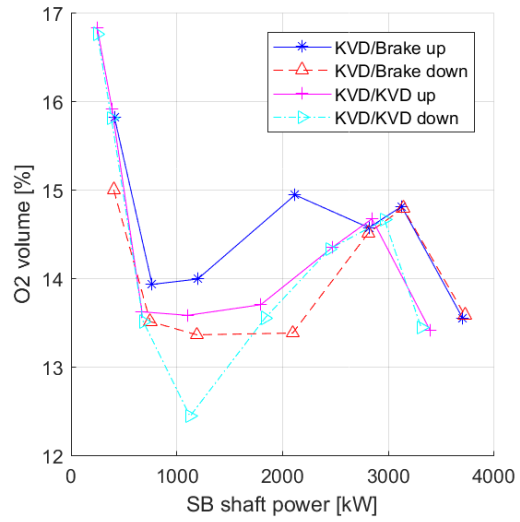

(a) W26 STC propcurve O2

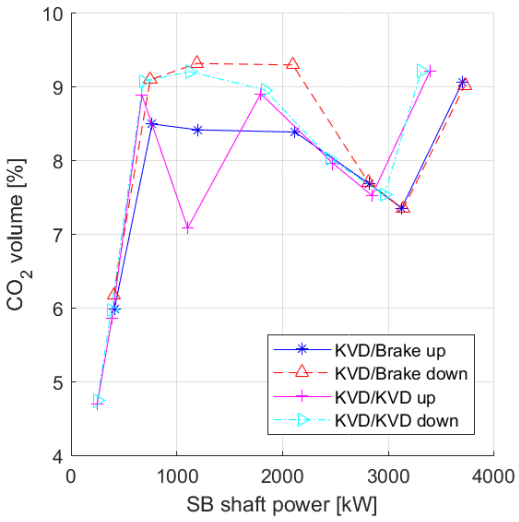

(b) W26 STC propcurve CO2

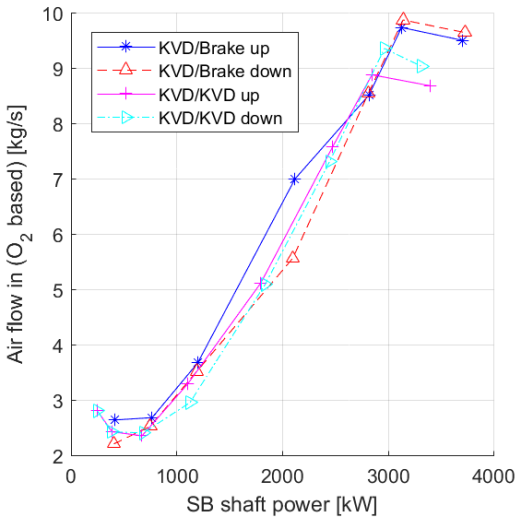

(c) W26 STC propcurve air O2

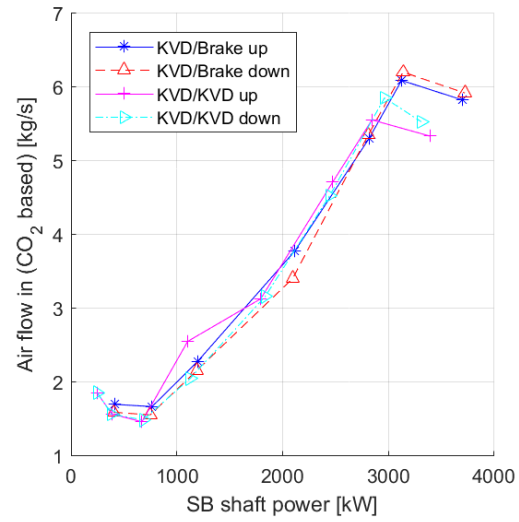

(d) W26 STC propcurve air CO2

Figure 67: W26-STC air flow measurement

If the mass flow based on the emission measurements is compared with the mass flow calculated based on the pressure measurement, turbocharger speed and compressor map the results of the CO2 method seem most reliable. Moreover, the values from the O2 measurement fall outside the compressor map after the switch point, and are therefore rejected. If the model predictions are then compared to the CO2 based mass flow calculation it can be seen that the model prediction is a bit low after the switchpoint. However, taking into account the calibration error in the charge pressure as seen in Figure 56a the low model prediction is explainable.

Charge air pressure [Pa]

Figure 68 shows the model predictions for the charge pressure in the inlet receiver.

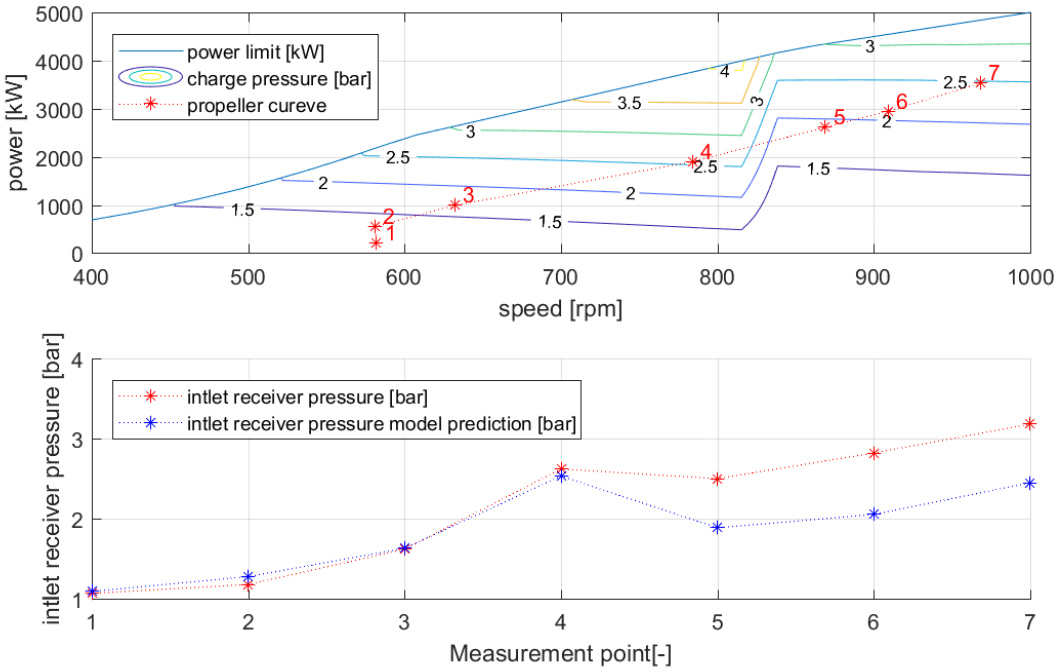

Figure 68: Charge pressure [bar]

The figure shows that the model prediction at the first four points slightly deviates from the measurements. After switching to two turbocharger operation (point 5) the pressure deviates significantly more. This is not totally unexpected since the FAT calibration of the model also showed an increase in error between the model and the FAT data at two turbocharger operation. The calibration error is around 0.25 [bar] as seen in Figure 56a, the resulting difference between the corrected model prediction and the measurement then becomes 0.25 [bar] or approximately 10%. Concluding, in two turbocharger operation the model prediction of the inlet receiver pressure is considerably lower than in measurements indicate. As a result, the model predictions of the mass flow and air excess ratio are also lower and the thermal loading is higher than in the actual engine.

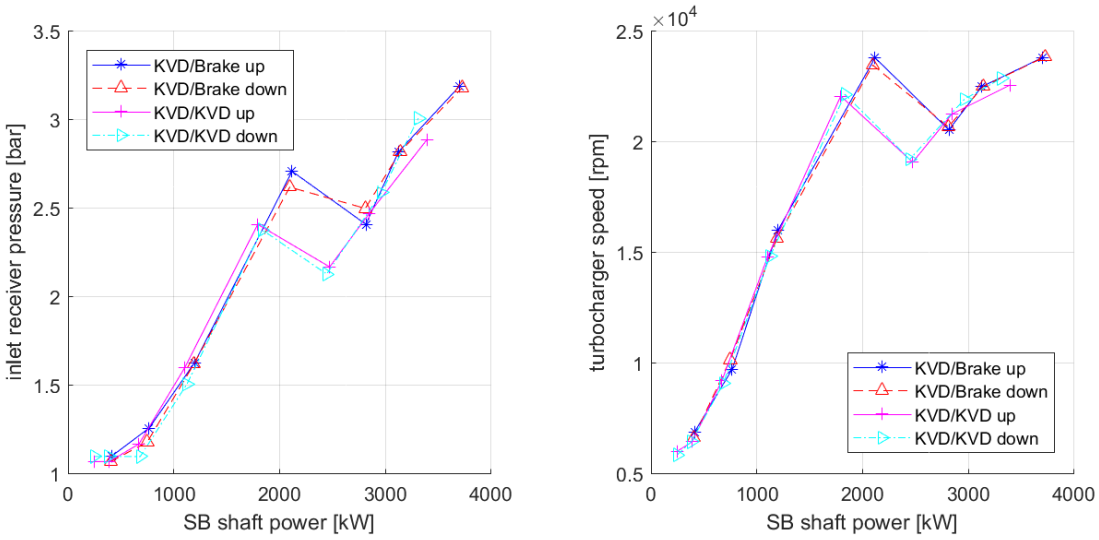

(a) W26 STC propcurve p IR

(b) W26 STC propcurve N TC2

Figure 69: W26-STC inlet receiver pressure and turbocharger speed

5.4. Conclusion

Although the measurement results give confidence in the models, especially the trends, a few phenomena encountered could not be explained sufficiently. The measurement results from the exhaust gasses showed quite some deviation. The calculations of the air mass flow resulting form the measurements show some of the deviations can be contributed to the change in measurement conditions. However, they also show an offset of around 4 [kg/s] which is very large. If the measurement data is compared with the compressor map data it can be concluded that the CO2 measurements are most logical to accept as the 'real' values. In two turbocharger operation the model prediction of the inlet receiver pressure is considerably lower than the measurements indicate. As a result, the model predictions of the mass flow of air and the air excess ratio are also lower than in the actual engine.

The fuel flow measurements showed a substantial measurement deviation from the FAT data and FAT calibrated model. This could have been resolved by measuring the actual engine power output and measuring the pressures in the cylinder. This would have lead to a stronger statement about the engines bsfc, the gearbox performance and the losses in these systems.

6

Results

In this section the effects of various charge air configurations on the diesel engine will be investigated. The investigation was performed using a MVFP model which has been validated by a measurement campaign as described in Section 5.

6.1. Introduction

In this section the results of the various turbocharging configurations that were modelled will be evaluated. Four turbocharger configurations were investigated: single turbocharging, single-hybrid turbocharging, 2-parallel-sequential turbocharging, and 2-parallel-sequential,hybrid turbocharging.

The models discussed here were based on the W26 as installed aboard the Zeven Provinciën class frigates. In order to make a quantitative comparison between the various charge air concepts, the nominal engine power and turbocharger size were kept constant. Inevitably, this leads to unfavourable matching. For the non sequentially turbocharged engines the mismatch is quite severe, the area where the engine is normally operating on one turbocharger is now operated on two turbochargers.

The operating envelope as given by the manufacturer was incorporated in the models and was explained in Section 5.3. For the single charge configuration, the operating envelope was reduced to a similar envelope as used on the single charged W26 engine. For the 2-parallel-sequential,hybrid configuration the operating envelope was increased to show the potential of this configuration.

In order to keep the explanation of the results as clear and succinctly as possible, the operation envelope was divided in four quadrants as depicted in Figure 70. The horizontal line was drawn at half the nominal rated power of the engine. The vertical line was determined by the moment of switching between one and two turbocharger operation, by definition this is called the *switch point*. Although single charge configurations do not have a switch, for comparison the same division as above will be applied.

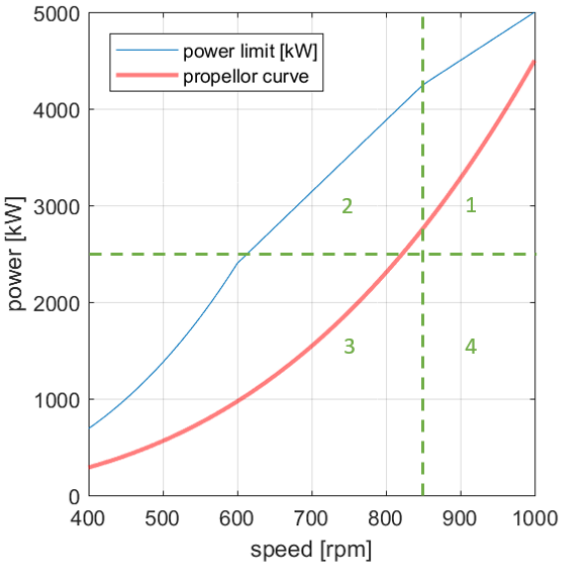

Figure 70: Operating envelope devided into four quadrants

For parallel-sequential turbocharging each quadrant has its own challenges. In quadrant **one**, the engine has just shifted from one to two turbocharger operation. Therefore, on the left side of the quadrant, the charge air pressure and air excess ratio is probably low, which could lead to overheating. In quadrant **two** the engine is operating just before switching to two turbochargers. Here the surge limit of the compressor and the maximum engine pressure have to be taken into account. In quadrant **three** especially in the lower region, the turbocharger is spinning at very low speed, resulting in a low the charge pressure and air excess ratio. Quadrant **four** is not used frequently during operation because the propeller curve only crosses the upper left corner of quadrant four. For single turbocharging, only quadrant three is of special importance, where the turbocharger speed is low, resulting in a low charge air pressure and air excess ratio.

6.2. Efficiency

First the effect of each charge air configuration on the efficiency of the diesel engine will be evaluated.

In Figure 71 the brake specific fuel consumption for each turbocharging configuration is shown over the complete operating envelope. In general it can be seen that the lowest specific fuel consumption was achieved at the boundary of the operating envelope in quadrant two. In this quadrant the engine already delivers a big part of its rated power while the engine speed and mechanical losses are still relatively low.

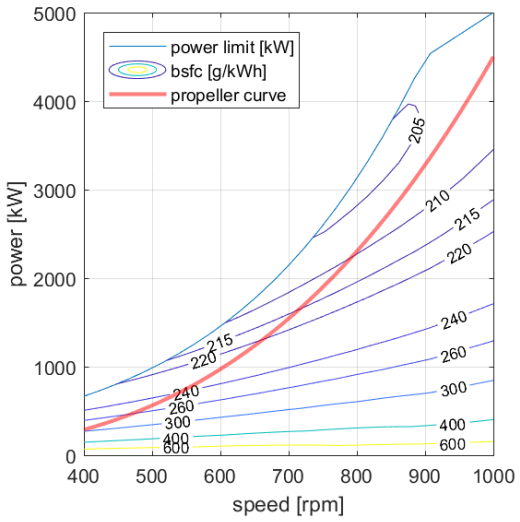

(a) Single charged

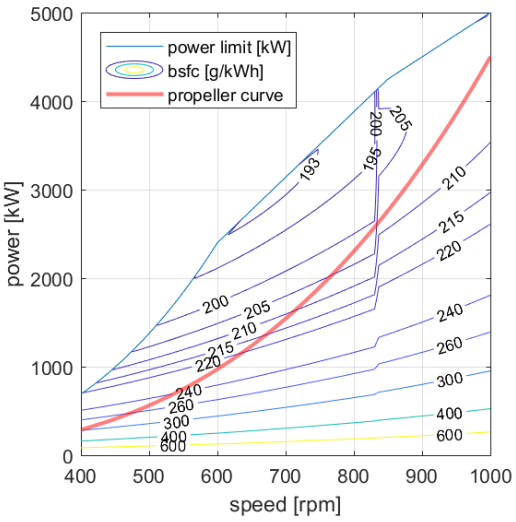

(b) Parallel,Sequential charged

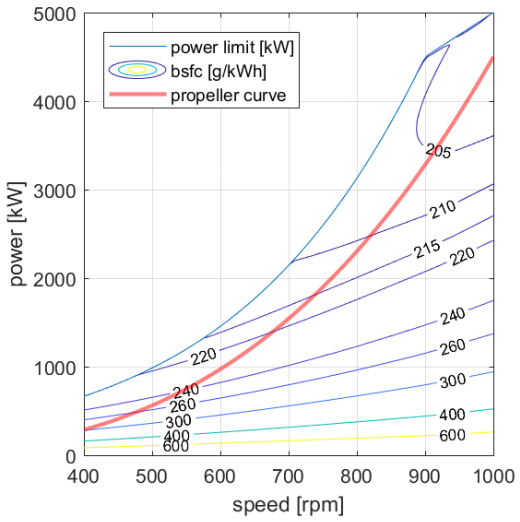

(c) Single - Hybrid charged

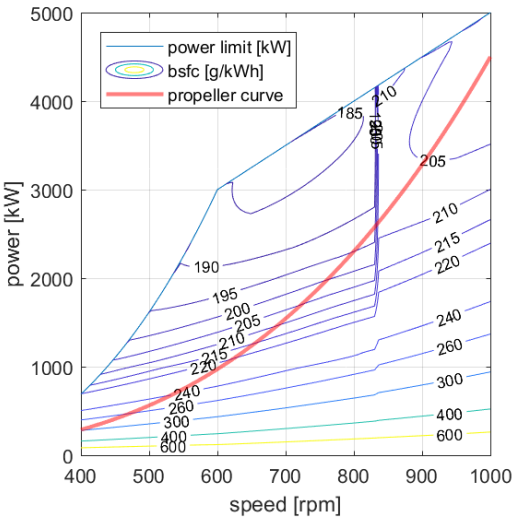

(d) 2-parallel-sequential,hybrid charged

Figure 71: Model predictions of the bsfc [g/kWh] of various charge air concepts

In order to make a quantitative comparison of the effect of the four different charge air concepts the bsfc of the four charge air concepts on the propeller curve was compared as shown in Figure 72. This is the third power theoretical propeller curve, with the nominal propulsion power on 90% of the maximum continuous rating of the engine. This corresponds with a sea state 2 $\sim$ 3 propeller curve on 32° pitch for the LCF frigate. The data points are depicted in Table 9, were the same notation (a), (b), (c), (d), as in Figure 71 is used.

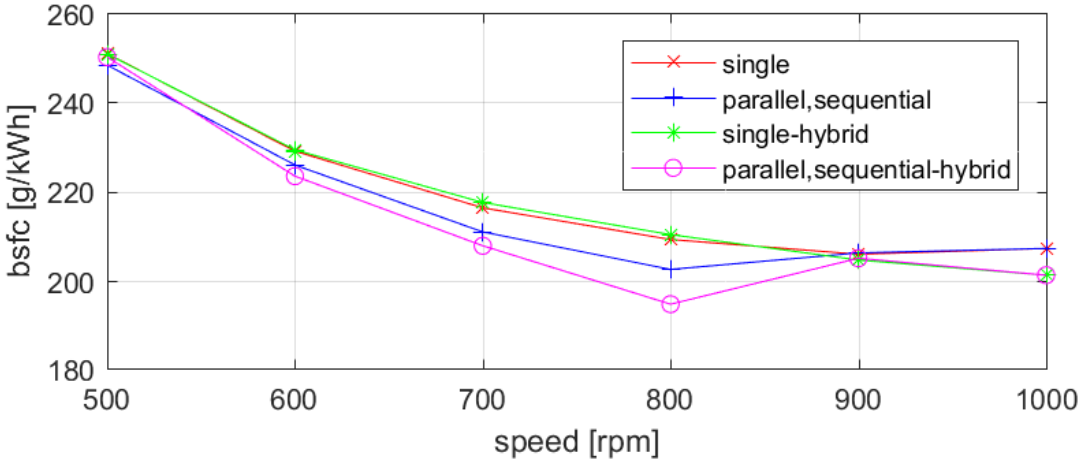

Figure 72: bsfc [g/kWh] of the four charge air configurations on the propeller curve

Table 9: The bsfc [g/kWh] of the four charge air configurations on the propeller curve and compared to the single charged concept (concept (a))

rpm	500	600	700	800	900	1000		500	600	700	800	900	1000
Concept	bsfc [g/kWh]							change ratio to concept a					
a	250,9	229	216,3	209,2	205,9	207,2		1	1	1	1	1	1
b	248,3	225,9	210,9	202,5	206,2	207,2		-0,01	-0,01	-0,02	-0,03	0,00	0,00
c	250,8	229,3	217,5	210,3	204,6	201,2		0	0,00	0,01	0,01	-0,01	-0,03
d	250,1	223,4	207,8	194,7	205	201,2		0	-0,02	-0,04	-0,07	0,00	-0,03

6.2.1. Effect of Parallel-Sequential turbocharging on effiency

Figure 71b and Figure 71d show an interesting phenomenon around the switch point. In quadrant two, left of the switch point the bsfc is considerably lower than right of the switch point in quadrant one. The explanation for this can be found in Figure 79b. It can be seen that before the switch point in quadrant 2 the air excess ratio was significantly higher than after the switch point. The higher air excess ratio is the result of a high charge air pressure. Which in return, is the result of the parallel-sequential turbocharging configuration. Table 9 shows that on the propeller curve, the effect of parallel-sequential turbocharging with respect to single turbocharging lead to an maximal bsfc decrease of approximately 3%.

6.2.2. Effect of hybrid turbocharging on effiency

In hybrid turbocharging configurations, power is added to the turbocharger to keep the air excess ratio at the required value of 2, which will increase the efficiency of the engine, but comes at the cost of the power supplied to the turbocharger. First, the single-hybrid turbocharger concept was investigated.

The amount of power eligible for PTO or requested for PTI can be seen in Figure 73a. If the power is actually subtracted or supplied to the turbocharger, the effect on the bsfc of the engine can be seen in Figure 73b.

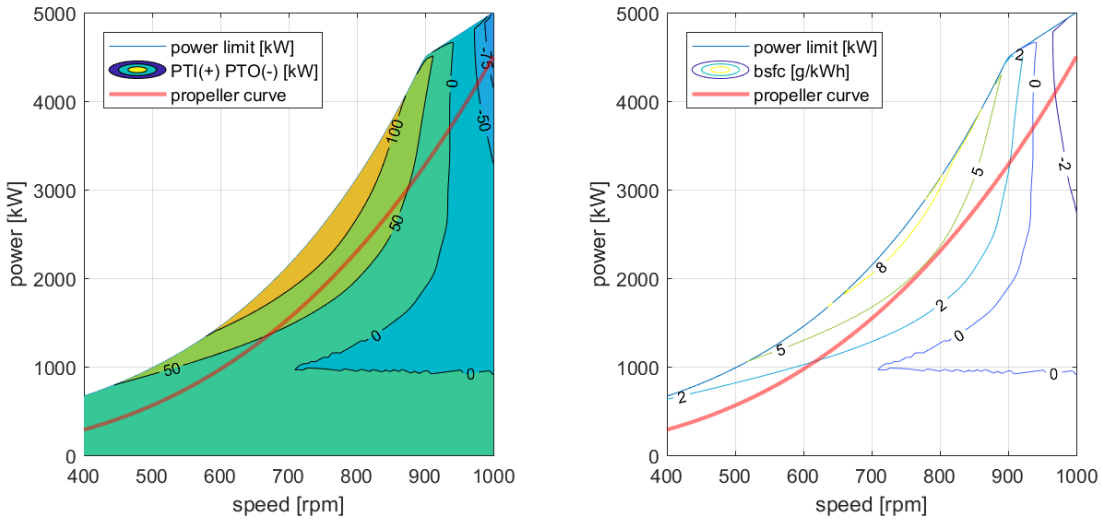

(a) Power [kW] available for PTO or PTI (b) Change in bsfc [g/kWh] for the diesel engine

Figure 73: Effects of PTO and PTI via the turbocharger on the bsfc [g/kWh]

On a large part of the operating envelope, the electric motor on the hybrid turbocharger is supplying additional power to the turbocharger. This is due to the mismatch of the turbocharger size with respect to the engine as mentioned earlier. As seen in Table 9 the hybrid turbocharger only had a positive effect on the bsfc around the nominal point of approximately 3%. Hence, this is what the charge configuration was matched for. On the lower part of the propeller curve the turbocharger was actually slightly decreasing the efficiency.

The second hybrid concept consist of the 2-parallel-sequential,hybrid turbocharger. Again, the amount of power eligible for PTO or requested for PTI can be seen in Figure 74a. If the power is actually subtracted or supplied to the turbocharger, the effect on the bsfc can be seen in Figure 74b.

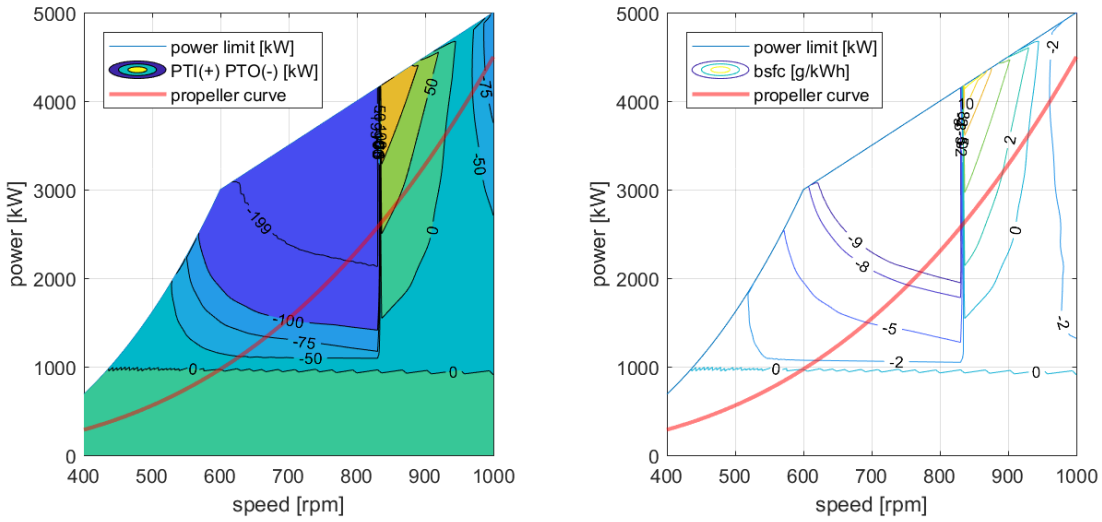

(a) Power [kW] available for PTO or PTI (b) Change in bsfc [g/kWh] for the diesel engine

Figure 74: Effects of PTO and PTI via the turbocharger on the bsfc [g/kWh]

The 2-parallel-sequential,hybrid turbocharger essential shows the same behaviour as the 2-parallel-sequential turbocharger concept. Before the switch point, the bsfc is very low, and as soon as the second charger kicks in the bsfc increases considerably. However, the bsfc before

the switch point is even lower than at the 2-parallel-sequential,hybrid concept due to the PTO. Table 9 shows that on the propeller curve, the effect of 2-parallel-sequential,hybrid turbocharging with respect to single turbocharging resulted into an maximal bsfc decrease of approximately 7%.

6.2.3. Effect of the operating point on efficiency

Figure 72 shows the bsfc on the propeller curve. It can be seen that although the bsfc changes significantly over the operating envelope , the points on the propeller curve show a more moderate change. This is due to the position of the propeller curve, which did not coincide with the most efficient areas in the operating envelope.

It is clear that the full potential of the turbocharging configurations is not utilized yet. In order to improve the efficiency further, the operating points of engine have to be shifted in the direction of the most efficient part of the operating envelope. For example, this could be done by applying a power take off on the propeller shaft as explained by Klein Woud et al. [26] and seen in Figure 75a. The power subtracted from the propeller shaft is fed to the electric grid of the ship. Another option is to transfer power from one shaft to a second shaft via electric machines, as currently done aboard the national security cutters of the U.S. Coast Guard and seen in Figure 75b. In the latter case, two shafts will be driven in parallel by one diesel engine.

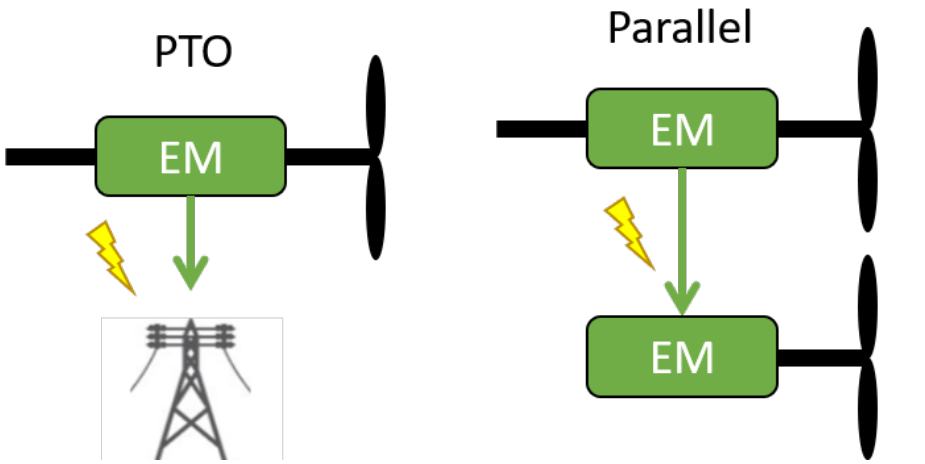

(a) PTO on propeller shaft

(b) Drive two shafts parallel with one diesel engine

Figure 75: Shifting the operating point of the diesel engine

The effect of PTO on the propeller shaft or driving two shafts parallel with one diesel engine are depicted in Figure 76. It can be seen that the propeller curve is altered to the regions where the bsfc is lower.

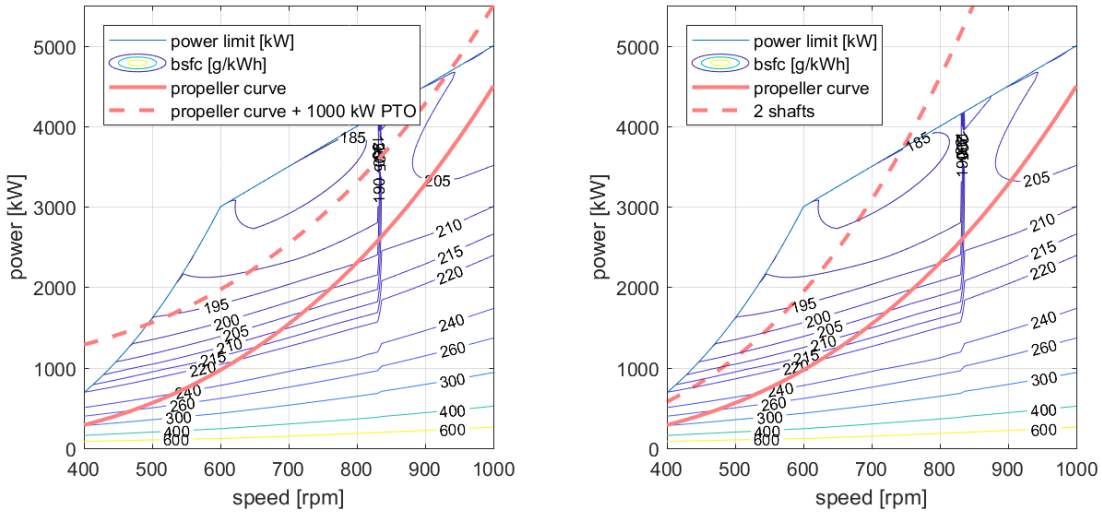

(a) Utilize PTO on propeller shaft

(b) Drive two shafts parallel

Figure 76: Shifted (propeller) load curves

The results of the altered propeller curve are given in Table 10 and Table 11, and show that the effect of the charge air configurations increases significantly if the propeller curve is altered. In comparison with a single charged diesel engine driving one shaft, without PTO, the bsfc decreases with more than 15% in part load.

Table 10: Two shafts driven by one diesel engine, compared to concept(a) with one shaft

rpm	500	600	700	rpm	500	600	700
Concept	bsfc [g/kWh]			Concept	change ratio to concept a		
a	250,9	229	216,3	a	1	1	1
b	207,5	196,7	192,8	b	-0,17	-0,14	-0,11
d	206,1	192,3	184,4	d	-0,18	-0,16	-0,15

Table 11: Propeller curve + 1000 kW PTO on shaft, compared to concept(a) without PTO

rpm	600	700	800	900	rpm	600	700	800	900
Concept	bsfc [g/kWh]				Concept	change ratio to concept a			
a	229	216,3	209,2	205,9	a	1	1	1	1
b	196,4	195	194,3	206,1	b	-0,14	-0,10	-0,07	0,00
d	191,8	187,1	185,6	207,8	d	-0,16	-0,13	-0,11	-0,01

6.2.4. Effect of charge air configurations on efficiency

The effect of the charge air concepts on the efficiency of the diesel engine is significant. 2-parallel-sequential, and 2-parallel-sequential,hybrid both show an increase of efficiency on the propeller curve of 3% and 7% respectively. If the propeller curve is altered to maximize the effect of the advanced charge air configurations the efficiency can be increased by more than 15% or 36,7 g/kWh.

6.3. Performance

The aim of this thesis is to evaluate the effect of various charge air concepts on the Measures Of Effectiveness (MOE) of a ship. As explained by Geertsma et al. [12] there is a difference between measures of effectivenes and Measures Of Performance (MOP). A measure of performance is usually obtained from a benchmark test and can be used to compare different models or objects to each other. This is very common in the automotive indsutry, for example, the world-harmonised light-duty vehicle test cycle as described in [27]. For ships Geerstma et al. [12] proposed several MOPs obtained from a series of manoeuvres. For example, the time it takes a ship to accelerate from 0 to 15 knots. The results obtained from a MOP can be used to analyse the effectiveness of a ship. In this section the effect of a various charge air concepts on the operating envelope, engine thermal loading and acceleration performance is investigated.

The same four charge air configurations as in the previous section were investigated. The operating envelopes were also chosen the same, except for the single-hybrid configuration. In order to show the potential of the addition of a hybrid turbocharger, the operating envelope of the single-hybrid configuration was chosen equal to the envelope of the 2-parallel-sequential configuration. Further, to show the effect of controlling the temperature the single-hybrid concept was modelled without power or temperature control.

6.3.1. Operating envelope and acceleration

The acceleration performance of a ship driven by diesel engines is, amongst others, limited by the ability of the diesel engine to supply power to the propeller. The more power the diesel engine can supply, the faster the ship is able to accelerate. The power which can be delivered by the diesel engine is limited by two factors. The operating envelope and the temperature limits of the engine. The operating envelope as seen in Figure 70 was given by the manufacturer. For the temperature limit, the exhaust valve temperature was chosen as estimator for the thermal loading of the engine as proposed by Grimmelius et al.[16]. The value indicating thermal loading is set at 1200 [K], corresponding to a value of $\lambda \approx 1.5$. A short explanation about the exhaust valve temperature is given in Section 3.6.2.

The mechanism of thermal loading the engine can be explained as follows: A low charge air pressure results in a low amount of trapped air in the cylinder and a low scavenge efficiency. The low amount of trapped air results in a low air excess ratio, resulting in a high temperature combustion as seen in Figure 30. The low scavenge efficiency results in sub optimal cooling of the cylinder between the power strokes. The combination of a high combustion temperature and insufficient cooling together cause thermal overloading of the engine.

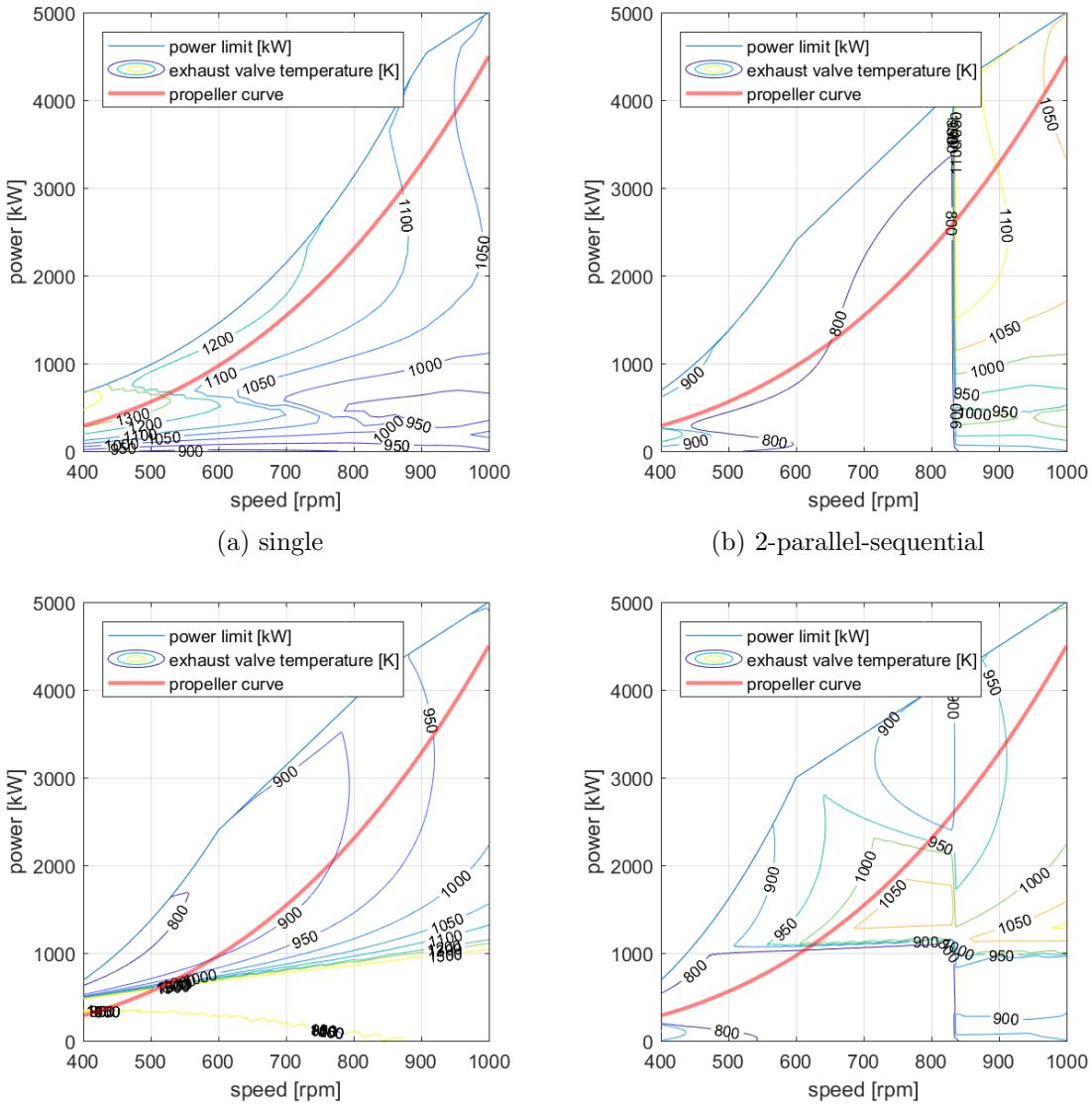

(a) single

(b) 2-parallel-sequential

(c) single-hybrid

(d) 2-parallel-sequential,hybrid

Figure 77: Model results of maximum temperature T4 [K]

In Figure 77 the exhaust valve temperature for each turbocharging configuration is shown over the complete operating envelope. It can be seen that the trends in the exhaust valve temperature of Figure 77a and 77b follow the trends in the air excess ratio as depicted in Figure 79a and 79b. This is in accordance with the work of Sapra et al. [38], who investigated the relation between exhaust valve temperature and air excess ratio.

The single charge configuration in Figure 77a shows a considerable higher temperature in quadrant 2 and 3 then the parallel-sequential concept in Figure 77b. This can be explained by the mismatching of the charge air configuration as explained in Section 6.2. The parallel-sequential configuration shows a rise in temperature just after the switch point. This was presumably caused by a slightly low model prediction of the charge air pressure encountered during the validation. The low charge air pressure results in a low air excess ratio, increasing the temperature of the engine.

Figure 77c depicts the temperature of the single-hybrid configuration. The air excess ratio was kept at $\lambda = 2.0$ over almost the complete operating envelope as seen in Figure 79c. The exhaust valve temperature in quadrant three and four exeeds 1500 [K] showing that the engine was thermally overloaded. This was caused by the PTO from the hybrid turbocharger. Figure 77d

shows the same trend although temperature control has prevented overheating. If the 1200 [K] boundary is compared with the air excess ratio in Figure 79a the boundary seems to correspond with the $\lambda = 2.2$ contour. Although the charge air pressure is very low here $p_b \approx 1.1[bar]$ the hybrid turbocharger starts to take off power since the lambda is higher then 2. This results in a charge air pressure of $p_b \approx 1.0[bar]$. It can be concluded that estimation of thermal loading of the diesel engine based on the air excess ratio as investigated by Sapra et al. [38] is not valid in this region. Therefore, extra measures to avoid power take off were implemented as discussed in Section 4.10.

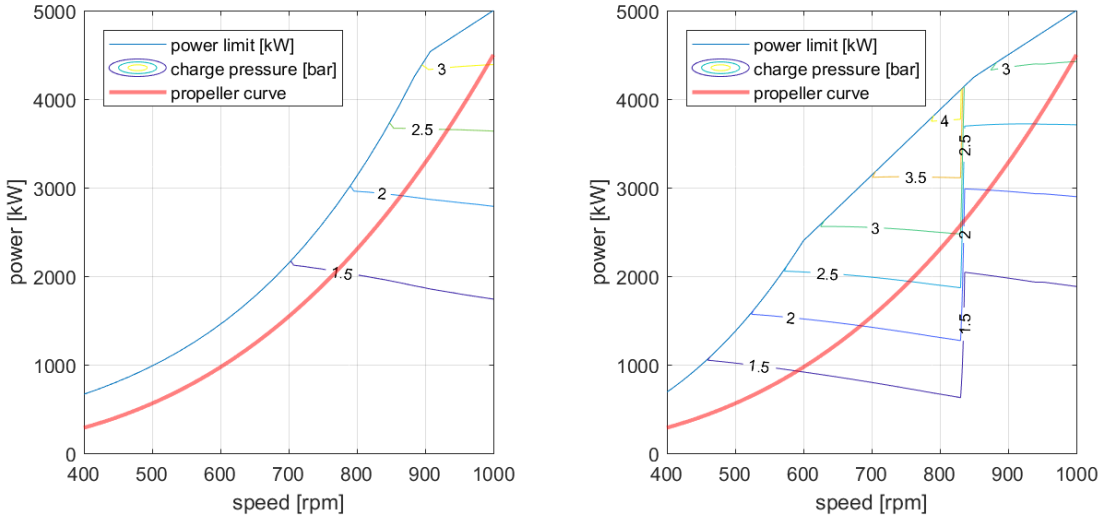

(a) single

(b) 2-parallel-sequential

(c) single-hybrid

(d) 2-parallel-sequential,hybrid

Figure 78: Model results of the charge air pressure [bar]

Figure 78 shows the model prediction for the charge air pressure p_b in [bar] for each configuration over the complete operating envelope. It can be seen that the charge pressure in the single configuration is shown in Figure 78a is low due to the mismatch of the turbocharger configuration. Further, in Figure 78d the contour line of $p_b = 1.5$ [bar] shows an interesting behaviour. This can be explained by the control strategy in which power take off was not allowed below 1000 [kW] engine power as explained in Section 4.10. Above 1000 [kW] engine power the hybrid turbocharger starts to take off power and charge air pressure drops back to $p_b = 1.5$ [bar] explaining the form of the contour.

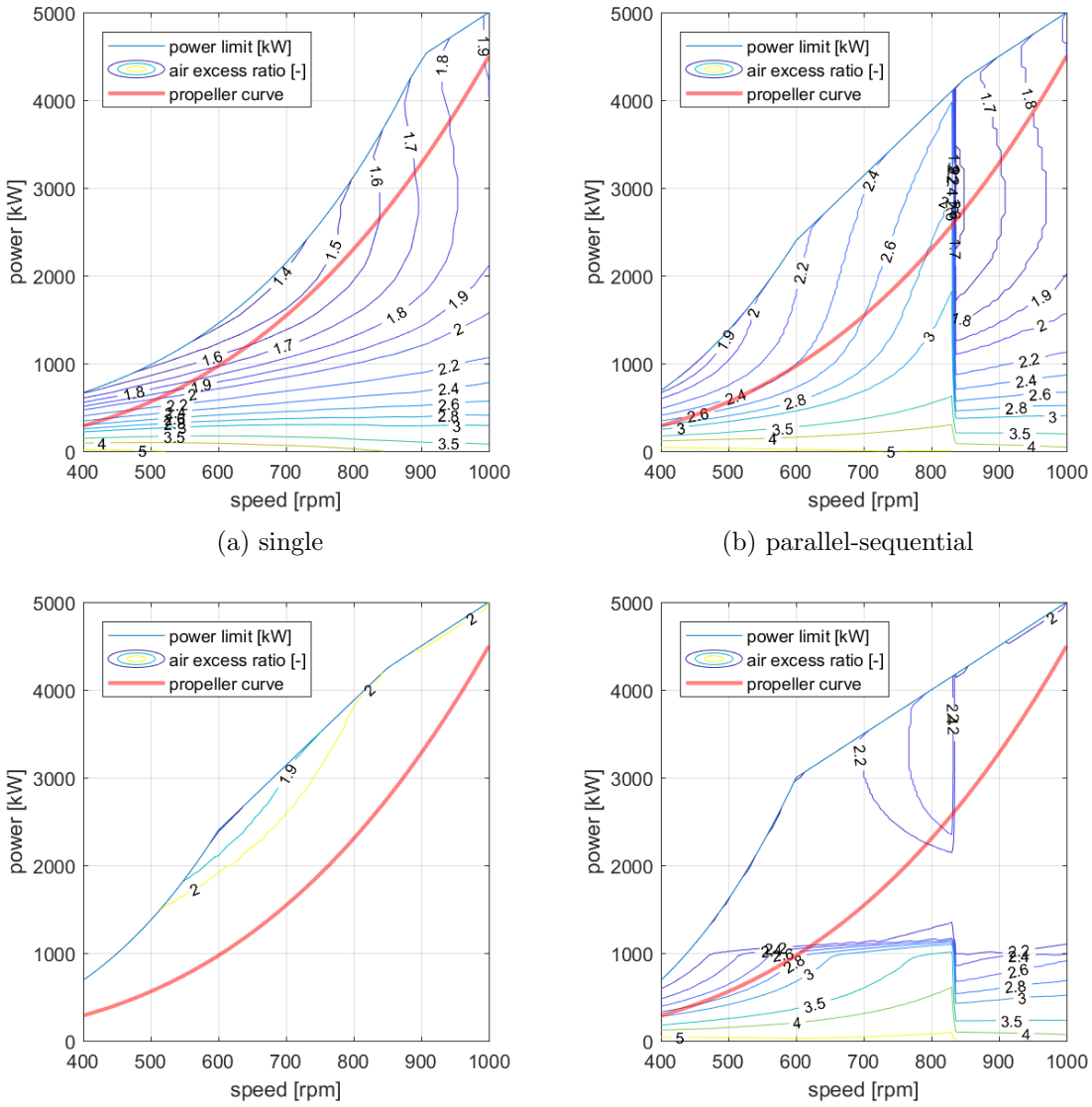

(a) single

(b) parallel-sequential

(c) single-hybrid

(d) parallel-sequential-hybrid

Figure 79: Model results of the air excess ratio λ [-]

Figure 79 shows the model prediction for the air excess ratio for each configuration over the complete operating envelope. It can be seen that the addition of a hybrid turbocharger makes it possible to keep the air excess ratio at $\lambda = 2.0$ over almost the complete operating envelope. In Figure 79c it can be seen that around the edge of the operating envelope the air excess ratio decreases a bit. The hybrid turbocharger is unable to deliver the required power to keep the air excess ratio at $\lambda = 2.0$. In Figure 79d the opposite occurs. The air excess ratio is higher than $\lambda = 2.0$. This indicates that the maximum power take off value is reached. In both cases this could be solved by installing an electric machine with a higher power rating than 200 [kW].

6.3.2. Effect of charge air configurations on the operating envelope

In order to make a quantitative comparison of the effect of the four charge air configurations on the operating envelope the power limit at 600 rpm was evaluated. The power limit was either determined by the air excess ratio which has to be higher than 2, or by the torque limit of the engine. The results are depicted in Table 12.

Table 12: power in kW at 600 rpm engine speed, and ratio to concept (a)

Concept	power at 600 rpm in [kW]	ratio to single concept [-]
1-single (a)	750	1
2-parallel-sequential (b)	2400	3,2
1-single-hybrid (c)	1867	2,49
2-parallel-sequential,hybrid (d)	3000	4

Figure 77d and 79d showed the parallel-sequential,hybrid concept keeps well within the limits of the maximum allowed exhaust valve temperature of 1200 [K] and the air excess ratio of $\lambda = 2.0$. Therefore, it can be concluded that the parallel-sequential,hybrid concept was able to extend the operating envelope with approximately 4.6% in area as seen in Figure 80. This resulted in a 25% increase in power output at 600 [rpm] engine speed, affecting the acceleration performance.

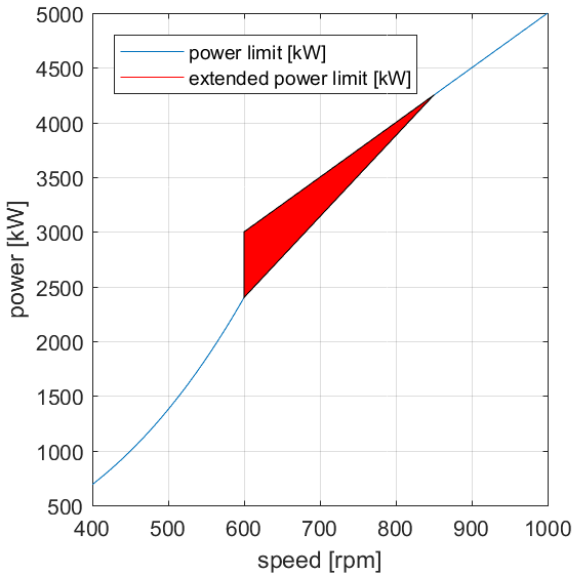

Figure 80: Operating envelope after addition of a hybrid turbocharger on the W26

6.3.3. Dynamic performance

In order to investigate the dynamic performance of the diesel engine with a hybrid turbocharger a simple engine acceleration test was performed. The single charged concept (a) and the single-hybrid charged concept (c) are compared in a simulation which resembles a acceleration manoeuvre of a ship. This research only includes a diesel engine and no ship model. Therefore, the engine and torque setting for the acceleration are chosen according the work of Geertsma et al. [12]. Geerstma et al. did a acceleration study on a complete ship model and showed that an acceleration manoeuvre is comparable to a linear speed and torque increase. This is quite a rough estimation, and the dynamic influences of waves and the propeller are not accounted for. Also the influence of controlling the pitch of the propeller is not included in the model. Figure 81a and 81b shows the increase in effective torque and engine speed as a function of time. The simulation starts at 750 [kW] engine power as depicted in Figure 81c and stops in the nominal point at 5000 [kW] at nominal engine speed. For the acceleration test, the hybrid turbocharger is configured to only perform power take in. The actual power supplied to the turbocharger is depicted in Figure 81d.It can be seen that the first 20 seconds of the the power output, contain a lot of noise. This is caused by the use of a PI controller and the offset of the air excess ratio at the start of the simulation.

This results in the charge air pressure as shown in Figure 82a and 82a, for a non-hybrid and a hybrid turbocharger respectively.

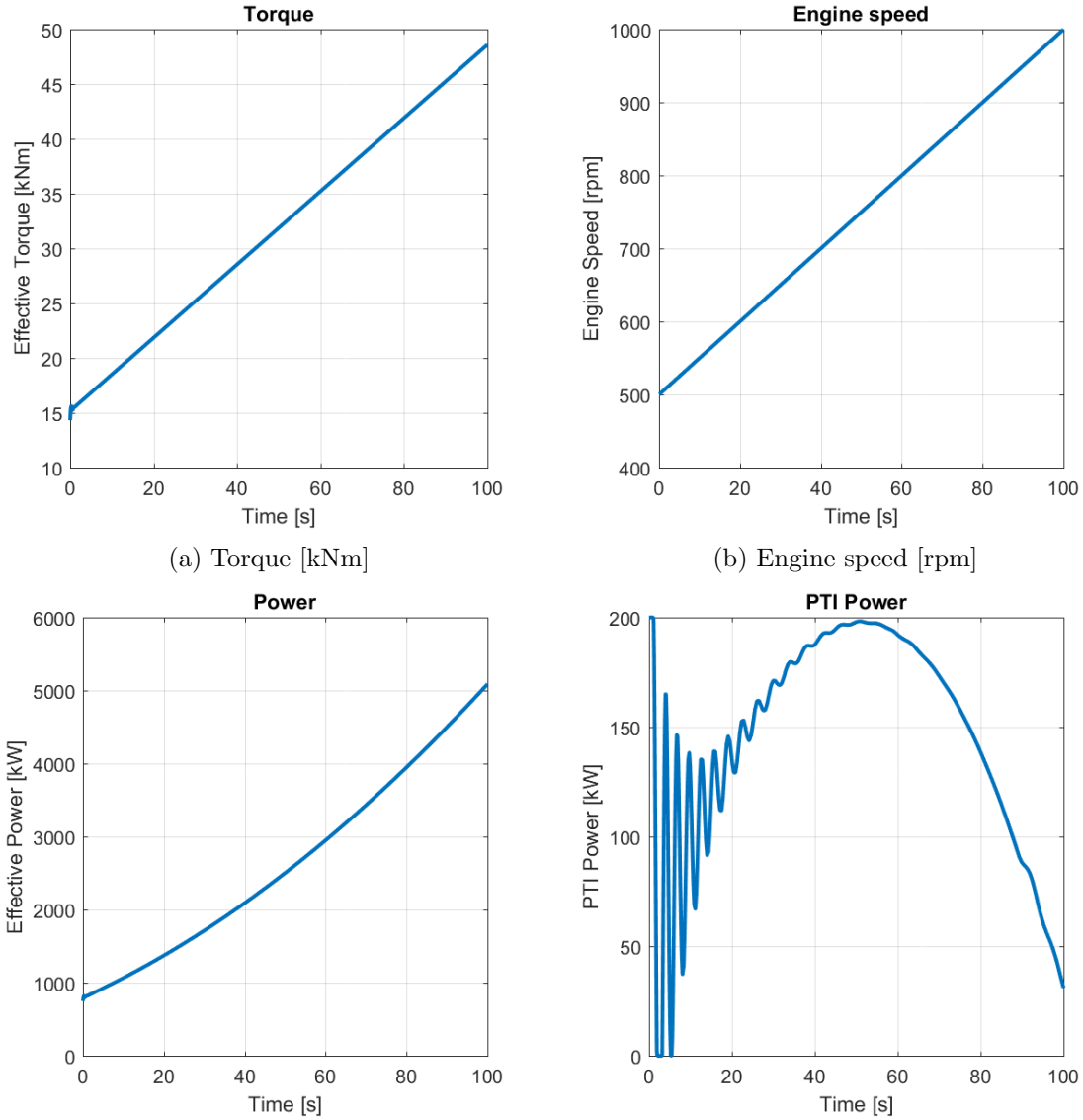

(a) Torque [kNm]

(b) Engine speed [rpm]

(c) Engine power [kW]

(d) Power take in [kW]

Figure 81: Model results for dynamic simulation

Figure 82b shows the air excess ratio of a non-hybrid and a hybrid turbocharger. It can be seen that the air excess ratio for during the acceleration is much better for the hybrid turbocharger. This has an positive effect on the temperatures in the engine as shown in Figure 82c and 82d. The exhaust valve temperature of the non hybrid turbocharged engine peeks at 1280 [K] at t=28.5. The exhaust valve temperature of the hybrid turbocharged engine is 850 [K] at that point. A difference of 430 [K].

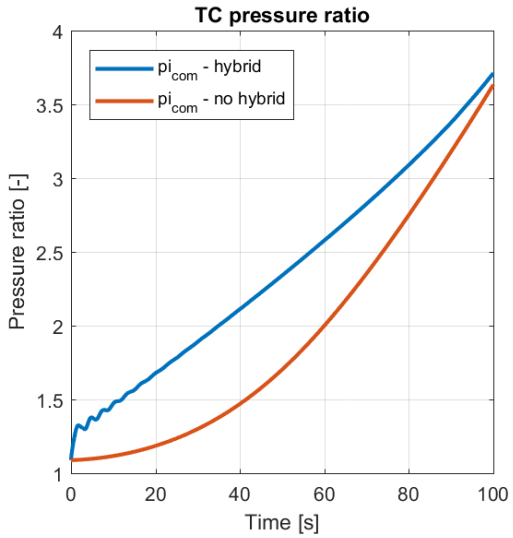

(a) Pressure ratio over the compressor

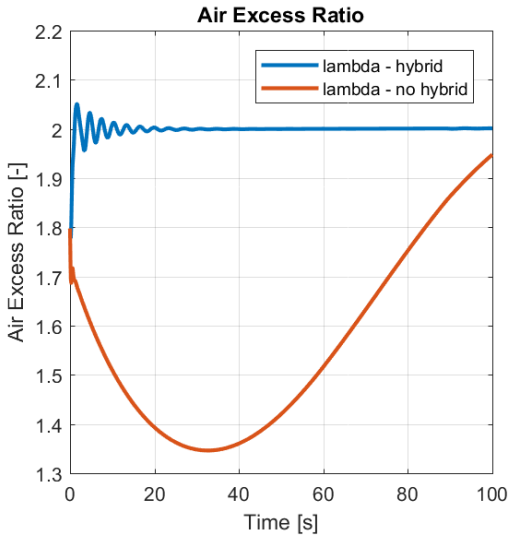

(b) Air excess ratio [-]

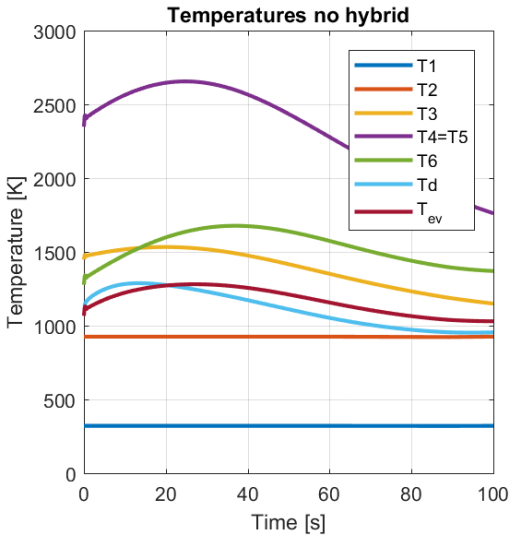

(c) Temperatures [K] - no hybrid

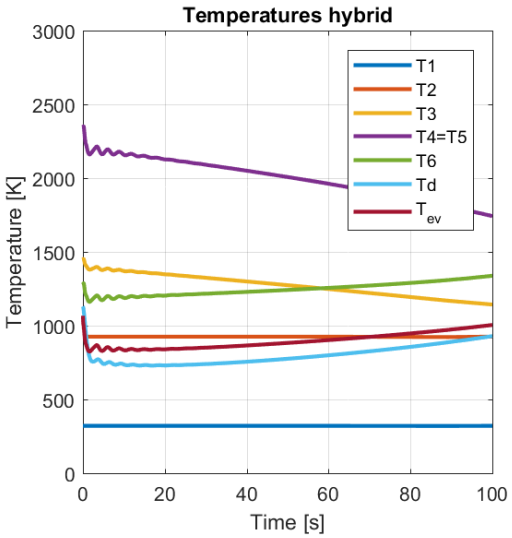

(d) Temperatures - Hybrid

Figure 82: Model results for dynamic simulation

6.4. Effect of charge air configurations on acceleration performance

The effect of the four compared charge air configurations on the acceleration and operating envelope is significant. The addition of hybrid turbocharger increases the available power at 600 rpm by at least 25% with respect to the parallel-sequential or single charged configuration. If the extra available power can be fully utilized, the acceleration time will presumably decrease significantly. Further, it was shown in a dynamic simulation that the exhaust valve temperature is 430 [K] lower during an engine acceleration from 30% nominal torque at 50% engine speed to full rated torque and engine speed. This proofs that hybrid turbocharging can have a significant effect on the thermal loads during acceleration of the diesel engine. To improve the estimation of the effects of hybrid turbocharging on the ships performance it is recommended to set up a dynamic simulation of a complete ship propulsion model. A dynamic simulation model will enable us to gain a better (quantitative) insight into the influences of advanced turbocharger performance on the performance of ship propulsion as a whole. The methods using the measures of performance as proposed by Geerstma et al. [12] are therefore recommended to investigate the thermal loading of the diesel engine in combination with various charge air configurations during acceleration of the ship.

7

Conclusions and Recommendations

7.1. Classification

After an extensive literature survey it was possible to divide different turbocharger configurations in a simple, effective and clear classification. The classification is based on electrical network theory and consists of the number of chargers, the configuration in which they are placed and finally, additional technology applied in the turbocharger.

$$\underbrace{number}_{1,2,3..} - \underbrace{configuration}_{single,\ series,\ parallel} - \underbrace{technology}_{sequential,\ hybrid,\ VTG}$$

The scope of this research was on efficiency increase over the complete operating envelope of the diesel engine and acceleration performance. Among the concepts investigated parallel-sequential turbocharging, hybrid turbocharging, or a combination of both are most promising to improve both efficiency and acceleration performance. Therefore, it was decided to limit the scope to these advanced charge air configurations. In order to make a comparison four turbocharging configurations were investigated:

(a) 1-single turbocharging

(b) 2-parallel-sequential turbocharging

(c) 1-single-hybrid turbocharging

(d) 2-parallel-sequential,hybrid turbocharging

7.2. Model approach

An extensive investigation in modelling hybrid turbochargers resulted in two turbocharger models, a model based on a compressor map and the equations of motion, and a model based on the Büchi power balance. In order to decide a model strategy it is important to understand the weaknesses and strengths of each approach. It was found that it was not possible to model a torque balance of a general compressor model with the current simple diesel model. However, through the addition of a general compressor model, a torque balanced turbocharger could be modelled. The general compressor model was matched within 5% accuracy of the actual compressor map of the compressor. Also, it was possible to match the compressor model to a data set obtained during an extensive measurement campaign under operating conditions aboard a fast naval combatant. This gives confidence that, if extensive FAT data is available, the general compressor model gives more accurate, and physical based predictions of the turbocharger behaviour. In conclusion, if the dynamic interaction of the turbocharger (for example with an electric machine) is important, it is advised to use the motion based turbocharger model. Otherwise, the Büchi based model is advised because of its simplicity.

7.3. Turbocharger strategy

It was concluded that the application of advanced charge air configurations can significantly improve the engine efficiency in part load. For example, the application of a 2-parallel-sequential,hybrid turbocharger leads to an increase in efficiency of 7% at 800 rpm on the propeller curve in comparison with a single charged engine as seen in Table 13. Furthermore, hybrid turbocharging enables extending the operating envelope of a parallel-sequential turbocharged engine with up to 25% at 60% engine speed as seen in Table 14. This enables the engine to deliver constant torque from 600 to 1000 rpm.

Table 13: The bsfc [g/kWh] of the four charge air configurations on the propeller curve and compared to the single charged concept (a)

rpm	500	600	700	800	900	1000		500	600	700	800	900	1000
Concept	bsfc [g/kWh]							change ratio to concept a					
a	250,9	229	216,3	209,2	205,9	207,2		1	1	1	1	1	1
b	248,3	225,9	210,9	202,5	206,2	207,2		-0,01	-0,01	-0,02	-0,03	0,00	0,00
c	250,8	229,3	217,5	210,3	204,6	201,2		0	0,00	0,01	0,01	-0,01	-0,03
d	250,1	223,4	207,8	194,7	205	201,2		0	-0,02	-0,04	-0,07	0,00	-0,03

Table 14: operating envelope power limit at 600 rpm

Concept	power at 600 rpm in [kW]	ratio to single concept [-]
1-single (a)	750	1
2-parallel-sequential (b)	2400	3,2
1-single-hybrid (c)	1867	2,49
2-parallel-sequential,hybrid (d)	3000	4

The potential created by hybrid and parallel turbocharging can only be fully utilized if the extended area of the operating envelope is actually used by the propulsor. Two approaches to shifting the engine load towards the extended operating envelope were investigated. The application of a 1 MW power take off on the propeller shaft resulted in an efficiency increase of 16% at 600 rpm as seen in Table 15. The other approach was to drive two propeller shafts in parallel with one diesel engine, resulting in an efficiency increase of 18% at 500 rpm as seen in Table 16. In both cases 1000 [kW] was delivered to the propeller(s). This corresponds to a ship speed of approximately 10 knots, which is often used for loitering.

Table 15: Propeller curve + 1000 kW PTO on the propeller shaft, compared to concept(a) without PTO on the propeller shaft

rpm	600	700	800	900	rpm	600	700	800	900
Concept	bsfc [g/kWh]				Concept	change ratio to concept a			
a	229	216,3	209,2	205,9	a	1	1	1	1
b	196,4	195	194,3	206,1	b	-0,14	-0,10	-0,07	0,00
d	191,8	187,1	185,6	207,8	d	-0,16	-0,13	-0,11	-0,01

Table 16: Two shafts driven parallel by one diesel engine, compared to concept(a) driving one shaft

rpm	500	600	700	rpm	500	600	700
Concept	bsfc [g/kWh]			Concept	change ratio to concept a		
a	250,9	229	216,3	a	1	1	1
b	207,5	196,7	192,8	b	-0,17	-0,14	-0,11
d	206,1	192,3	184,4	d	-0,18	-0,16	-0,15

Although the dynamic behaviour and control of the hybrid turbocharger should be investigated further, the results of the dynamic simulation showed the charge air pressure could be increased with approximately 0.5 [bar] during acceleration of the diesel engine. This resulted in a 430 [K] temperature drop of the exhaust valve temperatures while simulating a fast engine power increase, resembling a ship acceleration load.

Apart from the increase in performance in acceleration and operating envelope, the models showed that the air excess ratio can be controlled very accurately. Although not deeply investigated, better control of the air excess ratio could solve the problems with knock and misfire in gas engines under heavy load variation.

The effects of hybrid turbocharging on NOx emissions are positive. Hybrid turbocharging increases the pressure ratio over the cylinder resulting in a better scavenge process. Therefore, the cylinder will be cooler which is beneficial for NOx reduction. Further, it was shown that the thermal loading during acceleration could be reduced significantly. The exhaust valve temperatures were decreased with almost 430 [K].

Summarizing, advanced charge air configurations can contribute considerably in improving the efficiency, acceleration performance, and emissions of diesel engine driven fast naval combatants. Generally, in combination with shifting the operating point of the diesel engine, efficiency in part load can increase with approximately 15% in comparison with a single charged diesel engine. Depending on the actual operational profile, this can result in a significant contribution to the aim of reducing the logistic dependency, environmental impact and fuel costs of the ships of the Royal Netherlands Navy.

7.4. Recommendations

The conclusion of this research showed the potential of hybrid turbocharging. Hybrid turbocharging is relatively unexplored in the maritime world and therefore a lot of interesting questions remain. To improve the estimation of the effects of hybrid turbocharging on the ships performance it is recommended to set up a dynamic simulation of a complete ship propulsion model. A dynamic simulation model will enable us to gain a better (quantitative) insight into the influences of advanced turbocharger performance on the performance of ship propulsion as a whole. The methods using the measures of performance as proposed by Geerstma et al. [12] are therefore recommended to investigate the thermal loading of the diesel engine in combination with various charge air configurations during acceleration of the ship.

This thesis has investigated a very simple control strategy for the hybrid turbocharger to improve the air excess ratio. However the proposed model provides the opportunity to incorporate an electric motor model and its control strategy into the models. With these additional models alternative control strategies for the hybrid turbocharger and its influence on engine performance can be investigated. Also a deeper investigation in the behaviour of the turbocharger itself is interesting, since an electric motor can now easily be incorporated into the model. This gives the opportunity to investigate the control strategy of the turbocharger and its influence on the engine performance.

With respect to the validation of the models, al lot of uncertainties were encountered during the measurement campaign. Therefore it was hard to draw reliable conclusions. First of all, a measurement campaign in a controlled environment, for example a test bench, to validate the diesel model would give a more precise insight in the accuracy of the model predictions. After this it is advised to investigate the differences in the model predictions and the measured values aboard the Zeven provinciën class. It might be well possible that a significant performance degradation of the propulsion plant can be revealed. This performance degradation should be taken into account for the design choices of the replacement M-frigate. Moreover, performing similar measurement campaigns over the life of the vessel, or logging and analysing automation system data could reveal causes of the performance degradation and condition based maintenance strategies could subsequently be developed to address this performance degradation.

For the future frigate it is recommended to design the propulsion system in such a way that the ship uses the complete operating envelope of the diesel engine, which is not the case now. If the electric drive can be utilized for PTO and PTI on the propeller shaft, significant efficiency improvements are possible. Further, in order to determine whether it is feasible to install hybrid turbochargers aboard the replacement M-frigate the following recommendations are made: The hybrid turbocharger and the support systems should be investigated with respect to economic and technical feasibility. Further, the optimal power rating of the electric motor and support systems should be investigated. The potential energy savings have to make up for additional costs, space and increase of complexity.

The result from this thesis demonstrate that hybrid turbocharging has a big effect on the temperature in the cylinder, which might contribute in lowering the NOx emissions of the engine. Therefore, it is recommended to investigate the influence of a hybrid turbocharger on emissions. Finally, it is suspected that the hybrid turbocharger can play a major role in the application of alternative fuels by controlling the air excess ratio. Therefore, it is recommended to investigate the application of hybrid turbochargers on gas and dual fuel engines.

Acknowledgments

I would like to thank Rinze Geertsma for being the supervisor of my project. I learned a lot from him during the extensive discussions over the Royal Netherlands Navy, naval ships, and Marine Engineering in general. Also, I admire his patience, especially with my academic writing skills.

From the Defence Materiel Organisation I would like to thank Fred Driegen, my other supervisor. Fred, it was a pleasure to work with you, you gave me useful feedback, you were always in for a joke, and motivated me if needed. I wish you a great time aboard Zr. Ms. Van Amstel. I would also like to thank Youri Linden, for all his efforts to help me, and for the great time aboard Zr. Ms. De Ruyter, it was an unforgettable experience. I would like to thank all the other colleagues I had the pleasure to work with. The nice coffee breaks, discussions over craftsmanship, broken cars, fancy new cars, foreign navies, submarines, moving to Utrecht, I enjoyed them all. Also, the nice 'team uitjes' to Amsterdam, Utrecht and Den Helder, which provided the distraction needed to continue.

Special thanks has to go to Anneloe, Huib and Jeroen. My fellow students at DMO. We have had a lot of support, company, and fun with each other, many thanks for that.

Also, I would like to express my thanks to Menno van Leeuwen. We have been a great team in the last two years of our study. Studying, IWS, Vulcanus, The study tour and great friendship. You helped me when it was difficult, cheered me up when it was hard, and we laughed a lot. Thanks Menno, for everything.

Inevitable the people who loved me, adored me and always supported me unconditionally deserve a place here. Off course I'm talking about my parents. Pap, Mam, bedankt voor alle steun, voor mijn studie, het altijd fijne thuiskomen en alle zorgen. Natuurlijk mag ik Quint, Stein en Celine niet vergeten, you are the best.

Finally my thoughts go to my dearest Inés, for all the love she gave me, the support during this intensive year, and the moments we shared, i will never forget them.

Joris, 28 januari 2018

References

[1] How a Coriolis Mass Flow Meter Works - www.instrumentationtoolbox.com - 2018-01-05.

[2] Leith Acura Cary -Turbochargers, http://blog.leithacura.com/acura-sh-awd-turbocharger/, 2016.

[3] Habib Aghaali and Hans-Erik Ångström. A review of turbocompounding as a waste heat recovery system for internal combustion engines. *Renewable and Sustainable Energy Reviews*, 49:813–824, 2015.

[4] Syed Kamran Arshad-Ali. SUITABILITY OF HYBRID ELECTRIC POWERTRAINSWITH ELECTRIC TURBOCHARGER, 2015.

[5] Aleksandar Borisavljevic, Henk Polinder, and Jan Abraham Ferreira. On the speed limits of permanent-magnet machines. *IEEE Transactions on Industrial Electronics*, 57(1):220–227, 2010.

[6] Ennio Codan, Christoph Mathey, and Adrian Rettig. PAPER NO .: 293 2-Stage Turbocharging – Flexibility for Engine Optimisation. *CIMAC Congress 2010*, 2010.

[7] P. Colonna and H. van Putten. Dynamic modeling of steam power cycles. Part I-Modeling paradigm and validation. *Applied Thermal Engineering*, 27(2-3):467–480, 2007.

[8] S.L. Dixon and C.A. Hall. Fluid Mechanics and Thermodynamics of Turbomachinery. *Fluid Mechanics and Thermodynamics of Turbomachinery*, 1998.

[9] Gene F. Franklin, J. David Powell, and Abbas Emami-Naeini. *Digital Control*. Pearson, 1994.

[10] J. Galindo, J. R. Serrano, H. Climent, and O. Varnier. Impact of two-stage turbocharging architectures on pumping losses of automotive engines based on an analytical model. *Energy Conversion and Management*, 51(10):1958–1969, 2010.

[11] R D Geertsma, R R Negenborn, K Visser, and J J Hopman. Torque control for diesel mechanical and hybrid propulsion on naval vessels. 2016.

[12] R D Geertsma, R R Negenborn, K Visser, and J J Hopman. Pitch control for ships with mechanical and hybrid propulsion : Modelling , validation and performance quantification. *Applied Energy*, 2017.

[13] Rinze Geertsma, Jasper Vollbrandt, Rudy Negenborn, Klaas Visser, and Hans Hopman. A quantitative comparison of hybrid diesel-electric and gas-turbine-electric propulsion for future frigates.

[14] David Gerada, David Borg-Bartolo, Abdeslam Mebarki, Christopher Micallef, Neil L. Brown, and Chris Gerada. Electrical Machines for High Speed Applications with a Wide Constant-Power Region Requirement. *Journal of international Conference on Electrical Machines and Systems*, 1(3):274–281, 2012.

[15] H.T. Grimmelius, D. Boetius, P. Baan, and P.Baan H.T. Grimmelius, D. Boetius. The Influence of Sequential Turbocharging Control on Propulsion Behaviour , Proceedings of the 12 th Ship Control Systems Symposium. In *The Hague, The Royal Netherlands Navy, ISBN 90 - 9013016 - 0*. The hague, 1999.

[16] Hugo T. Grimmelius and Douwe Stapersma. Control optimisation and load prediction for marine diesel engines using a mean value simulation model. *ENSUS 2000, Conference Proceedings*, 2000.

[17] R C Hibbeler. *ENGINEERING MECHANICS - DYNAMICS*. Pearson Prentice Hall, New Jersey, 2010.

[18] H. Hiereth and P. Prenninger. *Charging the internal combustion engine*. Springer, 2003.

[19] Seiichi Ibaraki, Yukio Yamashita, Hiroshi Ogita, and Yasuaki Jinnai. Development of electrically assisted turbocharger, Hybrid turbo. *MItsubishi Heavy Industries Technical Review*, Technical:1–5, 2006.

[20] Yukio Ibaraki, Yamashita Seiichi, Kunio Ebisu, Sumida Motoki, Byeongil Ogita, and an Hiroshi. Development of Electric Supercharger to Facilitate the Downsizing of Automobile Engines. *Mitsubishi Heavy Industries Technical Review*, 47(December 2010):7–12, 2010.

[21] J.P. Jensen, A.F. Krinstensen, S.C. Sorenson, N. Houbak, and E. Hendricks. Mean value modeling of a small turbocharged diesel engine. *SAE 910070*, pages 20–54, 1991.

[22] M Kalikatzarakis. Tertiary control of hybrid tugboats. 2017.

[23] Jaime Karremann. Marineschepen.nl, 2009.

[24] Johannes Kech, Ronald Hegner, and Tobias Männle. Turbocharging : Key technology for high-performance engines. 2011.

[25] Shiraishi Keiichi, Yoshihisa Ono, Yamashita; Yukio, and Musashi Sakamoto. Energy Savings through Electric-assist Turbocharger for Marine Diesel Engines. *MItsubishi Heavy Industries Technical Review*, 52(1):36–41, 2015.

[26] Hans Klein woud and Douwe Stapersma. *Design of Propulsion and Electric Power Generation Systems*. IMarEst, London, 2002.

[27] Jinyoung Ko, Dongyoung Jin, Wonwook Jang, Cha Lee Myung, Sangil Kwon, and Simsoo Park. Comparative investigation of NOx emission characteristics from a Euro 6-compliant diesel passenger car over the NEDC and WLTC at various ambient temperatures. *Applied Energy*, 187(x):652–662, 2017.

[28] Görkem Kökkülünk, Adnan Parlak, and Hasan Hüseyin Erdem. Determination of performance degradation of a marine diesel engine by using curve based approach. *Applied Thermal Engineering*, 108(October 2017):1136–1146, 2016.

[29] Mike Ligtvoet. Meetplan KVD koppelmeting, 2017.

[30] Y Linden. *NO-emission prediction in a Diesel Engine*. PhD thesis, TU Delft, 2017.

[31] M. A. Loonstijn. Literature Study sequential turbocharging for marine 4-stroke diesel engines. 2016.

[32] M. A. Loonstijn. Faculty of Mechanical Engineering Diesel A-M Scavenge Model Proposal A Dynamic scavenge model based on physical principles. 2017.

[33] M.A. Loonstijn. A Study on the Effects of Sequential Turbocharged Diesel Engines. Technical report, TU Delft, Delft, 2016.

[34] M.A. Loonstijn. Faculty of Mechanical Engineering Diesel A-M (placeholder name) Model Proposal Expanding the Diesel A model for advanced turbocharging capabilities. 2017.

[35] S Miedema and Zhi-hua Lu. The dynamic behavior of a diesel engine. (December), 2014.

[36] M. Moran and N. Shapiro. *Fundamentals of Engineering Thermodynamics*. Wiley, Chichester, 2006.

[37] Panos Papalambros, Donald C Graham, Ann Arbor, and Douglass J Wilde. *Principles of Optimal Design Second Edition*. 2013.

[38] Harsh Sapra, Milinko Godjevac, Klaas Visser, Douwe Stapersma, and Chris Dijkstra. Experimental and simulation-based investigations of marine diesel engine performance against static back pressure. *Applied Energy*, 204:78–92, 2017.

[39] P Schulten and D Stapersma. Mean Value Modelling of the Gas Exchange of a 4-stroke Diesel Engine for Use in Powertrain Applications. *SAE paper 2003-01-0219*, (724), 2003.

[40] P.J.M. SChulten. *The interaction between diesel engines, ship and propellers during manouevring*. PhD thesis, TU Delft, 2005.

[41] K Shiraishi, Y Ono, and K Sugishita. Development of Large Marine Hybrid Turbocharger for Generating Electric Power with Exhaust Gas from the Main Engine. 47(3):53–58, 2010.

[42] Keiichi Shiraishi and Yoshihisa Ono. Hybrid Turbocharger with Integrated High Speed Motor- generator. *Review Literature And Arts Of The Americas*, 44(1):1–3, 2007.

[43] Gequn Shu, Youcai Liang, Haiqiao Wei, Hua Tian, Jian Zhao, and Lina Liu. A review of waste heat recovery on two-stroke IC engine aboard ships. *Renewable and Sustainable Energy Reviews*, 19:385–401, 2013.

[44] Dig Vijay Singh and Eilif Pedersen. A review of waste heat recovery technologies for maritime applications. *Energy Conversion and Management*, 111(X):315–328, 2016.

[45] D Stapersma. *Diesel Engines Volume 1 Performance Analysis*, volume 1. TU Delft, Delft, 2010.

[46] D Stapersma. *Diesel Engines Volume 2 Turbocharging*, volume 2. TU Delft, Delft, 2010.

[47] D Stapersma. *Diesel Engines Volume 3 Combustion*, volume 3. TU Delft, Delft, 2010.

[48] D Stapersma. A general model for off-design performance of a single stage turbomachine. Technical Report D, TU Delft, Delft, 2013.

[49] J.P. van Buijtenen. Gas Turbines WB4420 / 4421. pages 1–180, 2007.

[50] Ministerie van defensie. Operationele energiestrategie. Technical report, Ministerie van Defensie, Den Haag, 2015.

[51] P J van Spronsen and R L Tousain. An optimal control approach to preventing marine diesel engine overloading aboard Karel Doorman class frigates. *Control Applications in Marine Systems 2001*, 12(September):493–498, 2002.

[52] Jasper Vollbrandt. *Improving the maneuvering performance of diesel hybrid propulsion plants for fast naval combatants*. PhD thesis, Delft University of Technology, 2016.

[53] Arndt von Drathen. Charge Air Systems for Submarine Engines. *MTU*, 2014.

[54] A. Vrijdag, D. Stapersma, and T. Van Terwisga. Systematic modelling, verification, calibration and validation of a ship propulsion simulation model. *Proceedings of the Institute of Marine Engineering, Science and Technology Part A: Journal of Marine Engineering and Technology*, 4177(15):3–20, 2009.

[55] Arthur Vrijdag. *Control of Propeller Cavitation in Operational Conditions*. PhD thesis, TU Delft, 2009.

[56] Q. Zhang, A. Pennycott, and C. J. Brace. A review of parallel and series turbocharging for the diesel engine. *Proceedings of the Institution of Mechanical Engineers, Part D: Journal of Automobile Engineering*, 227(12):1723–1733, 2013.

[57] K. Zinner. *Aufladung von Verbrennungsmotoren*. Springer-Verlag, Berlin, Heidelberg, New York, 2nd edition, 1980.

A

Appendix

A.1. Operational Profile of a fast naval combatant

Speed	[kn]	1-3	3-5	5-7	7-9	9-11	11-13	13-15	15-17	17-19	19-21	21-23	23-25	25-27	>27
Time	[%]	<17					<76					<8			
PB	[kW]	53 – 138	138 – 214	214 – 369	369 – 676	676 – 1229	1229 – 2079	2079 – 3313	3313 – 4927	4927 – 7322	7322 – 10205	10205 – 13837	13837 – 18939	18939 – 26071	>26071

Table 17: Estimated brake power for operational profile of a LCF frigate [52]

A.2. Transmission losses Zeven Provinciën class

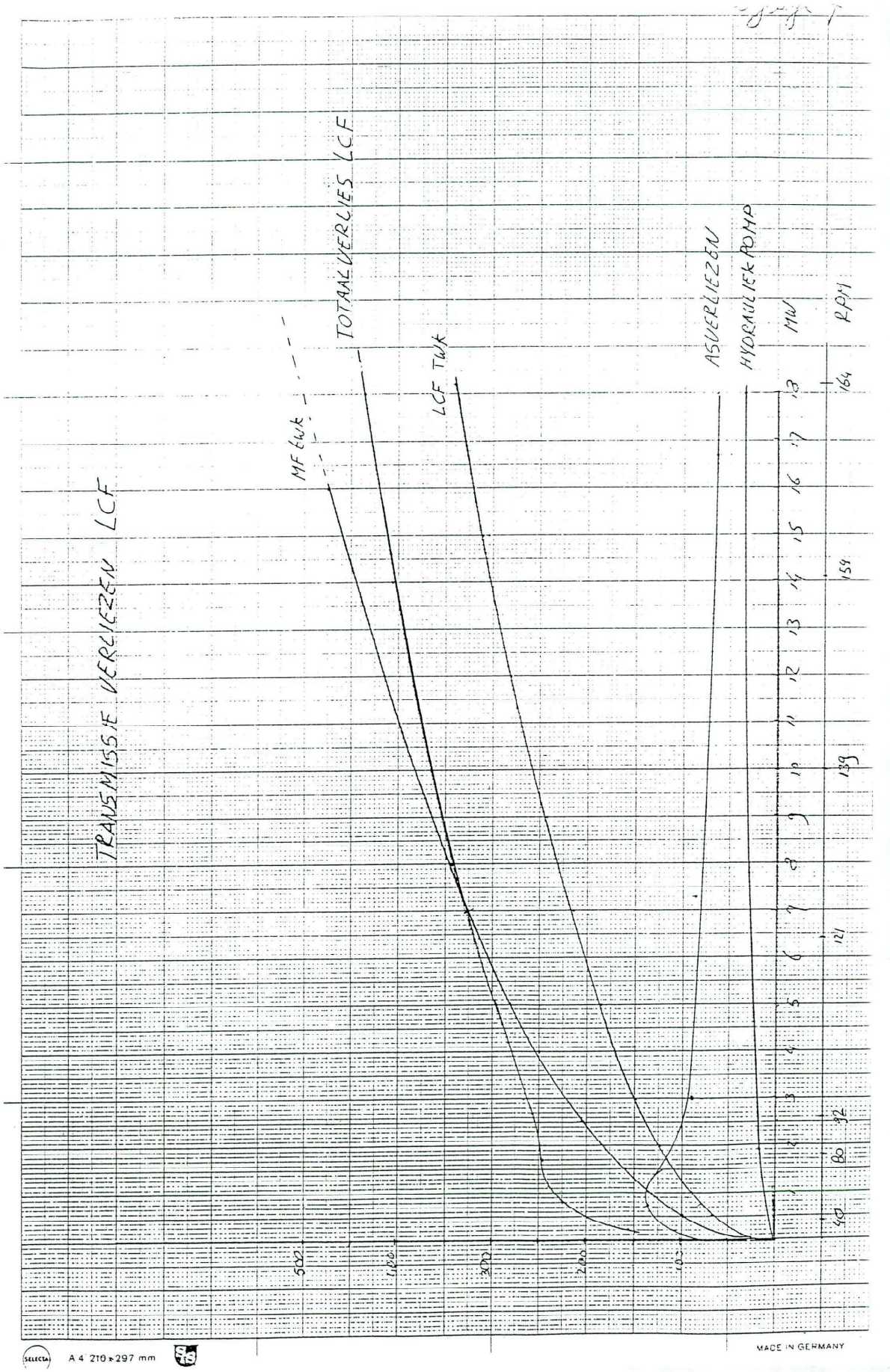

A.3. Compressor map Zeven Provinciën class